# Modelling of directional data using Kent distributions

### Parthan Kasarapu

PARTHAN.KASARAPU@MONASH.EDU

Faculty of Information Technology Monash University VIC 3800, Australia

### Abstract

The modelling of data on a spherical surface requires the consideration of directional probability distributions. To model asymmetrically distributed data on a three-dimensional sphere, Kent distributions are often used. The moment estimates of the parameters are typically used in modelling tasks involving Kent distributions. However, these lack a rigorous statistical treatment. The focus of the paper is to introduce a Bayesian estimation of the parameters of the Kent distribution which has not been carried out in the literature, partly because of its complex mathematical form. We employ the Bayesian informationtheoretic paradigm of Minimum Message Length (MML) to bridge this gap and derive reliable estimators. The inferred parameters are subsequently used in mixture modelling of Kent distributions. The problem of inferring the suitable number of mixture components is also addressed using the MML criterion. We demonstrate the superior performance of the derived MML-based parameter estimates against the traditional estimators. We apply the MML principle to infer mixtures of Kent distributions to model empirical data corresponding to protein conformations. We demonstrate the effectiveness of Kent models to act as improved descriptors of protein structural data as compared to commonly used von Mises-Fisher distributions.

**Keywords:** Minimum Message Length, von Mises-Fisher, Kent distribution, Protein modelling

### 1. Introduction

Directional statistics is a growing discipline with widespread applications in earth sciences, meteorology, physics, biology, and other areas. A sample of directional data corresponds to a collection of unit vectors. The modelling of directional data has been explored using several types of distributions described on surfaces of compact manifolds, such as spheres and tori (Fisher, 1953, 1993; Mardia and Jupp, 2000). The most popular amongst these distributions is the von Mises-Fisher (vMF) distribution (Watson and Williams, 1956). Its probability density function f at any point  $\mathbf{x}$  on a unit three-dimesional sphere has the form:

$$f(\mathbf{x}; \mathbf{\Theta}) \propto \exp{\kappa \boldsymbol{\gamma}_1^\mathsf{T} \mathbf{x}}$$

where  $\propto$  denotes proportionality,  $\Theta$  is the parameter vector comprising of the unit mean vector  $\gamma_1$  and the concentration parameter  $\kappa \geq 0$ . The vMF distribution is analogous to a symmetric Gaussian distribution, wrapped around a unit sphere. As such, it is useful for modelling directional data that is symmetrically distributed with respect to a mean direction. The modelling of asymmetrically distributed directional data, however, requires

distributions which generalize the vMF distribution. A generalization of vMF is called the Fisher-Bingham distribution (Mardia, 1975) which takes the form:

$$f(\mathbf{x}; \mathbf{\Theta}) \propto \exp\{\kappa \mathbf{\gamma}_1^\mathsf{T} \mathbf{x} + \beta_2 (\mathbf{\gamma}_2^\mathsf{T} \mathbf{x})^2 + \beta_3 (\mathbf{\gamma}_3^\mathsf{T} \mathbf{x})^2\}$$
 (1)

where the parameters  $\gamma_1, \gamma_2, \gamma_3$  are unit vectors with  $\gamma_2$  and  $\gamma_3$  being orthogonal to each other, the parameters  $\beta_2$  and  $\beta_3$  are real values with  $\beta_2 \geq \beta_3$ . As the distribution is characterized using an 8 real valued parameter vector  $\Theta$  (2 for  $\gamma_1$ , 3 for  $\gamma_2$  and  $\gamma_3$ , and 3 scalars  $\kappa, \beta_2, \beta_3$ ), it is also referred to as the FB<sub>8</sub> distribution. Notice that compared to the vMF, the FB<sub>8</sub> distribution has an exponential factor with additional quadratic terms.

Given more free parameters, the FB<sub>8</sub> distribution is a better choice compared to the vMF distribution in modelling real world three-dimensional directional data where symmetry cannot be assumed. However, the use of the FB<sub>8</sub> distribution in directional statistics poses difficulties owing to its complex mathematical form and also because of a lack of a natural understanding of its parameters (Kent, 1982). In order to achieve a balance between the highly simplified vMF model and the complex FB<sub>8</sub> distribution, Kent (1982) suggested an alternative form that is relatively easy to work with and whose parameters have natural interpretations. This distribution, referred to as the *Kent* distribution, is obtained from Equation 1 by assuming  $\gamma_1, \gamma_2, \gamma_3$  form an orthogonal system of vectors and are subject to the constraint  $\beta_2 = -\beta_3 = \beta$ . The probability density function is then given by

$$f(\mathbf{x}; \mathbf{\Theta}) = c(\kappa, \beta)^{-1} \exp\{\kappa \mathbf{\gamma}_1^\mathsf{T} \mathbf{x} + \beta [(\mathbf{\gamma}_2^\mathsf{T} \mathbf{x})^2 - (\mathbf{\gamma}_3^\mathsf{T} \mathbf{x})^2]\}$$
(2)

where  $\gamma_1, \gamma_2, \gamma_3$  are orthogonal unit vectors representing the *mean*, *major*, and *minor* axes respectively;  $\kappa$ , as before, measures the concentration, and  $0 \le \beta < \kappa/2$  describes the *ovalness*.

The Kent distribution was proposed as a spherical analogue of the general Gaussian distribution and serves as a natural extension to the vMF distribution. The distribution has ellipse-like contours of constant probability density on the spherical surface. Kent (1982) argued that by imposing the constraints  $\beta < \kappa/2$  and  $\gamma_1, \gamma_2, \gamma_3$  to be an orthogonal system, the distribution would be unimodal and have a behaviour similar to the Gaussian distribution but on a spherical surface.

As the Kent distribution is characterized using a 5 real valued parameter vector  $\boldsymbol{\Theta}$  (3 for  $\gamma_1, \gamma_2, \gamma_3$  because they are orthogonal and unit vectors, 2 for the scalar entities  $\kappa, \beta$ ), it is popularly referred to as the FB<sub>5</sub> distribution. We will denote the 5-parameter Fisher-Bingham distribution as FB<sub>5</sub>( $\mathbf{Q}, \kappa, \beta$ ), where  $\mathbf{Q} = (\gamma_1, \gamma_2, \gamma_3)$  is a 3 × 3 orthogonal matrix. The normalization constant  $c(\kappa, \beta)$  of the distribution is derived as an infinite series

$$c(\kappa, \beta) = 2\pi \sum_{j=0}^{\infty} \frac{\Gamma(j + \frac{1}{2})}{\Gamma(j+1)} \beta^{2j} \left(\frac{2}{\kappa}\right)^{2j + \frac{1}{2}} I_{2j + \frac{1}{2}}(\kappa)$$
 (3)

that depends on the Gamma function  $\Gamma$  and the modified Bessel function  $I_v$  of the first kind and order v (Abramowitz and Stegun, 1965; Kent, 1982).

The importance of vMF and FB<sub>5</sub> distributions in mixture modelling tasks has been well established: vMF mixtures have been used in large-scale text clustering (Banerjee et al., 2003; Gopal and Yang, 2014), clustering of protein dihedral angles (Dowe et al., 1996a;

Mardia et al., 2007), and gene expression analyses (Banerjee et al., 2005). Mixtures of FB<sub>5</sub> distributions have been employed by Peel et al. (2001) to identify joint sets in rock masses, and by Hamelryck et al. (2006) to sample random protein conformations. The FB<sub>5</sub> distribution has increasingly found support in machine learning tasks in structural bioinformatics (Kent and Hamelryck, 2005; Boomsma et al., 2006; Hamelryck, 2009).

The analysis of data using FB<sub>5</sub> distributions requires estimating the corresponding parameters. Due to the complex mathematical form of the density function, these estimates are approximated. Kent (1982) derived the moment estimates and suggested limiting case approximations. However, the use of simplified approximations can have considerable effects from a practical standpoint. To overcome this, we explore Bayesian estimation using the minimum message length (MML) principle as it results in reliable estimators as shown by the experiments in Section 9.

The parameter inference of a statistical distribution is typically done by maximum likelihood (ML) or Bayesian maximum a posteriori probability (MAP) estimation. Bayesian inference using MML differs from the traditional approaches as follows: (1) unlike ML, MML uses a prior over the parameters and considers their precision while encoding; (2) unlike MAP, MML estimators are invariant under non-linear transformations of the parameters (Oliver and Baxter, 1994). The estimation of parameters using ML ignores the cost of stating the parameters, and MAP based estimation uses the probability density of parameters instead of their probability measure. In contrast, the MML inference process takes into account the optimal precision to which parameters should be stated and uses it to determine a corresponding probability value. The MML framework decomposes the inference problem into two parts: lossless encoding of the parameters, and encoding the data given those parameters. It then selects the parameters that result in the least overall message length to explain the data. Thus, models with varying parameters are evaluated based on their resultant total message lengths.

The MML principle has been used in the inference of several probability distributions (Wallace, 2005). In particular, the MML parameter estimates of a three-dimensional vMF distribution were derived by Dowe et al. (1996b), wherein they demonstrated that the MML estimates outperform the traditional ML and MAP based ones. For modelling higher dimensional directional data, Kasarapu and Allison (2015) demonstrated the reliable performance of MML-based vMF estimates compared to other traditional estimates. In this work, we derive the MML-based parameter estimates of a FB<sub>5</sub> distribution and subsequently use them in the mixture modelling. The MML estimates are shown to perform better than the traditionally used moment and maximum likelihood estimates. Also, the invariance property of MML estimates makes them reliable candidates when compared to MAP estimates. We study the results of modelling the protein data using mixtures of vMF and FB<sub>5</sub> distributions. Furthermore, we demonstrate that FB<sub>5</sub> mixture models serve as better candidate models when compared to vMF mixtures in modelling protein directional data.

The paper is organized as follows: Section 2 describes the MML framework and highlights the key differences between the MML estimation procedure and others. Section 3 explains the  $FB_5$  distribution and the associated geometrical construction. Section 4 describes the existing moment and maximum likelihood parameter estimates of the  $FB_5$  distribution. Section 5 describes the MAP estimation procedure in the context of the  $FB_5$  distribution and emphasizes its dependency on the manner the distribution is parameterized. Section 6

describes the MML-based estimation of the parameters of the FB<sub>5</sub> distribution. Section 7 outlines the numerical implementation of methods to compute the normalization constant and the corresponding partial derivatives which are required as part of MML-based estimation. Section 8 describes mixture modelling using FB<sub>5</sub> distributions with emphasis on the search for the optimal number of mixture components. Section 9 presents the experimental results of the various parameter estimation methods. Section 10 discusses the application of FB<sub>5</sub> mixtures with respect to modelling protein structural data. Section 11 concludes with a summary of the work.

# 2. Minimum Message Length (MML) Inference

In this section, we describe the model selection paradigm using the Minimum Message Length criterion and proceed to give an overview of MML-based parameter estimation for any distribution.

### 2.1 Model selection using minimum message length criterion

Wallace and Boulton (1968) developed the first practical criterion for model selection based on information theory. As per Bayes's theorem:

$$\Pr(\mathcal{H} \& \mathcal{D}) = \Pr(\mathcal{H}) \times \Pr(\mathcal{D}|\mathcal{H}) = \Pr(\mathcal{D}) \times \Pr(\mathcal{H}|\mathcal{D})$$

where  $\mathcal{D}$  denotes observed data, and  $\mathcal{H}$  some hypothesis about that data. Further,  $\Pr(\mathcal{H} \& \mathcal{D})$  is the joint probability of data  $\mathcal{D}$  and hypothesis  $\mathcal{H}$ ,  $\Pr(\mathcal{H})$  and  $\Pr(\mathcal{D})$  are the prior probabilities of hypothesis  $\mathcal{H}$  and data  $\mathcal{D}$  respectively,  $\Pr(\mathcal{H}|\mathcal{D})$  is the posterior probability, and  $\Pr(\mathcal{D}|\mathcal{H})$  is the likelihood.

As per Shannon (1948), given an event E with probability  $\Pr(E)$ , the length of the optimal lossless code to represent that event requires  $I(E) = -\log_2(\Pr(E))$  bits. Applying Shannon's insight to Bayes's theorem, Wallace and Boulton (1968) got the following relationship between conditional probabilities in terms of optimal message lengths:

$$I(\mathcal{H} \& \mathcal{D}) = I(\mathcal{H}) + I(\mathcal{D}|\mathcal{H}) = I(\mathcal{D}) + I(\mathcal{H}|\mathcal{D})$$

The above equation can be interpreted as the *total* cost to encode a message comprising of the following two parts:

- 1. First part: the hypothesis  $\mathcal{H}$ , which takes  $I(\mathcal{H})$  bits,
- 2. Second part: the observed data  $\mathcal{D}$  using knowledge of  $\mathcal{H}$ , which takes  $I(\mathcal{D}|\mathcal{H})$  bits.

As a result, given two competing hypotheses  $\mathcal{H}$  and  $\mathcal{H}'$ ,

$$\Delta I = I(\mathcal{H} \& \mathcal{D}) - I(\mathcal{H}' \& \mathcal{D}) = I(\mathcal{H}|\mathcal{D}) - I(\mathcal{H}'|\mathcal{D}) \quad \text{bits.}$$
Hence,  $\Pr(\mathcal{H}'|\mathcal{D}) = 2^{\Delta I} \Pr(\mathcal{H}|\mathcal{D})$ 

gives the log-odds posterior ratio between the two hypotheses. The framework provides a rigorous means to objectively compare two competing hypotheses. Clearly, the message length can vary depending on the complexity of  $\mathcal{H}$  and how well it can explain  $\mathcal{D}$ . A more

complex  $\mathcal{H}$  may explain  $\mathcal{D}$  better but takes more bits to be stated itself. The trade-off comes from the fact that (hypothetically) transmitting the message requires the encoding of both the hypothesis and the data given the hypothesis, that is, the model complexity  $I(\mathcal{H})$  and the goodness of fit  $I(\mathcal{D}|\mathcal{H})$ .

### 2.2 MML-based parameter estimation

Wallace and Freeman (1987) introduced a generalized framework to estimate a set of parameters  $\boldsymbol{\Theta}$  given data  $\mathcal{D}$ . The method requires a reasonable prior  $h(\boldsymbol{\Theta})$  on the hypothesis and evaluating the *determinant* of the Fisher information matrix  $|\mathcal{F}(\boldsymbol{\Theta})|$  of the *expected* second-order partial derivatives of the negative log-likelihood function,  $\mathcal{L}(D|\boldsymbol{\Theta})$ . The parameter vector  $\boldsymbol{\Theta}$  that minimizes the message length expression (given by Equation 4) is the MML estimate according to Wallace and Freeman (1987).

$$I(\mathbf{\Theta}, \mathcal{D}) = \underbrace{\frac{d}{2} \log q_d - \log \left( \frac{h(\mathbf{\Theta})}{\sqrt{|\mathcal{F}(\mathbf{\Theta})|}} \right)}_{I(\mathbf{\Theta})} + \underbrace{\mathcal{L}(\mathcal{D}|\mathbf{\Theta}) + \frac{d}{2}}_{I(\mathcal{D}|\mathbf{\Theta})}$$
(4)

where d is the number of free parameters in the model, and  $q_d$  is the d-dimensional lattice quantization constant (Conway and Sloane, 1984). The total message length  $I(\Theta, \mathcal{D})$ , therefore, comprises of two parts: (1) the cost of encoding the parameters,  $I(\Theta)$ , and (2) the cost of encoding the data given the parameters,  $I(\mathcal{D}|\Theta)$ . A concise description of the MML method is presented in Oliver and Baxter (1994).

The key differences between ML, MAP, and MML estimation techniques are as follows: in ML estimation, the encoding cost of parameters is, in effect, considered constant, and minimizing the message length corresponds to minimizing the negative log-likelihood of the data (the second part). In MAP based estimation, a probability density rather than the probability is used. It is self evident that continuous parameter values can only be stated to some finite precision; MML incorporates this in the framework by determining the region

of uncertainty in which the parameter is located. The value of  $V = \frac{q_d^{-d/2}}{\sqrt{|\mathcal{F}(\Theta)|}}$  gives a measure of the volume of the region of uncertainty in which the parameter  $\Theta$  is centered. This multiplied by the probability density  $h(\Theta)$  gives the *probability* of a particular  $\Theta$  as  $\Pr(\Theta) = h(\Theta)V$ . This probability is used to compute the message length associated with encoding the continuous valued parameters (to a finite precision).

### 3. The FB<sub>5</sub> distribution and its parameterization

The FB<sub>5</sub> distribution defined by Equation 2 comprises of three directional parameters and two scalar parameters. We describe the following parameterization of the distribution that is intuitive and relatively easy to comprehend. Let  $\mathbf{X}_1 = (1\ 0\ 0)^\mathsf{T}, \mathbf{X}_2 = (0\ 1\ 0)^\mathsf{T}, \mathbf{X}_3 = (0\ 0\ 1)^\mathsf{T}$  be the unit vectors along the standard coordinate axes. Let  $\mathbf{R}$  be the rotation matrix that transforms the orientation axes  $\gamma_1, \gamma_2, \gamma_3$  supporting a FB<sub>5</sub> distribution to align with the standard coordinate axes. Then,  $\mathbf{R}^\mathsf{T} = (\gamma_1, \gamma_2, \gamma_3) = \mathbf{Q}$  based on the following reasoning.

Let  $\alpha \in [0, \pi]$  and  $\eta \in [0, 2\pi]$  be the co-latitude and longitude that determine the mean axis  $\gamma_1$  (shown in Figure 1a). A clockwise rotation by an angle  $\eta$  about  $\mathbf{X}_1$  brings  $\gamma_1$  into

the  $\mathbf{X}_1\mathbf{X}_2$  plane. This operation transforms the axes to  $\gamma_1', \gamma_2', \gamma_3'$  respectively (Figure 1b). A subsequent clockwise rotation by an angle  $\alpha$  about  $\mathbf{X}_3$  aligns  $\gamma_1'$  with  $\mathbf{X}_1$ . This rotation brings the major and minor axes into the  $\mathbf{X}_2\mathbf{X}_3$  plane (as orthogonality should be preserved). In this orientation (Figure 1c), let  $\psi \in [0, \pi]$  be the angle between the transformed axis  $\gamma_2''$  and  $\mathbf{X}_2$ . A clockwise rotation by  $\psi$  about  $\mathbf{X}_1$  aligns  $\gamma_2''$  with  $\mathbf{X}_2$  and  $\gamma_3''$  with  $\mathbf{X}_3$ .

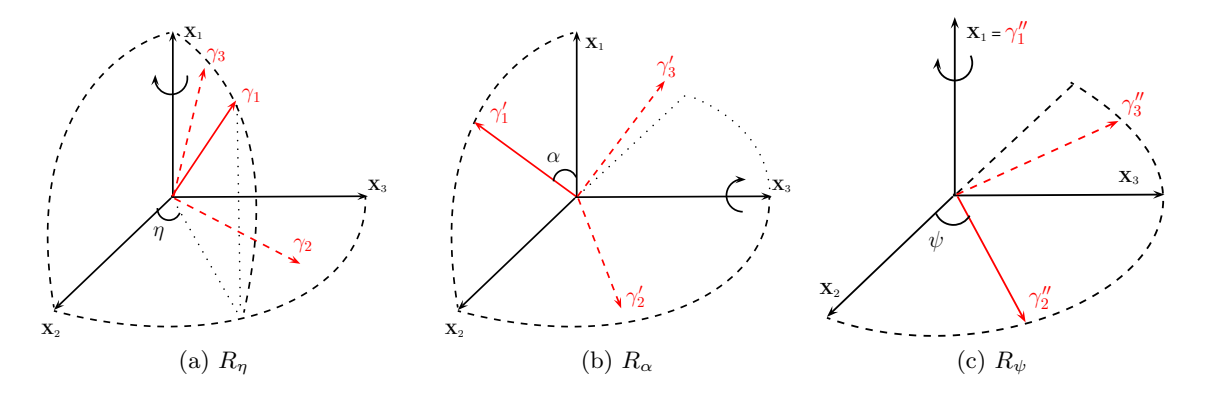


Figure 1: The series of rotations to orient  $\gamma_1, \gamma_2, \gamma_3$  with the standard coordinate axes. The red dashed lines indicate the axis that is not in the first octant. For example, in (b),  $\gamma'_2$  is below the  $\mathbf{X}_2\mathbf{X}_3$  plane whereas  $\gamma'_3$  is above the  $\mathbf{X}_2\mathbf{X}_3$  plane but behind the  $\mathbf{X}_1\mathbf{X}_3$  plane.

If  $\mathbf{R}_{\eta}, \mathbf{R}_{\alpha}, \mathbf{R}_{\psi}$  denote the respective rotation matrices given by

$$\mathbf{R}_{\eta} = \begin{bmatrix} 1 & 0 & 0 \\ 0 & \cos \eta & \sin \eta \\ 0 & -\sin \eta & \cos \eta \end{bmatrix}, \ \mathbf{R}_{\alpha} = \begin{bmatrix} \cos \alpha & \sin \alpha & 0 \\ -\sin \alpha & \cos \alpha & 0 \\ 0 & 0 & 1 \end{bmatrix}, \ \mathbf{R}_{\psi} = \begin{bmatrix} 1 & 0 & 0 \\ 0 & \cos \psi & \sin \psi \\ 0 & -\sin \psi & \cos \psi \end{bmatrix}$$

then the complete rotation matrix that effects the transformation from  $(\gamma_1, \gamma_2, \gamma_3)$  to  $(\mathbf{X}_1, \mathbf{X}_2, \mathbf{X}_3)$  is given by their product  $\mathbf{R} = \mathbf{R}_{\psi} \mathbf{R}_{\alpha} \mathbf{R}_{\eta}$ . By construction, any  $\mathbf{X}_i = \mathbf{R} \boldsymbol{\gamma}_i$ , (i = 1, 2, 3), and consequently,  $\mathbf{Q} = \mathbf{R}^{\mathsf{T}}$ . Hence, the three orthogonal axes  $\boldsymbol{\gamma}_i$  of a FB<sub>5</sub> distribution can effectively be described using the three angular parameters  $\psi$ ,  $\alpha$ ,  $\eta$  as follows:

$$\boldsymbol{\gamma}_{1} = (\cos \alpha, \sin \alpha \cos \eta, \sin \alpha \sin \eta)^{\mathsf{T}}$$

$$\boldsymbol{\gamma}_{2} = (-\cos \psi \sin \alpha, \cos \psi \cos \alpha \cos \eta - \sin \psi \sin \eta, \cos \psi \cos \alpha \sin \eta + \sin \psi \cos \eta)^{\mathsf{T}}$$

$$\boldsymbol{\gamma}_{3} = (\sin \psi \sin \alpha, -\sin \psi \cos \alpha \cos \eta - \cos \psi \sin \eta, -\sin \psi \cos \alpha \sin \eta + \cos \psi \cos \eta)^{\mathsf{T}}$$
(5)

The parameters  $\kappa$  and  $\beta$  are interpreted as scalars controlling the concentration and ovalness of the distribution. Also, since the distribution has ellipse-shaped contours on the spherical surface, it is easier to visualize the distribution and relate  $\kappa$  and  $\beta$  terms using eccentricity. Kent (1982) defined the eccentricity<sup>1</sup> as  $2\beta/\kappa$ , which is constrained to be less

<sup>1.</sup> The definition of eccentricity in this context differs from the traditional definition of eccentricity for a conic section such as a parabola, an ellipse, or a hyperbola defined in the Euclidean plane.

than 1 (by definition), allowing correspondence between a specific Kent distribution and its elliptical nature. In order to better understand the interaction of  $\kappa$  and eccentricity terms, we provide examples in Figure 2.

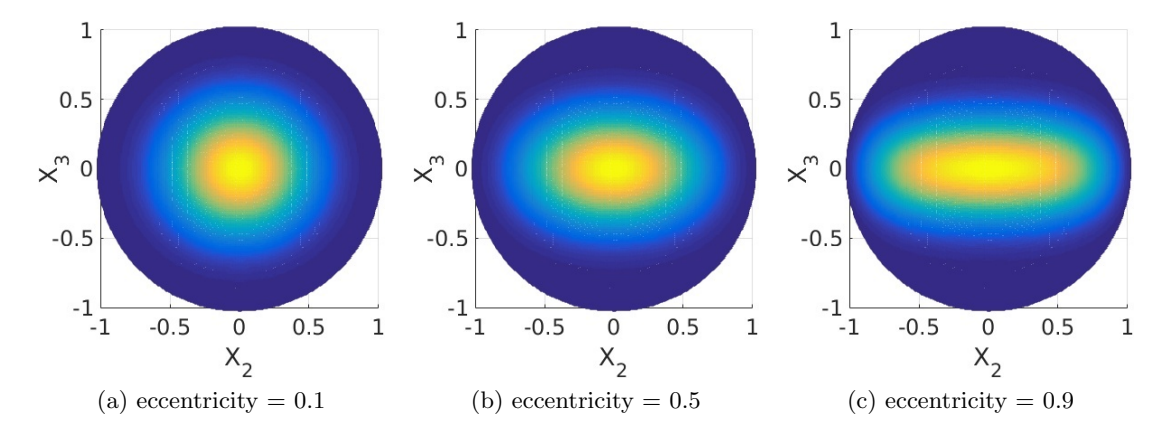


Figure 2: An example of a FB<sub>5</sub> distribution with varying eccentricities for  $\kappa = 10$ .

For a given  $\kappa=10$ , an eccentricity of 0.1 results in (almost) spherical contours (Figure 2a) (reminiscent of a vMF distribution); an eccentricity of 0.5 results in contours which are moderately eccentric (Figure 2b); an eccentricity of 0.9 further disperses the data along the major axis (Figure 2c).

# 4. Existing methods of parameter estimation of the FB<sub>5</sub> distribution

The traditional methods of maximum likelihood (ML) estimation or maximum a priori (MAP) based estimation require the optimization of negative log-likelihood or the posterior density functions respectively. They, however, don't result in closed form solutions and present difficulties because of the complex form of the probability distribution. Hence, the widely used method of estimating the parameters of a FB<sub>5</sub> distribution is done using moment estimation. Kent (1982) formulated a procedure to obtain these estimates that may be subsequently used as starting points to obtain the ML or MAP estimates. Kent (1982) derived the moment estimates and suggested approximations based on these estimates.

### 4.1 Moment estimation

The moment estimates were proposed as an alternative to the maximum likelihood estimates. The approach adopted by Kent (1982) is described here: let data  $\mathcal{D} = \{\mathbf{x}_1, \dots, \mathbf{x}_N\}$  be a random sample from FB<sub>5</sub>( $\mathbf{Q}, \kappa, \beta$ ). The sample mean  $\bar{\mathbf{x}}$  and sample dispersion  $3 \times 3$  matrix  $\mathbf{S}$  of the data are then given as:

$$\bar{\mathbf{x}} = \frac{1}{N} \sum_{i=1}^{N} \mathbf{x}_i$$
 and  $\mathbf{S} = \frac{1}{N} \sum_{i=1}^{N} \mathbf{x}_i \mathbf{x}_i^\mathsf{T}$ 

Let  $\widetilde{\kappa}, \widetilde{\beta}, \widetilde{\mathbf{Q}} = (\widetilde{\gamma}_1, \widetilde{\gamma}_2, \widetilde{\gamma}_3)$  be the respective moment estimates of  $\kappa, \beta$ , and  $\mathbf{Q}$ . Then the moment estimate  $\widetilde{\gamma}_1$  of the unit mean vector is obtained by normalizing  $\bar{\mathbf{x}}$ . The moment

estimates  $\widetilde{\gamma}_2$  and  $\widetilde{\gamma}_3$  are obtained by diagonalizing **S**. The matrix  $\widetilde{\mathbf{Q}}$  is obtained using the following two steps:

- 1. Choose an orthogonal matrix  $\mathbf{H}$  to rotate  $\bar{\mathbf{x}}$  to align with the  $\mathbf{X}_1 = (1 \ 0 \ 0)^\mathsf{T}$  axis (based on the discussion in Section 3,  $\mathbf{H} = \mathbf{R}_{\alpha} \mathbf{R}_{\eta}$ , where  $\alpha$  and  $\eta$  are the co-latitude and longitude of  $\bar{\mathbf{x}}$  respectively). Let  $\mathbf{B} = \mathbf{H}^\mathsf{T} \mathbf{S} \mathbf{H}$ , so that  $\mathbf{B}$  is the dispersion matrix in the transformed frame of reference.
- 2. The moment estimates of the major and minor axis correspond to the respective directions of maximum and minimum variance of the data in this transformed reference frame. If the angle between the direction of maximum variance and the  $\mathbf{X}_2 = (0\ 1\ 0)^\mathsf{T}$  axis is  $\psi$ , then a rotation defined by the orthogonal matrix  $\mathbf{K}$  about  $\mathbf{X}_1$  by  $\psi$ , aligns the maximum and minimum variance directions with the  $\mathbf{X}_2$  and  $\mathbf{X}_3 = (0\ 0\ 1)^\mathsf{T}$  axes respectively. To compute these directions, it is required to diagonalize  $\mathbf{B}_L$ , the lower  $2 \times 2$  submatrix of  $\mathbf{B}$ . The eigenvalue decomposition of  $\mathbf{B}_L$  gives the angle  $\psi$  between the maximum variance direction and  $\mathbf{X}_2$ , which can be subsequently used to determine  $\mathbf{K}$ . If the  $3 \times 3$  dispersion matrix  $\mathbf{B} = [b_{ij}], 1 \le i, j \le 3$ , the expression for  $\psi$  is

$$\tan 2\psi = \frac{2b_{23}}{b_{22} - b_{33}} \quad \text{where} \quad \mathbf{B}_L = \begin{bmatrix} b_{22} & b_{23} \\ b_{23} & b_{33} \end{bmatrix}$$
(6)

The two rotations defined by the orthogonal transformations  $\mathbf{H}$  followed by  $\mathbf{K}$  transform the axes of a FB<sub>5</sub> distribution to align with the standard coordinate axes. In effect, the original data  $\mathcal{D}$  is transformed to  $\mathcal{D}' = \{\mathbf{y}_1, \dots, \mathbf{y}_N\}$  such that  $\mathcal{D}'$  corresponds to a random sample drawn from FB<sub>5</sub>( $\mathbf{I}, \kappa, \beta$ ), where  $\mathbf{I}$  is the identity matrix. Hence, an inverse transformation of the coordinate axes yields the moment estimates  $\widetilde{\mathbf{Q}}$  of the axes of the FB<sub>5</sub> distribution.

Further, for  $\mathbf{y} = (y_1, y_2, y_3)^\mathsf{T}$ , Kent (1982) provided the moment expressions given below:

$$\mathbb{E}[y_1] = c_{\kappa}/c, \quad \mathbb{E}[y_2^2 - y_3^2] = c_{\beta}/c, \text{ where } c = c(\kappa, \beta), c_{\kappa} = \partial c/\partial \kappa, c_{\beta} = \partial c/\partial \beta$$
 (7)

For data  $\mathcal{D}$ , if  $\|\bar{\mathbf{x}}\|$  is the magnitude of the sample mean  $\bar{\mathbf{x}}$  and  $l_1 > l_2$  are the eigenvalues of  $\mathbf{B}_L$ , then Kent (1982) defines the *shape* and *size* and quantities as  $r_1$  and  $r_2$  respectively and are given as

$$r_1 = \mathbb{E}[y_1] = \|\bar{\mathbf{x}}\| \quad \text{and} \quad r_2 = \mathbb{E}[y_2^2 - y_3^2] = l_1 - l_2$$
 (8)

Hence, solving these two simultaneous equations in conjunction with Equation 7 results in the moment estimates  $\widetilde{\kappa}$  and  $\widetilde{\beta}$ . As the expressions of the partial derivatives  $c_{\kappa}$  and  $c_{\beta}$  are difficult to work with, the following limiting case approximations of  $\widetilde{\kappa}$  and  $\widetilde{\beta}$  are often used.

$$\widetilde{\kappa} \approx (2 - 2r_1 - r_2)^{-1} + (2 - 2r_1 + r_2)^{-1}$$

$$\widetilde{\beta} \approx \frac{1}{2} \{ (2 - 2r_1 - r_2)^{-1} - (2 - 2r_1 + r_2)^{-1} \}$$
(9)

These asymptotic approximations can also be used as starting points to accurately determine  $\widetilde{\kappa}$  and  $\widetilde{\beta}$  using an optimization library.

### 4.2 Maximum likelihood estimation

To obtain the maximum likelihood estimates, the negative log-likelihood function  $\mathcal{L}(\mathcal{D}|\Theta)$  of the data  $\mathcal{D}$ , given by Equation 10, needs to be minimized. It is to be noted that  $\gamma_1, \gamma_2, \gamma_3$  are expressed in terms of  $\psi, \alpha, \eta$  (Equation 5), so that  $\Theta = \{\psi, \alpha, \eta, \kappa, \beta\}$  is a vector of parameters.

$$\mathcal{L}(\mathcal{D}|\mathbf{\Theta}) = N \log c(\kappa, \beta) - \kappa \boldsymbol{\gamma}_1^\mathsf{T} \sum_{i=1}^N \mathbf{x}_i - \beta \boldsymbol{\gamma}_2^\mathsf{T} \left( \sum_{i=1}^N \mathbf{x}_i \mathbf{x}_i^\mathsf{T} \right) \boldsymbol{\gamma}_2 + \beta \boldsymbol{\gamma}_3^\mathsf{T} \left( \sum_{i=1}^N \mathbf{x}_i \mathbf{x}_i^\mathsf{T} \right) \boldsymbol{\gamma}_3 \quad (10)$$

The maximum likelihood estimates are given as solutions to the equation  $\frac{\partial \mathcal{L}}{\partial \mathbf{\Theta}} = 0$ . These estimates are obtained through numerical optimization as the solution cannot be written in an analytical form. The optimization routine often requires some initial values of the roots. These starting points are taken to be the moment estimates that were discussed previously.

# 5. Maximum a posteriori (MAP) based parameter estimation

The moment estimates of a FB<sub>5</sub> distribution are typically used in a variety of applications (Peel et al., 2001; Kent and Hamelryck, 2005; Boomsma et al., 2006; Hamelryck et al., 2006). In this section, we explore MAP based parameter estimation, which we will later use in our discussion to compare the various estimators (see Section 9). The estimation procedure requires the maximization of the posterior density given some observed data  $\mathcal{D}$ . If  $h(\Theta)$  is an appropriate prior density of the parameters and  $Pr(\mathcal{D}|\Theta)$  is the likelihood of data given the parameters, then the posterior density  $Pr(\Theta|\mathcal{D})$  is given as

$$\Pr(\boldsymbol{\Theta}|\mathcal{D}) \propto h(\boldsymbol{\Theta}) \times \Pr(\mathcal{D}|\boldsymbol{\Theta})$$

For an independent and identically distributed sample  $\mathcal{D} = \{\mathbf{x}_1, \dots, \mathbf{x}_N\}$ , and a probability distribution  $f(\mathbf{x}; \mathbf{\Theta})$ , the likelihood term  $\Pr(\mathcal{D}|\mathbf{\Theta}) = \prod_{i=1}^N f(\mathbf{x}_i; \mathbf{\Theta})$ . The MAP estimator corresponds to the mode of the posterior distribution. The mode is, however, not the same under varying parameterizations. As a result, the MAP estimate is *not* invariant under some non-linear transformation of the parameter space (Murphy, 2012). This drawback is exemplified in the context of estimating the parameters of a FB<sub>5</sub> distribution. A prior  $h_{\mathbf{\Theta}}$  is described on the parameter vector  $\mathbf{\Theta}$ . It is formulated based on the choice of priors for the individual elements of the parameter vector. We also consider its reparameterization in a transformed space and demonstrate that the modes of the posterior in these alternative parameterizations are not given by the same transformation of the parameter space.

### 5.1 Prior density of the parameters

The formulation of the prior density of the 5-parameter vector  $\mathbf{\Theta}$  is derived as a product of the priors of the three angular parameters  $\psi$ ,  $\alpha$ ,  $\eta$  and two scalar parameters  $\kappa$ ,  $\beta$ . Hence, the prior density of the complete set of parameters is given by  $h_{\mathbf{\Theta}}(\psi, \alpha, \eta, \kappa, \beta) = h_A(\psi, \alpha, \eta) \times h_S(\kappa, \beta)$ .

# 5.1.1 Prior density $(h_A)$ on the angular parameters $\psi, \alpha, \eta$

By construction (see Section 3), the pair  $\alpha$ ,  $\eta$  uniquely defines the mean direction  $\gamma_1$  of a FB<sub>5</sub> distribution. The mean may be considered to be uniformly distributed on the spherical surface, and hence, its prior density is  $\frac{\sin \alpha}{4\pi}$ . The angle  $\psi$  which determines the orientation of the major and minor axis in a plane perpendicular to  $\gamma_1$  is treated to be uniformly distributed on  $[0,\pi]$ . The joint prior of the angular parameters is, therefore, given by  $h_A(\psi,\alpha,\eta) = \frac{\sin \alpha}{4\pi^2}$ .

### 5.1.2 Prior density $(h_S)$ on the scale parameters $\kappa, \beta$

The prior of the concentration parameter  $\kappa$  corresponds to the one used by Dowe et al. (1996b) in their analysis of vMF distributions defined on the two-sphere and is given as:  $h(\kappa) = \frac{4\kappa^2}{\pi(1+\kappa^2)^2}$ . For a given  $\kappa$ , as per the definition of a FB<sub>5</sub> distribution, the parameter  $\beta \in [0, \kappa/2)$ . A uniform prior is considered for  $\beta$  within this range, that is, the conditional density  $h(\beta|\kappa) = 2/\kappa$ . Therefore, the joint prior density of the scalar parameters is  $h_S(\kappa, \beta) = (2/\kappa)h(\kappa)$ . The joint prior density  $h_{\Theta}$  is, hence, given as:

$$h_{\Theta}(\psi, \alpha, \eta, \kappa, \beta) = \frac{2\kappa \sin \alpha}{\pi^3 (1 + \kappa^2)^2}$$
(11)

### 5.2 Non-linear transformations of the parameter space

The reason for considering another parameterization is to show that MAP estimates are not invariant under non-linear transformations of the parameter space. If  $T(\Theta) = \Theta'$  denotes a transformation T on the parameter vector  $\Theta$ , then for invariance, the parameter estimates in both the parameterizations should be affected by the same transformation. The parameter estimate  $\widehat{\Theta}'$  in the transformed space and the estimate  $\widehat{\Theta}$  should be related as  $T(\widehat{\Theta}) = \widehat{\Theta}'$ . With the help of an example, we demonstrate that the invariance property is not a characteristic of MAP-based estimation, thus, making it an inconsistent estimator.

### 5.2.1 An alternative parameterization involving $\beta$

An alternative parameterization is considered where the eccentricity  $e = 2\beta/\kappa$  (see Section 3) is used instead of  $\beta$ . This is an example of a non-linear transformation of the parameter  $\beta$ . The prior density  $h_{\Theta'}$  (Equation 12) of the modified parameter vector  $\Theta' = \{\psi, \alpha, \eta, \kappa, e\}$  is obtained by dividing the prior density  $h_{\Theta}$  by the Jacobian of the transformation given by  $J = \partial e/\partial \beta = 2/\kappa$ . The prior density  $h_{\Theta'}$  (after reparameterization) is:

$$h_{\Theta'}(\psi, \alpha, \eta, \kappa, e) = \frac{h_{\Theta}(\psi, \alpha, \eta, \kappa, \beta)}{J} = \frac{\kappa^2 \sin \alpha}{\pi^3 (1 + \kappa^2)^2}$$
(12)

### 5.2.2 Alternative forms of the posterior distribution

Based on the definitions of prior densities in varying parameter spaces, one can estimate the parameters by maximizing the posterior density in the corresponding parameterization. The different expressions for the posterior density are summarized here.

Posterior(
$$\Theta | \mathcal{D}$$
)  $\propto h_{\Theta}(\psi, \alpha, \eta, \kappa, \beta) \times \prod_{i=1}^{N} f(\mathbf{x}_{i}; \Theta)$   
Posterior( $\Theta' | \mathcal{D}$ )  $\propto h_{\Theta'}(\psi, \alpha, \eta, \kappa, e) \times \prod_{i=1}^{N} f(\mathbf{x}_{i}; \Theta')$  (13)

The expression for  $f(\mathbf{x}, \mathbf{\Theta}')$  is obtained by substituting  $\beta = \kappa e/2$  in the FB<sub>5</sub> probability density function  $f(\mathbf{x}, \mathbf{\Theta})$  (given by Equation 2). It should be noted that the value of likelihood expression is the same across different parameterizations.

### 5.3 An example demonstrating the effects of alternative parameterizations

An example of estimating parameters using the various posterior distributions for a given dataset is shown here. A random sample of size N=10 is generated from a FB<sub>5</sub> distribution (Kent et al., 2013). The true parameters of the distribution are  $\{\psi, \alpha, \eta\} = \pi/2$  each,  $\kappa = 10$ , and  $\beta = 2.5$  (eccentricity = 0.5). To obtain the MAP estimates, the objective functions corresponding to the posterior density (Equation 13) need to be maximized. To solve for the parameter estimates, the non-linear optimization library NLopt (Johnson) in conjunction with derivative-free optimization (Powell, 1994) is used. Maximizing the two versions of the posterior density results in the following MAP estimates of  $\psi, \alpha, \eta$ :

$$\begin{split} \widehat{\psi} &= 2.071, \ \widehat{\alpha} = 1.493, \ \widehat{\eta} = 1.522 \quad \text{using } h_{\pmb{\Theta}} \\ \widehat{\psi} &= 2.071, \ \widehat{\alpha} = 1.493, \ \widehat{\eta} = 1.522 \quad \text{using } h_{\pmb{\Theta}'} \end{split}$$

It is observed that the MAP estimates of  $\psi, \alpha, \eta$  are not different from their counterparts obtained using the two variations of the posterior density. However, the estimates  $\widehat{\kappa}$  and  $\widehat{\beta}$  under the parameterizations  $\Theta$  and  $\Theta'$  do not correspond to each other as illustrated in the results below.

$$\widehat{\kappa} = 17.023, \ \widehat{\beta} = 5.493 \quad \text{using } h_{\Theta}$$

$$\widehat{\kappa} = 20.549, \ \widehat{e} = 0.701 \implies \widehat{\beta} = \widehat{\kappa} \, \widehat{e}/2 = 7.199 \quad \text{using } h_{\Theta'}$$

Ideally, the values of  $\widehat{\kappa}$  and  $\widehat{\beta}$  obtained through the use of  $h_{\Theta'}$  should be the same as that obtained when the posterior density is maximized using  $h_{\Theta}$  prior. Clearly, with MAP-based estimation, the end results are different for the two cases.

The modes of the posterior in the  $\kappa$ ,  $\beta$  and  $\kappa$ , e parameterizations are shown in Figure 3(a) and (b) respectively. It is expected that the modes of the posterior shift as per the parameter space. However, they should be invariant regardless of the transformation affecting the two parameter spaces. It is observed that the mode in  $\kappa$ , e space, when mapped back to the  $\kappa$ ,  $\beta$  space, results in a posterior density as shown in Figure 3(c). This is different from the posterior density shown in Figure 3(a), as the modes are at different locations. We emphasize that the invariance property of parameter estimates is central to inductive inference. The example considered here shows that MAP estimation of the parameters of a FB<sub>5</sub> distribution does not satisfy the invariance property, thus resulting in unreliable estimators.

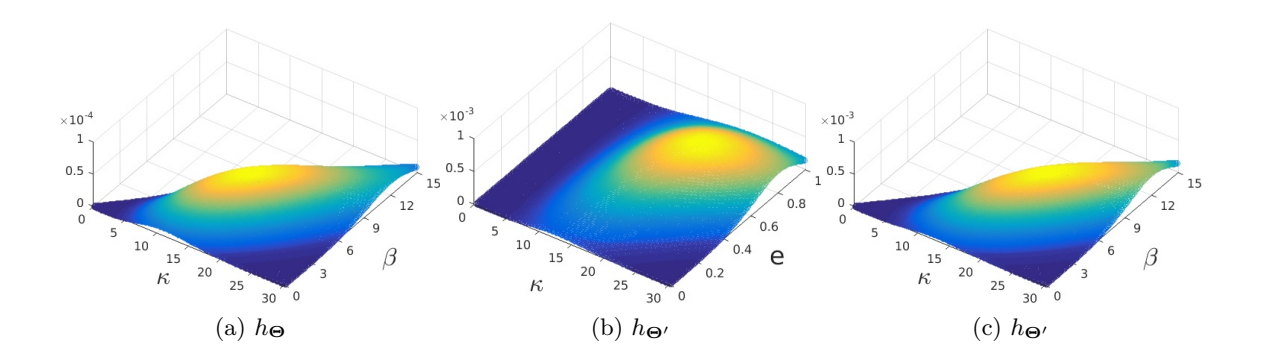


Figure 3: Heat maps depicting the modes (MAP estimate) of the posterior density as a function of  $\kappa$ ,  $\beta$  and  $\kappa$ , e parameterizations. The Z-axis denotes the posterior density value in the respective parameterization.

The aforementioned eccentricity transform is a straightforward transformation involving  $\beta$ . The remaining four parameters are left unchanged in this case. Another parameterization involving all five parameters of the FB<sub>5</sub> distribution is outlined in Appendix A.

# 6. MML-based estimation of the parameters of the FB<sub>5</sub> distribution

We now shift our focus to deriving the MML-based parameter estimates of a FB<sub>5</sub> distribution which is among the main contributions of this work. As explained in Section 2, derivation of the MML estimates requires the formulation of the message length expression (Equation 4) for encoding some observed data using the FB<sub>5</sub> distribution. The formulation requires the use of a suitable prior density on the parameters (see Section 5.1). The prior for  $\kappa$  is taken as  $h(\kappa)$  (see Section 5.1), the prior of  $\kappa$  for the vMF distribution on the two-sphere (Dowe et al., 1996b). This results in the joint prior density  $h_{\Theta}(\psi, \alpha, \eta, \kappa, \beta)$  (Equation 11). The main bottleneck involved in the MML-based parameter estimation is, however, the evaluation of the Fisher information matrix. As shown later, its computation involves the first and second order moments corresponding to a FB<sub>5</sub> distribution. The details are presented here.

**Notations** Before we proceed with describing the approach based on MML inference, we define the following notations which are used subsequently. We require the use of partial derivatives of the normalization constant  $c(\kappa, \beta)$  given by Equation 3. The following are the adopted notations to represent them.

$$c(\kappa, \beta) = c, \quad c_{\kappa} = \partial c/\partial \kappa, \quad c_{\beta} = \partial c/\partial \beta$$
$$c_{\kappa\kappa} = \partial^{2} c/\partial \kappa^{2}, \quad c_{\beta\beta} = \partial^{2} c/\partial \beta^{2}, \quad c_{\kappa\beta} = \partial^{2} c/\partial \kappa \partial \beta$$

# 6.1 Derivation of the moments of a general FB5 distribution

Kent (1982) provided the moment expressions in the case of a FB<sub>5</sub> distribution whose mean, major and minor axes are aligned with the standard coordinate axes. In this setup,

consider a random vector  $\mathbf{y} \sim \mathrm{FB}_5(\mathbf{I}, \kappa, \beta)$ , where  $\mathbf{I}$  is the identity matrix. Then, Kent (1982) provided the following moments:

$$\mathbb{E}[\mathbf{y}] = \begin{pmatrix} c_{\kappa}/c & 0 & 0 \end{pmatrix}^{\mathsf{T}}, \text{ and}$$

$$\mathbb{E}[\mathbf{y}\mathbf{y}^{\mathsf{T}}] = \mathbf{\Lambda} = \begin{pmatrix} \lambda_1 & 0 & 0 \\ 0 & \lambda_2 & 0 \\ 0 & 0 & \lambda_3 \end{pmatrix}, \text{ where}$$

$$\lambda_1 = \frac{c_{\kappa}}{c}, \lambda_2 = \frac{c - c_{\kappa\kappa} + c_{\beta}}{2c}, \lambda_3 = \frac{c - c_{\kappa\kappa} - c_{\beta}}{2c}$$
(14)

We derive here the moments in the case of a general FB<sub>5</sub> distribution, that is, whose three mutually orthogonal axes can be oriented in any fashion. Let  $\mathbf{x} \sim \mathrm{FB}_5(\mathbf{Q}, \kappa, \beta)$ , a generic distribution whose axes are not aligned with the coordinate axes. Recall, from Section 3, that  $\mathbf{Q}$  is the rotation matrix that aligns the standard coordinate axes with the axes of a FB<sub>5</sub> distribution. Based on the parameterization of the FB<sub>5</sub> distribution, we can deduce that  $\forall \mathbf{x}, \exists \mathbf{y} \sim \mathrm{FB}_5(\mathbf{I}, \kappa, \beta)$  such that  $\mathbf{x} = \mathbf{Q}\mathbf{y}$ , and hence,  $\mathbf{x}\mathbf{x}^\mathsf{T} = \mathbf{Q}\mathbf{y}\mathbf{y}^\mathsf{T}\mathbf{Q}^\mathsf{T}$ . Using the results from Equation 14, we have

$$\mathbb{E}[\mathbf{x}] = \mathbf{Q} \,\mathbb{E}[\mathbf{y}] = \begin{pmatrix} \boldsymbol{\gamma}_1 & \boldsymbol{\gamma}_2 & \boldsymbol{\gamma}_3 \end{pmatrix} \begin{pmatrix} c_{\kappa}/c & 0 & 0 \end{pmatrix}^{\mathsf{T}} = c_{\kappa}/c \,\boldsymbol{\gamma}_1$$
and 
$$\mathbb{E}[\mathbf{x}\mathbf{x}^{\mathsf{T}}] = \mathbf{Q} \,\mathbb{E}[\mathbf{y}\mathbf{y}^{\mathsf{T}}] \,\mathbf{Q}^{\mathsf{T}} = \mathbf{Q}\boldsymbol{\Lambda}\mathbf{Q}^{\mathsf{T}}$$
(15)

### 6.2 Computation of the Fisher information

The computation of the determinant of the Fisher information matrix requires the evaluation of the second order partial derivatives of the negative log-likelihood function with respect to the parameters of the distribution. As per the density function (Equation 2), the negative log-likelihood of a datum  $\mathbf{x}$  is given by

$$\mathcal{L}(\mathbf{x}|\mathbf{\Theta}) = \log c(\kappa, \beta) - \kappa \boldsymbol{\gamma}_1^\mathsf{T} \mathbf{x} - \beta \boldsymbol{\gamma}_2^\mathsf{T} \mathbf{x} \mathbf{x}^\mathsf{T} \boldsymbol{\gamma}_2 + \beta \boldsymbol{\gamma}_3^\mathsf{T} \mathbf{x} \mathbf{x}^\mathsf{T} \boldsymbol{\gamma}_3$$
 (16)

For the FB<sub>5</sub> distribution, the 5-parameter vector  $\mathbf{\Theta} = \{\psi, \alpha, \eta, \kappa, \beta\}$ . Let  $\mathcal{F}_1(\mathbf{\Theta})$  denote the Fisher information for a *single* observation. The Fisher information matrix  $\mathcal{F}_1(\mathbf{\Theta})$  associated with the parameters of a FB<sub>5</sub> distribution is a 5 × 5 *symmetric* matrix whose  $(i, j)^{\text{th}}$  element corresponding to parameters  $\theta_i$ ,  $\theta_j \in \mathbf{\Theta}$  is  $\mathcal{F}_{\theta_i \theta_j} = \mathbb{E}\left[\frac{\partial^2 \mathcal{L}}{\partial \theta_i \partial \theta_j}\right]$ . Further, as explained later, the determinant  $|\mathcal{F}_1(\mathbf{\Theta})|$  is decomposed as a product of  $|\mathcal{F}_A|$  and  $|\mathcal{F}_S|$ , where  $\mathcal{F}_A$  is the Fisher matrix associated with the angular parameters  $\psi, \alpha, \eta$ , and  $\mathcal{F}_S$  is the Fisher matrix associated with the scale parameters  $\kappa, \beta$ .

### 6.2.1 Fisher matrix $(\mathcal{F}_A)$ associated with $\psi, \alpha, \eta$

 $\mathcal{F}_A$  is a  $3 \times 3$  symmetric matrix whose elements are the expected values of the second order partial derivatives of  $\mathcal{L}$  with respect to  $\theta_i, \theta_i \in \{\psi, \alpha, \eta\}$ . Let the *expectation* be given as

$$\mathbb{E}\left[\frac{\partial^2 \mathcal{L}}{\partial \theta_i \partial \theta_i}\right] = -\kappa T(\gamma_1) - \beta T(\gamma_2) + \beta T(\gamma_3)$$
(17)

where the individual terms  $T(\gamma_m)$ ,  $m \in \{1, 2, 3\}$  are comprised of the expectations of the corresponding partial differentials of  $\gamma_m$ . They are computed using the following identities:

$$T(\boldsymbol{\gamma}_{1}) = \mathbb{E}\left[\frac{\partial^{2}(\boldsymbol{\gamma}_{1}^{\mathsf{T}}\mathbf{x})}{\partial\theta_{i}\partial\theta_{j}}\right] = \mathbb{E}\left[\mathbf{x}\right]^{\mathsf{T}} \frac{\partial^{2}\boldsymbol{\gamma}_{1}}{\partial\theta_{i}\partial\theta_{j}}, \text{ and}$$

$$T(\boldsymbol{\gamma}_{m}) = \mathbb{E}\left[\frac{\partial^{2}(\boldsymbol{\gamma}_{m}^{\mathsf{T}}\mathbf{x}\mathbf{x}^{\mathsf{T}}\boldsymbol{\gamma}_{m})}{\partial\theta_{i}\partial\theta_{j}}\right] \quad \text{(for } m = 2, 3)$$

$$= 2\left(\boldsymbol{\gamma}_{m}^{\mathsf{T}}\mathbb{E}\left[\mathbf{x}\mathbf{x}^{\mathsf{T}}\right] \frac{\partial^{2}\boldsymbol{\gamma}_{m}}{\partial\theta_{i}\partial\theta_{j}} + \left(\frac{\partial\boldsymbol{\gamma}_{m}}{\partial\theta_{i}}\right)^{\mathsf{T}}\mathbb{E}\left[\mathbf{x}\mathbf{x}^{\mathsf{T}}\right] \left(\frac{\partial\boldsymbol{\gamma}_{m}}{\partial\theta_{j}}\right)\right)$$

$$(18)$$

The terms  $T(\gamma_m)$  depend on the expressions for the constituent first and second order partial differentials of  $\gamma_m$ , which we provide in Appendix B. Using Equations 15, 17 and 18, the elements of the Fisher information matrix  $\mathcal{F}_A$  are derived as follows:

$$\mathcal{F}_{\psi\psi} = 4 \beta c_{\beta}/c; \quad \mathcal{F}_{\alpha\psi} = 0; \quad \mathcal{F}_{\eta\psi} = (\cos \alpha) 4 \beta c_{\beta}/c$$

$$\mathcal{F}_{\alpha\alpha} = \kappa c_{\kappa}/c + 2\beta \left\{ (\lambda_1 - \lambda_3) \sin^2 \psi - (\lambda_1 - \lambda_2) \cos^2 \psi \right\}$$

$$\mathcal{F}_{\eta\alpha} = \beta (1 - 3\lambda_1) \sin 2\psi \sin \alpha$$

$$\mathcal{F}_{\eta\eta} = (\sin^2 \alpha) \kappa c_{\kappa}/c$$

$$+2\beta \left\{ \begin{array}{l} \lambda_2 (\cos^2 \psi \cos^2 \alpha + \sin^2 \psi) + (\lambda_2 - \lambda_3) \cos^2 \alpha \\ -\lambda_3 (\sin^2 \psi \cos^2 \alpha + \cos^2 \psi) + \lambda_1 \sin^2 \alpha \cos 2\psi \end{array} \right\}$$
(19)

# 6.2.2 Fisher matrix $(\mathcal{F}_S)$ associated with $\kappa, \beta$

 $\mathcal{F}_S$  is a 2 × 2 symmetric matrix whose elements are the *expectations* of the second order partial derivatives of  $\mathcal{L}$  with respect to  $\kappa$  and  $\beta$ . From Equation 16, we have

$$\frac{\partial \mathcal{L}}{\partial \kappa} = \frac{c_{\kappa}}{c} - \boldsymbol{\gamma}_{1}^{\mathsf{T}} \mathbf{x} \quad \text{and} \quad \frac{\partial \mathcal{L}}{\partial \beta} = \frac{c_{\beta}}{c} - \boldsymbol{\gamma}_{2}^{\mathsf{T}} \mathbf{x} \mathbf{x}^{\mathsf{T}} \boldsymbol{\gamma}_{2} + \boldsymbol{\gamma}_{3}^{\mathsf{T}} \mathbf{x} \mathbf{x}^{\mathsf{T}} \boldsymbol{\gamma}_{3}$$

$$\frac{\partial^{2} \mathcal{L}}{\partial \kappa^{2}} = \frac{c c_{\kappa \kappa} - c_{\kappa}^{2}}{c^{2}} = \mathcal{F}_{\kappa \kappa}$$

$$\frac{\partial^{2} \mathcal{L}}{\partial \beta^{2}} = \frac{c c_{\beta \beta} - c_{\beta}^{2}}{c^{2}} = \mathcal{F}_{\beta \beta}, \quad \text{and}$$

$$\frac{\partial^{2} \mathcal{L}}{\partial \kappa \partial \beta} = \frac{c c_{\kappa \beta} - c_{\kappa} c_{\beta}}{c^{2}} = \mathcal{F}_{\kappa \beta}$$
(20)

### 6.2.3 Fisher matrix $\mathcal{F}(\mathbf{\Theta})$ associated with the 5-parameter vector $\mathbf{\Theta}$

It is to be noted that for  $\theta_i \in \{\kappa, \beta\}$  and  $\theta_j \in \{\psi, \alpha, \eta\}$ ,  $T(\gamma_m) = 0$  as  $\frac{\partial \gamma_m}{\partial \theta_i} = 0$  ( $\gamma_m$  given by Equation 5 are independent of  $\kappa, \beta$ ). Consequently,  $\mathcal{F}_{\theta_i \theta_j} = 0$ . This allows for the

computation of  $|\mathcal{F}_1(\mathbf{\Theta})|$  as the product of  $|\mathcal{F}_A|$  and  $|\mathcal{F}_S|$ . Thus,

$$|\mathcal{F}_{1}(\mathbf{\Theta})| = \begin{vmatrix} \mathcal{F}_{\psi\psi} & \mathcal{F}_{\psi\alpha} & \mathcal{F}_{\psi\eta} & 0 & 0 \\ \mathcal{F}_{\alpha\psi} & \mathcal{F}_{\alpha\alpha} & \mathcal{F}_{\alpha\eta} & 0 & 0 \\ \mathcal{F}_{\eta\psi} & \mathcal{F}_{\eta\alpha} & \mathcal{F}_{\eta\eta} & 0 & 0 \\ 0 & 0 & 0 & \mathcal{F}_{\kappa\kappa} & \mathcal{F}_{\kappa\beta} \\ 0 & 0 & 0 & \mathcal{F}_{\beta\kappa} & \mathcal{F}_{\beta\beta} \end{vmatrix} = |\mathcal{F}_{A}||\mathcal{F}_{S}|$$

Then, the Fisher information for some observed data  $\mathcal{D} = \{\mathbf{x}_1, \dots, \mathbf{x}_N\}$  is given by  $|\mathcal{F}(\mathbf{\Theta})| = N^5 |\mathcal{F}_1(\mathbf{\Theta})|$  (as each element in  $|\mathcal{F}_1(\mathbf{\Theta})|$  is multiplied by the sample size N).

### 6.3 Message length formulation

The message length to encode some observed data  $\mathcal{D}$  can now be formulated by substituting the prior density  $h_{\Theta}$  (Equation 11), the Fisher information  $|\mathcal{F}(\Theta)|$  and the negative log-likelihood of the data (Equation 10) in the message length expression (Equation 4). The MML parameter estimates are the ones that minimize the entire message length. As there is no analytical form of the MML estimates, the solution is obtained, as for the maximum likelihood and MAP case, by using the NLopt<sup>2</sup> optimization library (Johnson). At each stage of the optimization routine, the Fisher information needs to be calculated. However, this involves the computation of complex entities such as the normalization constant  $c(\kappa, \beta)$  and its partial derivatives. The computation of these intricate mathematical forms using numerical methods is discussed in Section 7.

# 7. Computation of the normalization constant and the associated derivatives

The computation of the negative log-likelihood function and the message length is hindered because of the presence of the normalization constant and its associated derivatives. Kent (1982) provided an asymptotic formula for  $c(\kappa, \beta)$  as  $2\pi \exp(\kappa)[(\kappa^2 - 4\beta^2)]^{-1/2}$ . However, this approximation is valid for large  $\kappa$  and when  $2\beta/\kappa$  is sufficiently small. In this section, we describe the methods that can be employed to efficiently compute these complex functions without making any assumptions.

# 7.1 Computing $\log c(\kappa,\beta)$ and the logarithm of the derivatives: $c_{\kappa} = \partial c/\partial \kappa$ and $c_{\kappa\kappa} = \partial^2 c/\partial \kappa^2$

The expressions of  $c, c_{\kappa}, c_{\kappa\kappa}$  are related. to each other. These are explained by defining the quantity  $S_1^{(m)}$ , a logarithm sum where  $m \in \{0, 1, 2\}$ ,  $p = 2j + \frac{1}{2}$ ,  $\delta_1 = 2\pi\sqrt{\frac{2}{\kappa}}$ , and  $e = \frac{2\beta}{\kappa} < 1$  (by definition).

$$S_1^{(m)} = \log \delta_1 + \log \sum_{j=0}^{\infty} \frac{\Gamma(j + \frac{1}{2})}{\Gamma(j+1)} e^{2j} I_{p+m}(\kappa)$$
(21)

<sup>2.</sup> http://ab-initio.mit.edu/nlopt

Computation of the series  $S_1^{(m)}$ : We first establish that  $f_{j+1} < f_j \, \forall j \geq 0$  and show that  $S_1^{(m)}$  converges to a finite sum as  $j \to \infty$ . Consider the logarithm of the ratio of consecutive terms  $f_j$  and  $f_{j+1}$  in  $S_1^{(m)}$ .

$$\log \frac{f_{j+1}}{f_j} = \log \frac{j + \frac{1}{2}}{j+1} + 2\log e + \log \frac{I_{p+m+2}(\kappa)}{I_{p+m}(\kappa)}$$
 (22)

For p, v > 0,  $I_{p+v} < I_p$ , and the ratio  $\frac{I_{p+v}}{I_p} \to 0$  for large v (Amos, 1974). Further, e < 1 implies the above equation is the sum of negative terms. Hence,  $\log \frac{f_{j+1}}{f_j} < 0$ , which means  $f_{j+1} < f_j$ . Also,

$$\lim_{j \to \infty} \log \frac{f_{j+1}}{f_j} = 0 + 2\log e + \lim_{j \to \infty} \log \frac{I_{2j + \frac{1}{2} + 2}(\kappa)}{I_{2j + \frac{1}{2}}(\kappa)} = -\infty$$

Hence, as  $\lim_{j\to\infty} \frac{f_{j+1}}{f_j} = 0$ ,  $S_1^{(m)}$  is a convergent series.

For practical implementation of the sum, we express  $S_1^{(m)}$  as the modified summation,

$$S_1^{(m)} = \log \delta_1 + \log f_0 + \log \sum_{j=0}^{\infty} t_j$$
 (23)

where each  $f_j$  is divided by the maximum term  $f_0$ . For each j > 0,  $\log f_j$  is calculated using the previous term  $\log f_{j-1}$  (Equation 22). The new term  $t_j = f_j/f_0$  is then computed<sup>3</sup> as  $\exp(\log f_j - \log f_0)$  (computing the difference with the maximum value and then taking the exponent ensures numerical stability). The summation is terminated when the ratio  $\frac{t_j}{\sum_{k=1}^j t_k} < \epsilon \text{ (a small threshold } \sim 10^{-6}\text{)}.$ 

- Let  $S(c) = \log c(\kappa, \beta)$ : Substituting m = 0 in Equation 21 gives the logarithm of the normalization constant (given in Equation 3). Hence,  $S(c) = S_1^{(0)}$ .
- Let the  $j^{th}$  term dependent on  $\kappa$  in Equation 3 be represented as  $g_j(\kappa) = I_p/\kappa^p$ , where  $I_p$  implicitly refers to  $I_p(\kappa)$ . We use the relationship between the Bessel functions  $I_p, I_{p-1}$ , and the derivative  $I'_p$  in Equation 24 (Abramowitz and Stegun, 1965), to derive the expressions for the first and second derivatives of  $g_j(\kappa)$  (Equation 25).

$$\kappa I_p' = \kappa I_{p-1} - pI_p \tag{24}$$

$$g'_j(\kappa) = \frac{I_{p+1}}{\kappa^p}$$
 and  $g''_j(\kappa) = \frac{I_{p+2}}{\kappa^p} + \frac{1}{\kappa} \cdot \frac{I_{p+1}}{\kappa^p}$  (25)

Let  $S(c_{\kappa}) = \log c_{\kappa}$ : Because of the similar forms of  $g_j(\kappa)$  and  $g'_j(\kappa)$ , the expression for  $S(c_{\kappa})$  will be similar to S(c) with a change in *order* of the Bessel functions from m = 0 in Equation 21 to m = 1. Hence,  $S(c_{\kappa}) = S_1^{(1)}$  and an expression akin to Equation 23 can be derived for  $S(c_{\kappa})$ .

<sup>3.</sup> Because of the nature of Bessel functions,  $\log f_j$  can get very large and can result in overflow when calculating the exponent  $\exp(\log f_j)$ . However, dividing by  $f_0$  results in  $f_j/f_0 < 1$ .

• Let  $S(c_{\kappa\kappa}) = \log c_{\kappa\kappa}$ : Substituting m=2 in Equation 21 gives the logarithm sum  $S_1^{(2)}$  corresponding to the series with terms  $\frac{I_{p+2}}{\kappa^p}$ . Based on the nature of  $g_j''(\kappa)$  (Equation 25), and noting that  $S(c_{\kappa}) > S_1^{(2)}$  (as  $I_{p+1} > I_{p+2} \, \forall \, p \geq 0$ ), we can formulate  $S(c_{\kappa\kappa})$  as given below.

$$S(c_{\kappa\kappa}) = S(c_{\kappa}) + \log\left(\exp(S_1^{(2)} - S(c_{\kappa})) + \frac{1}{\kappa}\right)$$

# 7.2 The logarithm of the derivatives: $c_{\beta} = \partial c/\partial \beta$ , $c_{\kappa\beta} = \partial^2 c/\partial \kappa \partial \beta$ , and $c_{\beta\beta} = \partial^2 c/\partial \beta^2$

The expressions of  $c_{\beta}$  and  $c_{\kappa\beta}$  are related and are explained using the logarithm sum  $S_2^{(n)}$  where  $n \in \{0,1\}$ ,  $\delta_2 = \frac{4\pi}{\beta} \sqrt{\frac{2}{\kappa}}$ ,  $p = 2j + \frac{1}{2}$ , and  $e = \frac{2\beta}{\kappa}$ .

$$S_2^{(n)} = \log \delta_2 + \log \sum_{j=1}^{\infty} \underbrace{\frac{\Gamma(j + \frac{1}{2})}{\Gamma(j)}} e^{2j} I_{p+n}(\kappa)$$

$$(26)$$

We note that  $S_2^{(n)}$  is a convergent series (proof is based on the same reasoning as in Section 7.1).

Let the  $j^{th}$  term dependent on  $\beta, \kappa$  in Equation 3 be represented as  $g_j(\beta, \kappa) = \beta^{2j} \frac{I_p}{\kappa^p}$ . Its partial derivatives are given below. These derivatives are the terms in the series  $S_2^{(n)}$  (after factoring out the common elements as  $\delta_2$ ).

$$\frac{\partial g_j}{\partial \beta} = 2j\beta^{2j-1} \frac{I_p}{\kappa^p}$$
 and  $\frac{\partial^2 g_j}{\partial \kappa \partial \beta} = 2j\beta^{2j-1} \frac{I_{p+1}}{\kappa^p}$ 

- Let  $S(c_{\beta}) = \log c_{\beta}$ : this is obtained by substituting n = 0 in Equation 26. Hence,  $S(c_{\beta}) = S_2^{(0)}$ .
- Similarly,  $S(c_{\kappa\beta}) = \log c_{\kappa\beta} = S_2^{(1)}$ .
- The expression to compute  $S(c_{\beta\beta}) = \log c_{\beta\beta}$  is given by

$$S(c_{\beta\beta}) = \log\left(\frac{\delta_2}{\beta}\right) + \log\sum_{j=1}^{\infty} \underbrace{\frac{\Gamma(j + \frac{1}{2})}{\Gamma(j)}(2j - 1)e^{2j}I_p(\kappa)}_{f_j}$$

The practical implementation of  $S_2^{(n)}$  and  $S(c_{\beta\beta})$  is similar to that of  $S_1^{(m)}$  given by Equation 23. However, in these cases, the expressions of  $f_j$  and consequently  $t_j$ , are modified accordingly. Also, the series begin from j=1, and hence, the maximum terms will correspond to  $f_1$ .

# 8. Mixture modelling of FB<sub>5</sub> distributions

In this section, we provide an overview of the mixture modelling apparatus in the context of modelling directional data using  $FB_5$  distributions. The probability distribution of a mixture  $\mathcal{M}$  is of the form:

$$f(\mathbf{x}; \mathbf{\Phi}) = \sum_{j=1}^{K} w_j f_j(\mathbf{x}; \mathbf{\Theta}_j)$$

where K is the number of component FB<sub>5</sub> distributions,  $w_j \geq 0$  is the component weight such that  $\sum_{j=1}^{K} w_j = 1$ , and  $\Theta_j$  denotes the 5-parameter vector of the  $j^{\text{th}}$  FB<sub>5</sub> distribution. The parameters of the mixture are collectively given by  $\mathbf{\Phi} = \{w_1, \dots, w_K, \mathbf{\Theta}_1, \dots, \mathbf{\Theta}_K\}$ .

# 8.1 Estimating the mixture parameters

For a mixture with K number of components, the traditional method of estimating the mixture parameters is done by minimizing the negative log-likelihood function of the data given by

$$\mathcal{L}(\mathcal{D}|\mathbf{\Phi}) = -\sum_{i=1}^{N} \log \sum_{j=1}^{K} w_j f_j(\mathbf{x}_i; \mathbf{\Theta}_j)$$
(27)

where  $\mathcal{D} = \{\mathbf{x}_1, \dots, \mathbf{x}_N\}$  is the observed data of size N. The maximum likelihood estimation procedure, in this case, involves an *expectation-maximization* (EM) algorithm (Dempster et al., 1977; Krishnan and McLachlan, 1997) which is decomposed into the following steps:

• Expectation (E-step): The membership of each datum  $\mathbf{x}_i \in \mathcal{D}$  in a mixture component  $j \in \{1, K\}$  is updated as:

$$r_{ij} = \frac{w_j f(\mathbf{x}_i; \mathbf{\Theta}_j)}{\sum_{k=1}^{K} w_k f(\mathbf{x}_i; \mathbf{\Theta}_k)}, \quad \text{and} \quad n_j = \sum_{i=1}^{N} r_{ij}$$

where the table of memberships  $r_{ij}$  is termed the responsibility matrix and  $n_j$  is the effective membership of the  $j^{\text{th}}$  component.

• Maximization (M-step): The parameters of each component are updated by their respective maximum likelihood estimates. These are obtained by minimizing  $\mathcal{L}(\mathcal{D}|\Phi)$ . Differentiating Equation 27 with respect to  $\Theta_i$  leads to the following modified form

$$\mathcal{L}(\mathcal{D}|\mathbf{\Theta}_{j}) = n_{j} \log c(\kappa_{j}, \beta_{j}) - \kappa_{j} \boldsymbol{\gamma}_{1j}^{\mathsf{T}} \sum_{i=1}^{N} r_{ij} \mathbf{x}_{i}$$
$$- \beta_{j} \boldsymbol{\gamma}_{2j}^{\mathsf{T}} \left( \sum_{i=1}^{N} r_{ij} \mathbf{x}_{i} \mathbf{x}_{i}^{\mathsf{T}} \right) \boldsymbol{\gamma}_{2j} + \beta_{j} \boldsymbol{\gamma}_{3j}^{\mathsf{T}} \left( \sum_{i=1}^{N} r_{ij} \mathbf{x}_{i} \mathbf{x}_{i}^{\mathsf{T}} \right) \boldsymbol{\gamma}_{3j}$$
(28)

where  $\Theta_j = \{\psi_j, \alpha_j, \eta_j, \kappa_j, \beta_j\}$  and  $\gamma_{1j}, \gamma_{2j}, \gamma_{3j}$  are functions of  $\psi_j, \alpha_j, \eta_j$  (Equation 5). The above equation resembles the negative log-likelihood function due to a single FB<sub>5</sub> component (Equation 10) after accounting for the partial memberships of data within that component. Minimizing Equation 28 yields the maximum likelihood estimate of  $\Theta_j$ . The component weights are updated as  $w_j = n_j/N$ .

### 8.2 Estimating the mixture parameters using the MML framework

The seminal work on minimum message length inference of mixture models was carried out by Wallace and Boulton (1968). As per the MML framework (Section 2), the estimation of parameters of a mixture distribution requires the encoding of the parameters and the data given those parameters. The resultant total message length expression needs to be minimized to obtain the MML estimates. The formulation of a mixture modelling problem using MML framework can be decomposed into:

- 1. First part: encoding the mixture parameters  $\mathbf{\Phi}$ , namely, number of components K, mixture weights  $\mathbf{w} = \{w_1, \dots, w_K\}$ , and the component parameters  $\mathbf{\Theta}_i$ .
- 2. Second part: encoding the data  $\mathcal{D}$  given the parameters  $\Phi$ .

The schemes for encoding K and  $\mathbf{w}$  are generic (Wallace, 2005) and are summarized in Kasarapu and Allison (2015). However, encoding the component parameters requires the evaluation of the corresponding Fisher information. Using the appropriate encoding schemes, the general form of the total message length expression provided by Wallace and Freeman (1987) is:

$$I(\mathbf{\Phi}, \mathcal{D}) = I(K) + I(\mathbf{w}) + \sum_{j=1}^{K} I(\mathbf{\Theta}_j) + \underbrace{\mathcal{L}(\mathcal{D}|\mathbf{\Phi}) + \text{constant}}_{\text{second part}: I(\mathcal{D}|\mathbf{\Phi})}$$
(29)

where I(K) and  $I(\mathbf{w})$  are the message lengths to encode K and  $\mathbf{w}$  respectively. The cumulative Fisher information of mixtures for the components' parameters is given by the

summation 
$$\sum_{j=1}^{K} I(\Theta_j)$$
, where  $I(\Theta_j) = -\log \frac{h(\Theta_j)}{\sqrt{|\mathcal{F}(\Theta_j)|}}$  is the message length to encode the

parameters of the  $j^{\text{th}}$  component (Section 2.2). The second part of the message  $I(\mathcal{D}|\Phi)$  is a measure of the goodness of fit to the data and corresponds to the negative log-likelihood (Equation 27).

To obtain the MML estimates, an EM algorithm is employed to minimize the two-part message length  $I(\Phi, \mathcal{D})$ . In the E-step, the memberships of the data are updated, while in the M-step, the component parameters are updated using their respective MML estimates (Section 6.3). The EM algorithm is continued until there is no change in message length, that is, when the algorithm converges to a local minimum.

### 8.3 Determining the optimal number of mixture components

The parameters of a mixture can be estimated once the number of mixture components are known. A mixture modelling problem also needs to address the issue of selection of optimal number of components. The EM algorithms that are used in the estimation of mixture parameters are carried out with a fixed number of components. As the number of mixture components K increases, the negative log-likelihood (Equation 27) decreases and consequently results in an improvement to the quality of fit to the data. However, increasing K results in the mixtures becoming overly complex. Thus, a reliable tradeoff in terms of

balancing the model complexity and the quality of fit should be achieved. There are two aspects concerning the determination of suitable number of mixture components:

- 1. a scoring function to evaluate a given mixture
- 2. a search strategy to infer such a mixture

Scoring function: There have been numerous scoring functions proposed in the literature that aim to evaluate a given mixture model. A review of these methods is presented in McLachlan and Peel (2000). The common motivation is to balance the model complexity and the quality of fit. The scoring functions which quantify the model complexity based on the number of components are Akaike Information Criterion (AIC) (Akaike, 1974), Bayesian Information Criterion (BIC) (Schwarz, 1978; Rissanen, 1978), and Integrated Completed Likelihood (ICL) criterion (Biernacki et al., 2000). It is to be noted that AIC and BIC are shown to be approximations of the general MML framework (Figueiredo and Jain, 2002). The information-theoretic criteria that account for not just the number of components but also the components' parameters are ICOMP (Bozdogan, 1993), Laplace empirical criterion (LEC) (Roberts et al., 1998), and approximated MML criterion (Oliver et al., 1996; Figueiredo and Jain, 2002). Further, these criteria are derived using a MML interpretation. However, as detailed in Kasarapu and Allison (2015), these criteria are oversimplified versions of the generic MML framework and are incomplete in objectively addressing the tradeoff associated with selecting a suitable mixture model.

Search strategy: To determine the optimal number of mixture components using the aforementioned criteria (Akaike, 1974; Schwarz, 1978; Oliver et al., 1996; Roberts et al., 1998; Biernacki et al., 2000), mixtures are inferred for varying number of components using the EM algorithm, and the mixture that has the least score is treated as the optimal one. As the EM only guarantees convergence to a local optimum, a few trials are conducted with different starting points in an effort to minimize the possibility of getting trapped in a local optimum (Krishnan and McLachlan, 1997; McLachlan and Peel, 2000). In order to rectify the issues arising from the use of EM method which plays a central role in identifying the right mixture model, methods based on iteratively splitting and merging constituent mixture components have been proposed so as to enable the intermediate mixtures to escape from local optima. The notable amongst these are split-merge based EM (SMEM) method proposed by Ueda et al. (2000) and component-deletion based unsupervised learning approach proposed by Figueiredo and Jain (2002).

Given a mixture with K components, the SMEM method selects the top three candidates, merges two of them, and splits the other into two, thus, leaving the effective number of components unchanged. Further, the potential candidates are chosen depending on the improvement to the complete data log-likelihood function (used to formulate the ICL criterion). In contrast, the method of Figueiredo and Jain (2002) starts off by assuming a large number of components and iteratively eliminates those that are deemed redundant as per their objective function (a simplified MML-like formulation). Figueiredo and Jain (2002) demonstrated their competitive edge against the contemporary BIC (Schwarz, 1978), LEC (Roberts et al., 1998), and ICL criterion (Biernacki et al., 2000).

The SMEM algorithm does not facilitate an increase or decrease in the mixture size. In contrast, the method of Figueiredo and Jain (2002) progressively reduces the mixture size,

and hence, has no provision for recovering a component if it is deleted by chance. Also, the assumptions made in formulating their MML-like scoring function lack the rigor to objectively weigh the mixture model complexity against the quality of data fit, as explained in Kasarapu and Allison (2015). In order to address the limitations resulting from approximating the scoring functions and the search strategies, more recently, Kasarapu and Allison (2015) proposed a search heuristic in conjunction with a comprehensive MML formulation (with no approximations) to infer a suitable mixture model. This was demonstrated in the context of inference of mixtures of multivariate Gaussian and vMF distributions. In our previous work (Kasarapu and Allison, 2015), we have established that the proposed approach outperforms the widely used method of Figueiredo and Jain (2002).

### 8.4 The optimal number of components of a FB<sub>5</sub>-component mixture

We briefly review the search method of Kasarapu and Allison (2015) here that extended the MML-based Snob program (Wallace and Boulton, 1968; Wallace, 1986) for unsupervised learning. The method is adapted to the present scenario of mixture modelling of FB<sub>5</sub> distributions. The general idea is to perform a series of perturbations (split, delete, and merge operations) to a current sub-optimal mixture to obtain an improved mixture with a lower message length. The method begins by assuming a one-component mixture. The mixture is split into two children which are locally optimized. If the resultant mixture has a lower message length, the current mixture is updated. If, at any stage, a mixture has K components, each component is separately split into two, deleted, and merged with an appropriate component. The split operation results in a (K+1)-component mixture, while the delete and merge operations result in (K-1)-component mixtures. Each of the intermediate mixtures are optimized using an EM algorithm (Section 8.2). The perturbation corresponding to a component that results in the greatest reduction in message length is considered. This heuristic exhaustively considers all possible operations giving the K-component mixture the best chance to escape from a sub-optimal state. The method terminates when none of the perturbations result in improved mixtures. Each of these operations are explained below in the context of FB<sub>5</sub> distributions.

### 8.4.1 Splitting a component

The split operation is critical as it leads to mixtures with greater number of components. It is not desirable to have overly complex mixtures unless required. While splitting a (parent) component, the initial means of the two children should be reasonably apart so that they form distinct components and the K-component mixture has the best chance to move from a sub-optimal state to a more optimal state (if one exists). After the initial means are chosen, an EM is carried out just on the two child components until they are stabilized, leaving the remaining (K-1)-components unchanged. After optimizing the children, they are then integrated with the original K-1 components and an EM is subsequently performed on the K+1 components to reach an optimal state. If the new (K+1)-component mixture results in a lower total message length, that implies the perturbation of the K-component mixture resulted in an improved mixture.

Selection of initial means of the two child components: In the case of Gaussian distributions, Kasarapu and Allison (2015) chose the initial means such that they are one standard deviation away on either side of the component mean along the direction of maximum variance. In the present work, for directional distributions (vMF and FB<sub>5</sub>) defined on the three-dimensional spherical surface, we provide an analogous form. As described in Section 4.1, the procedure for moment estimation of the major and minor axes of a FB<sub>5</sub> distribution involves the eigenvalue decomposition of the matrix  $\mathbf{B}_L$ , the submatrix derived from the dispersion matrix  $\mathbf{B}$ . If  $l_1$  and  $l_2$  are the eigenvalues of  $\mathbf{B}_L$  (Equation 6), then  $l_1, l_2$  are roots of the characteristic equation:

$$l^2 - (b_{22} + b_{33})l + b_{22}b_{33} - b_{23}^2 = 0$$
 so that  $l_1 + l_2 = b_{22} + b_{33}$ 

According to Equation 8, we have  $l_1 - l_2 = r_2$ , and hence,  $l_1 = (b_{22} + b_{33} + r_2)/2$ . The maximum variance is along the direction of major axis and is equal to the eigenvalue  $l_1$ . Hence, one standard deviation would correspond to  $\sqrt{l_1}$ . It is to be noted that these calculations are done in the  $\mathbf{X}_2\mathbf{X}_3$  plane which contains the major and minor axes (that is, after the mean of the parent, as part of moment estimation, is aligned with  $\mathbf{X}_1$ ). However, it is now required to map this point back onto the *unit* sphere.

Consider Figure 4(a) where  $\gamma_2''$  and  $\gamma_3''$  are the major and minor axes in the  $\mathbf{X}_2\mathbf{X}_3$  plane respectively. The mean axis  $\gamma_1''$  of the parent component being split is aligned with  $\mathbf{X}_1$ . The segment OP is of length  $\sqrt{l_1}$  corresponding to unit standard deviation along  $\gamma_2''$ . Let  $M_1$  be the mean of one of the children. Then, for  $M_1$  such that  $M_1P$  is perpendicular to the  $\mathbf{X}_2\mathbf{X}_3$  plane, we have  $M_1P = \sqrt{1-l_1}$  (as  $OM_1 = 1$  is the radius of the sphere). If  $\theta \in [0, 180^\circ]$  measures the co-latitude of the mean  $M_1$  as shown, we have  $\theta = \arccos\sqrt{1-l_1}$ . The mean  $M_2$  (not shown in the figure) of the second child component lies in the plane containing  $OM_1P$  such that the angle between  $OM_2$  and  $OX_1$  is  $\theta$ . The two means are then transformed in order to conform with the axes of the parent FB<sub>5</sub> component. With these as starting points for the EM algorithm, the two child components are locally optimized. The children along with the untouched (K-1)-components serve as a starting point for estimating the parameters of the (K+1)-component mixture using the EM algorithm.

### 8.4.2 Deletion of a component

While deleting a component, its memberships are adjusted by proportionally distributing among the remaining K-1 components. With this new starting point, the parameters of the (K-1)-component mixture are estimated using an EM algorithm.

### 8.4.3 Merging two components

The choice of merging a pair of components is determined by their closeness. To identify the closest component, Kasarapu and Allison (2015) compute the Kullback-Leibler (KL) divergence (Kullback and Leibler, 1951) of the component in consideration with the remaining K-1 components in the mixture. The chosen pair is then merged to form a single component whose initial weight and memberships are given by the sum of the individual components' weights and memberships respectively. This acts as the starting point for the EM algorithm to estimate the parameters of the merged (K-1)-component mixture.

Kullback-Leibler divergence of  $FB_5$  distributions: The analytical form of the KL divergence between two  $FB_5$  distributions is derived below. The KL divergence between two probability distributions  $f_a$  and  $f_b$  is defined as

$$D_{KL}(f_a||f_b) = \mathbb{E}_a \left[ \log \frac{f_a(\mathbf{x})}{f_b(\mathbf{x})} \right]$$

where  $\mathbb{E}_a[.]$  is the expectation of the quantity [.] using  $f_a$ .

Let  $f_a(\mathbf{x}) = \mathrm{FB}_5(\kappa_a, \beta_a, \mathbf{Q}_a)$  and  $f_b(\mathbf{x}) = \mathrm{FB}_5(\kappa_b, \beta_b, \mathbf{Q}_b)$  be two distributions such that  $\mathbf{Q}_a = (\gamma_{a1}, \gamma_{a2}, \gamma_{a3})$  and  $\mathbf{Q}_b = (\gamma_{b1}, \gamma_{b2}, \gamma_{b3})$ . Let  $c_a$  and  $c_b$  be the respective normalization constants. Then,

$$\mathbb{E}_{a} \left[ \log \frac{f_{a}(\mathbf{x})}{f_{b}(\mathbf{x})} \right] = \log \frac{c_{b}}{c_{a}} + (\kappa_{a} \boldsymbol{\gamma}_{a1}^{\mathsf{T}} - \kappa_{b} \boldsymbol{\gamma}_{b1}^{\mathsf{T}}) \mathbb{E}_{a}[\mathbf{x}] 
+ \beta_{a} \boldsymbol{\gamma}_{a2}^{\mathsf{T}} \mathbb{E}_{a}[\mathbf{x}\mathbf{x}^{\mathsf{T}}] \boldsymbol{\gamma}_{a2} - \beta_{b} \boldsymbol{\gamma}_{b2}^{\mathsf{T}} \mathbb{E}_{a}[\mathbf{x}\mathbf{x}^{\mathsf{T}}] \boldsymbol{\gamma}_{b2} 
- \beta_{a} \boldsymbol{\gamma}_{a3}^{\mathsf{T}} \mathbb{E}_{a}[\mathbf{x}\mathbf{x}^{\mathsf{T}}] \boldsymbol{\gamma}_{a3} + \beta_{b} \boldsymbol{\gamma}_{b3}^{\mathsf{T}} \mathbb{E}_{a}[\mathbf{x}\mathbf{x}^{\mathsf{T}}] \boldsymbol{\gamma}_{b3}$$
(30)

gives the analytical form of the KL divergence of two FB<sub>5</sub> distributions. The expressions for  $\mathbb{E}_a[\mathbf{x}]$  and  $\mathbb{E}_a[\mathbf{x}\mathbf{x}^\mathsf{T}]$  are derived in Equation 15.

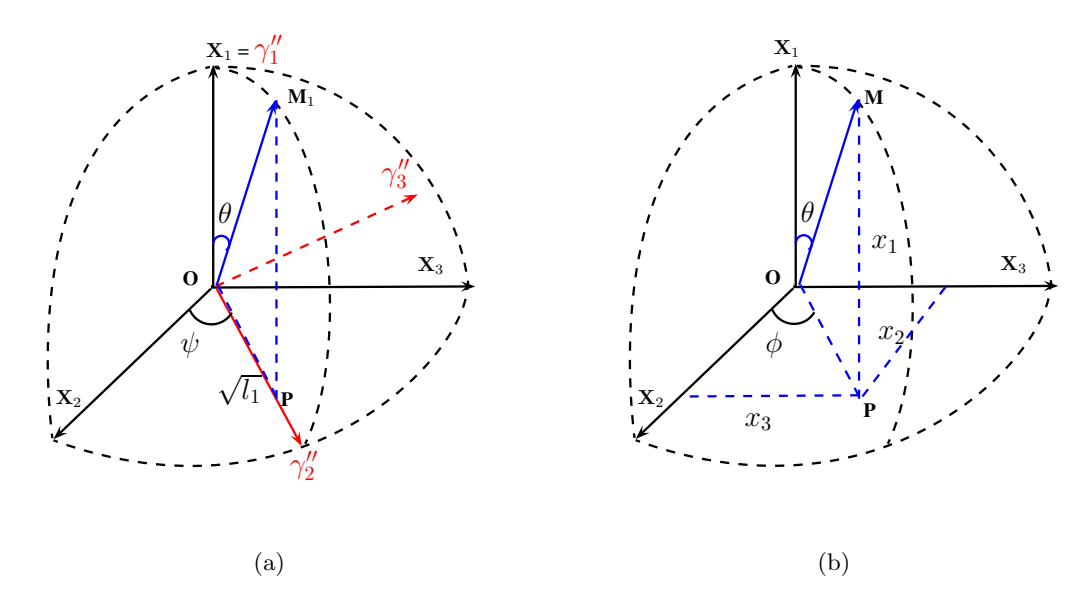


Figure 4: (a) Selection of initial means of children during splitting a parent component (see Section 8.4.1). (b) Transformation between spherical and Cartesian coordinates.

Through these perturbations, the search method aims to find an optimal state by leveraging information about the sub-optimal state. In doing so, we are cautiously splitting, deleting, or merging potential candidate components. The heuristic attempts to find improved mixtures without compromising the optimality of the intermediate solution.

### 8.5 An illustrative example of the search procedure

The mechanics of the inference of a suitable  $FB_5$  mixture model has been explained previously in Section 8.4. For further details of the search method, we refer the reader to Kasarapu and Allison (2015). To better illustrate the search process, this subsection presents a detailed example.

Consider a mixture with three FB<sub>5</sub> components (Figure 5) that have equal mixing proportions, the same concentration parameter  $\kappa=100$  and different eccentricities. The red component has eccentricity e=0.1 and the angular parameters defining its axes are  $(\psi, \alpha, \eta) = (0.60^{\circ}, 45^{\circ})$ . The green component has e=0.5 and  $(\psi, \alpha, \eta) = (150^{\circ}, 45^{\circ}, 30^{\circ})$ . The blue component has e=0.9 and  $(\psi, \alpha, \eta) = (30^{\circ}, 45^{\circ}, 60^{\circ})$ . The parameters are chosen such that the components are close to each other. A sample of size N=1000 was generated from the mixture using the method of Kent et al. (2013). The mixture density is shown as

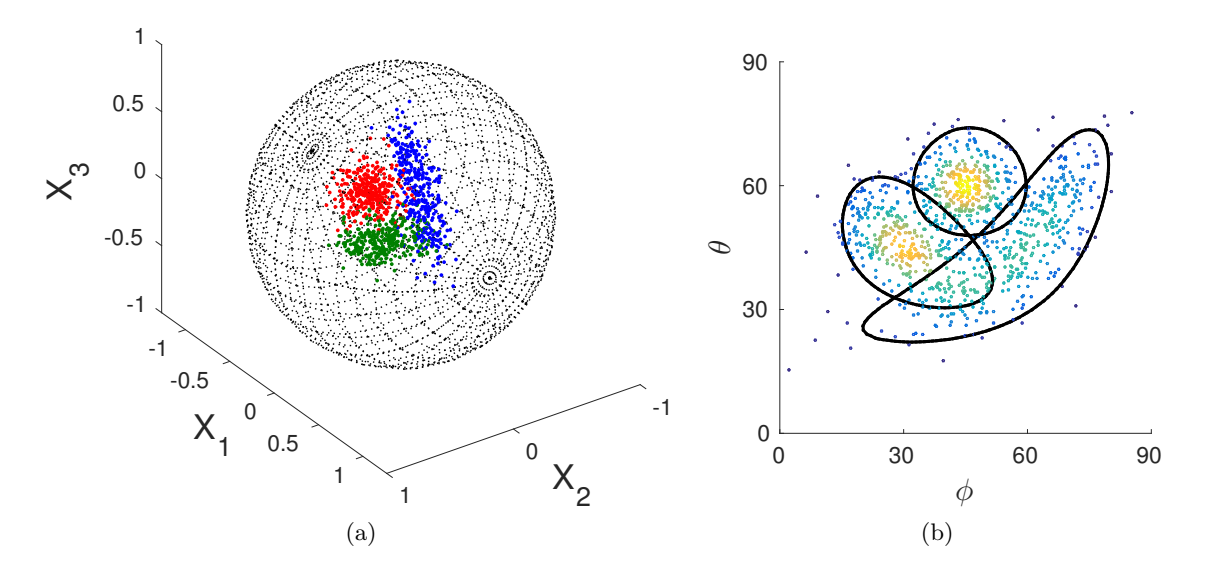


Figure 5: Original mixture consisting of three components with equal weights and  $\kappa=100$ . (a) individual components with varying eccentricities: e=0.1 (red), e=0.5 (green), and e=0.9 (blue) (b) simulated data plotted in degrees in the  $\theta\phi$  space (contours encompass 90% of the data),

a heat map in Figure 5(b). For ease of visualization, the density is represented in  $\theta\phi$  space, where  $\theta$  is the co-latitude and  $\phi$  is the longitude (Figure 4(b)). The Cartesian coordinates of each datum  $\mathbf{x}=(x_1,x_2,x_3)$  in the sampled data are transformed into the spherical coordinates defined by unit radius, co-latitude, and longitude. The transformation<sup>4</sup> is effected by:

$$x_1 = \cos \theta$$
,  $x_2 = \sin \theta \cos \phi$ ,  $x_3 = \sin \theta \sin \phi$ 

<sup>4.</sup> It is to be noted that transforming data generated from a FB<sub>5</sub> distribution (that has elliptical contours on the spherical surface) and representing in the  $\theta\phi$  space produces shapes that do not have any decipherable pattern as can be seen through this example.

### 8.5.1 The seach method explained

The search begins by inferring a one-component mixture  $\mathcal{M}_1$  (Figure 6a). It has an associated message length of I=19364 bits. Before splitting the component, the means of the children are initialized as shown in Figure 6(b). These means are determined as explained in Section 8.4.1. The children are optimized using the EM algorithm to generate the two-component mixture  $\mathcal{M}_2$  (Figure 6c).  $\mathcal{M}_2$  has a message length of I=19319 bits, and hence improves  $\mathcal{M}_1$  by 45 bits.

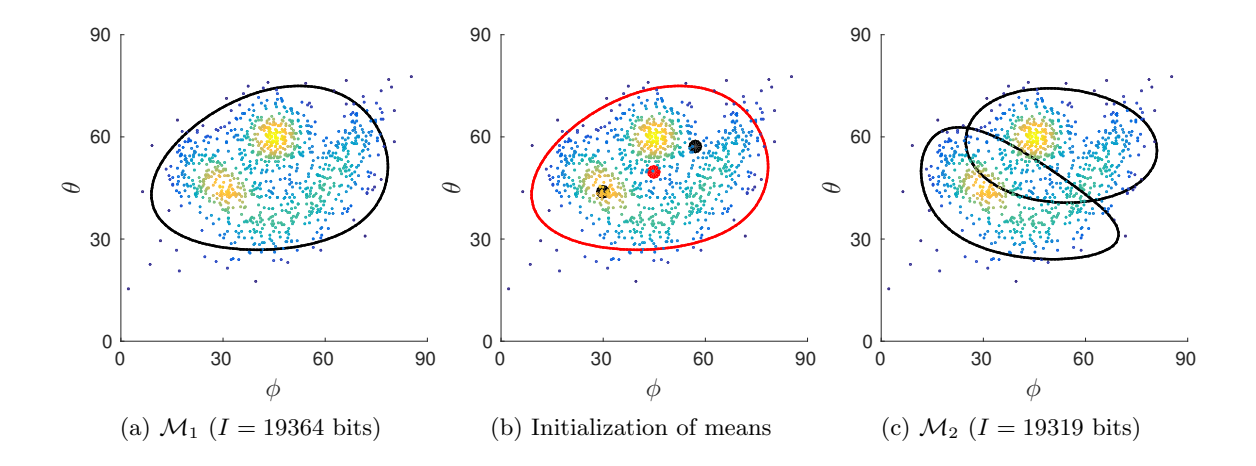


Figure 6: Iteration 1 (a) one-component mixture, (b) Red colour denotes the parent component being split, the red dot indicates the mean of the parent and the black dots (on either side) indicate the initial means of the children, (c) improved mixture.

In the second iteration, each of the two components in  $\mathcal{M}_2$  are split, deleted, and merged. Figure 7(a)-(c) illustrates the splitting of component  $P_1$ . After integrating the optimized children and subsequently optimizing the resulting 3-component mixture using an EM algorithm, an improved mixture  $\mathcal{M}_3$  is obtained. Figure 7(d)-(f) illustrates the splitting of component  $P_2$ . In this case, splitting  $P_2$  results in the same 3-component mixture  $\mathcal{M}_3$ . It is to be noted that while splitting  $P_1$  and  $P_2$  produce different intermediate states, as shown in Figure 7(b) and (e), the EM converges to the same optimal state in these cases. Figure 8(a)-(f) illustrate the deletion of  $P_1$  and  $P_2$ . While their deletions also have different intermediate starting points, as shown in Figure 8(b) and (e), the EM algorithm results in the same sub-optimal state (same as  $\mathcal{M}_1$ ). As this one-component mixture has a greater message length than that of  $\mathcal{M}_2$ , the deletion operations do not result in improved mixtures. The merging of  $P_1$  and  $P_2$  components, as shown in Figure 8(g)-(i), also does not improve on  $\mathcal{M}_2$ . Hence, after the second iteration, it is observed that amongst all perturbations, the splitting of  $P_1$  or  $P_2$  results in an improved mixture  $\mathcal{M}_3$ .

In the third iteration, all perturbations are carried out exhaustively. Figure 9 depicts the splitting, deletion, and merging of one of the three components  $(P_1)$  in  $\mathcal{M}_3$ . During splitting, observe the initial selection of means of the child components. The procedure outlined in Section 8.4.1 faithfully separates the two children and results in a mixture

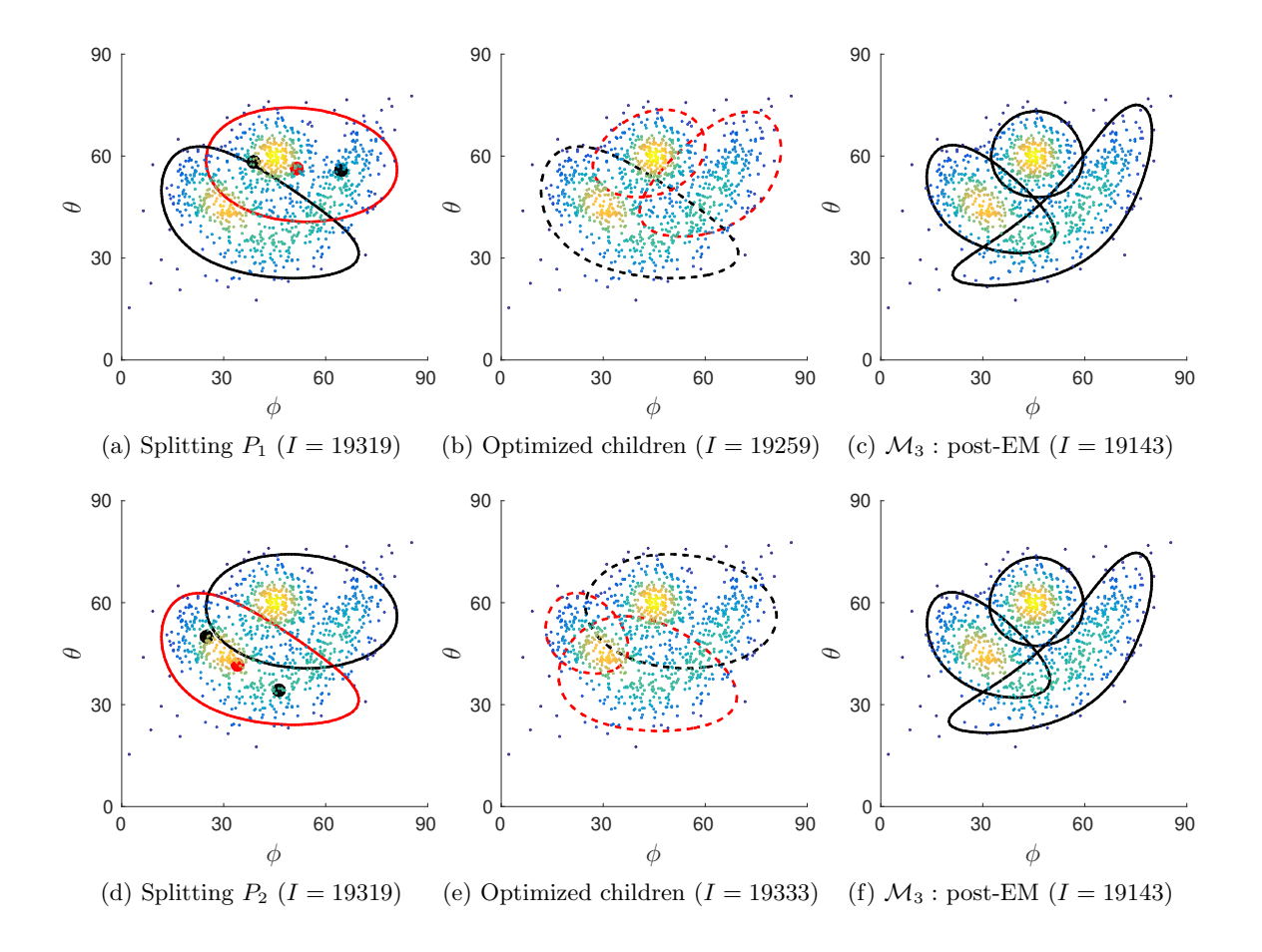


Figure 7: Iteration 2 – Split operations. (a)-(c) splitting the first component  $P_1$  in  $\mathcal{M}_2$ , and (d)-(f) splitting the second component  $P_2$  in  $\mathcal{M}_2$ . The red dashed lines in (b),(e) represent the optimized children (prior to integration), and black dashed lines in (b),(e) represent the unchanged components.

with a greater number of components. However, in this case, the optimized mixture  $\mathcal{M}_4$  (Figure 9c) does not improve the message length. Similarly, the deletion of  $P_1$  does not lead to an improved mixture (Figure 9f). While merging  $P_1$ , KL divergence is used to determine an appropriate candidate that is closest. Accordingly, the pair is selected (Figure 9g) which also does not result in an improved mixture (Figure 9i). The other two components in  $\mathcal{M}_3$  are also perturbed similarly. However, the operations do not result in an improvement (the series of steps and the resulting mixtures are included in Appendix C).

### 8.5.2 Variation of the two-part message length

Let us now explain the evolution of the mixture model in terms of the two-part message length (Equation 29). While increasing the number of mixture components leads to increased mixture complexity, the fit to the data improves. The first part of the message

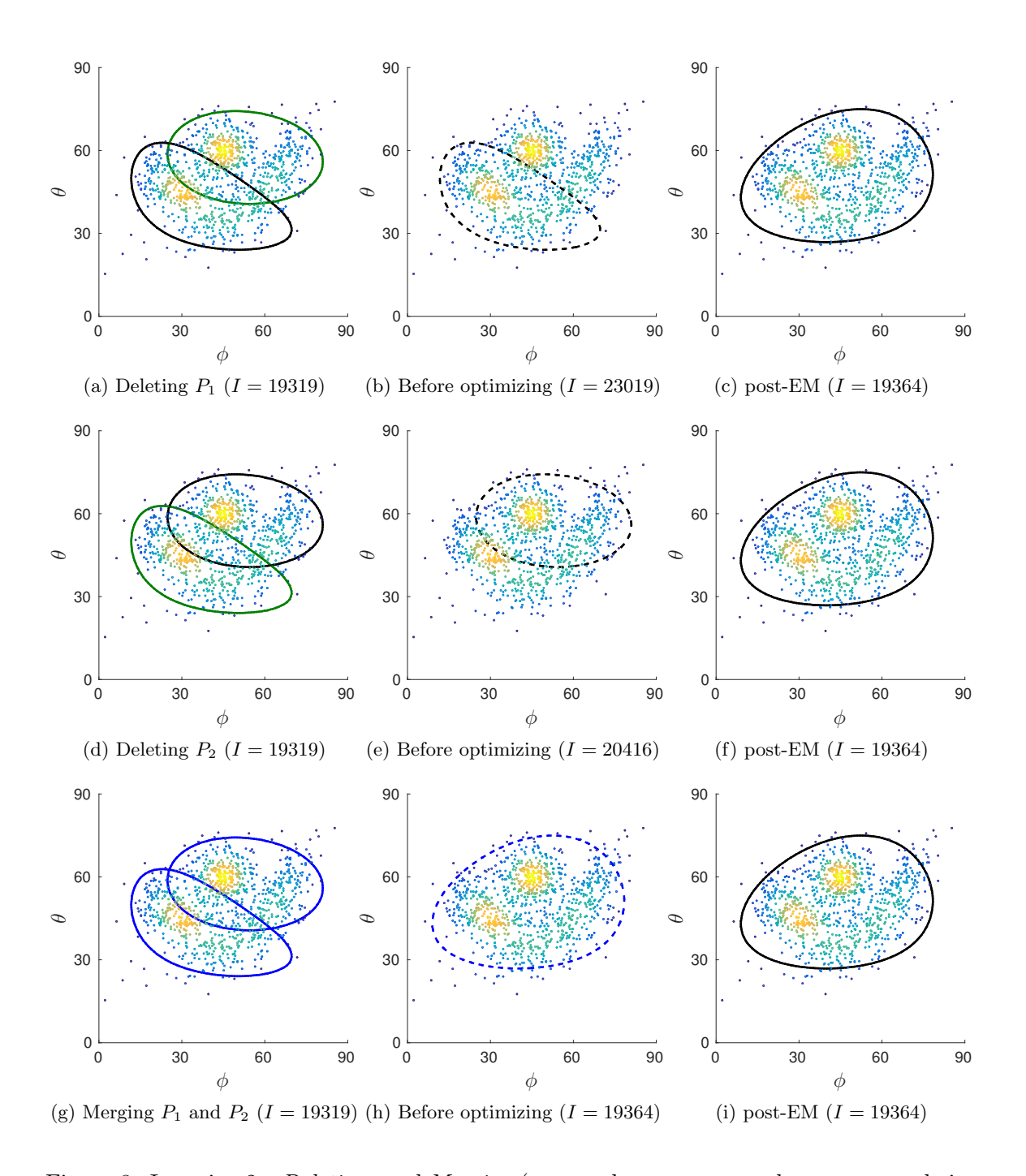


Figure 8: Iteration 2 - Deletions and Merging (green colour represents the component being deleted and blue denotes the pair being merged).

corresponds to the overhead related to encoding the mixture parameters (number of components, weights, and constituent components' parameters). The second part mainly cor-

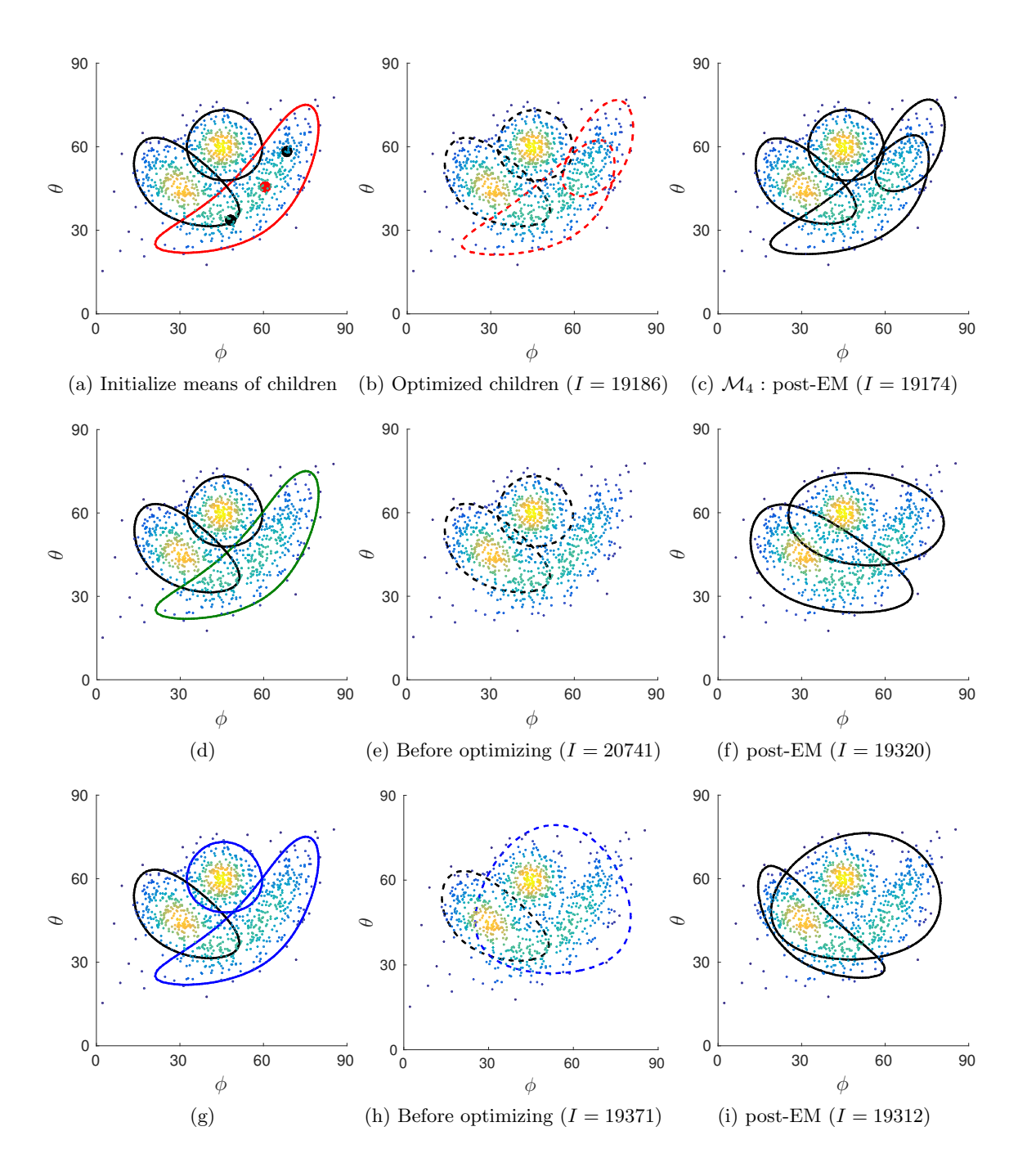


Figure 9: Iteration 3 – perturbations of  $P_1$  (a)-(c) splitting, (d)-(f) deletion, (g)-(i) merging

responds to the negative log-likelihood of the data using a given mixture model. In the previous example, the search method infers three components and terminates thereafter. The message lengths corresponding to the optimal mixtures during the associated search

process are plotted in Figure 10. It is observed that, until K=3, the total message length (green curve) decreases. We wanted to examine the variation of the message length beyond the inferred number of components. For this, starting from K=4 until K=10, we estimated the mixture parameters using the EM algorithm (Section 8.2) for each value of K>3. The results indicate that the total message length steadily increases beyond K=3. The reason is that although the negative log-likelihood of the data decreases (with increasing K), the second part of the message (blue curve) only changes marginally, while the first part continually increases. Thus, as mixtures become overly complex, there is a greater cost associated with encoding their parameters. This affects the total message length as the minimal gain in negative log-likelihood is overshadowed by the increase in the first part of the message. Hence, this example demonstrates the effectiveness of the search method in the context of FB<sub>5</sub> distributions. Furthermore, it also demonstrates the ability of the MML criterion to balance the tradeoff between the model complexity and the quality of data fit.

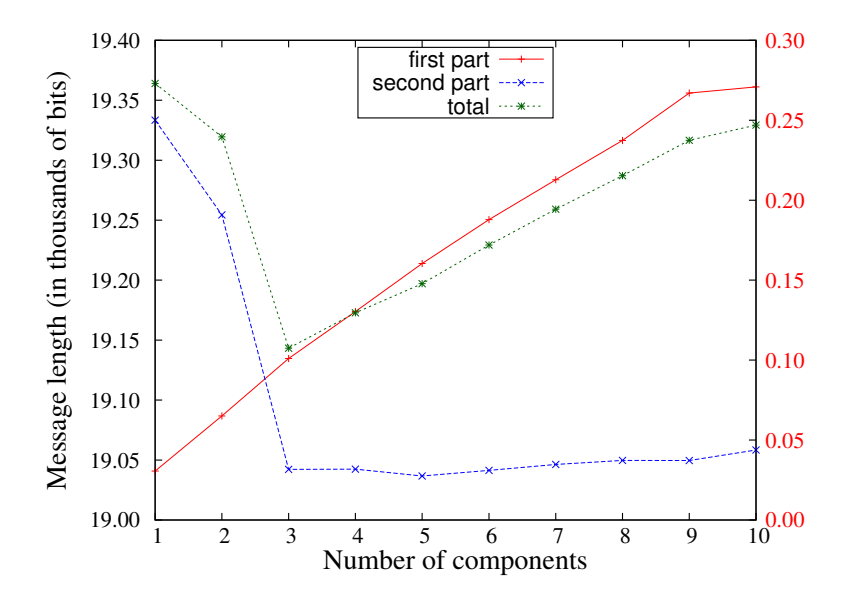


Figure 10: Variation of the individual parts of the total message length with increasing number of components (note that the two Y-axes have different scales: the first part of the message follows the right side Y-axis; while the second part of the message and total message lengths follow the left side Y-axis)

# 9. Experimental analyses of the various parameter estimates

For a given FB<sub>5</sub> distribution characterized by concentration  $\kappa$  and eccentricity e, a random sample of size N is generated using the method proposed by Kent et al. (2013). We set the true distribution to have  $\{\psi, \alpha, \eta\} = \pi/2$  each. The scale parameters  $\kappa$  and e are varied to obtain different FB<sub>5</sub> distributions and corresponding random samples. The parameters are estimated using the sampled data and the different estimation methods. The procedure is repeated 1000 times for each combination of N,  $\kappa$ , and e.

### 9.1 Methods of comparison

We conduct a comparison between the moment, maximum likelihood (ML), MAP, and MML-based estimates. The results include the two versions of MAP estimates resulting from the two forms of the posterior distributions (Equation 13): MAP1 corresponds to the posterior with parameterization  $\kappa, \beta$ , and MAP2 corresponds to the posterior with parameterization  $\kappa, e$ . The two versions are considered so as to show that MAP estimates are inconsistent and are dependent on the parameterization used.

The MML estimates are obtained by minimizing the message length expression. Naturally, the estimates due to other methods do not result in lower message lengths. Similarly, if we use the negative log-likelihood as the comparison criterion, the maximum likelihood estimates have a lower value compared to the other estimates. As each estimation technique optimizes a different objective function, it is required to have a metric that impartially evaluates the different estimates. The mean squared error of the estimates and Kullback-Leibler (KL) divergence (Kullback and Leibler, 1951) are therefore used to compare the various estimates. The estimates are also compared using statistical hypothesis testing.

### 9.1.1 Mean squared error of the estimates

For a parameter vector  $\boldsymbol{\Theta}$ , and its estimate  $\widehat{\boldsymbol{\Theta}}$ , the mean squared error (MSE) is given by  $\mathbb{E}[(\widehat{\boldsymbol{\Theta}} - \boldsymbol{\Theta})^2]$ . Further, the MSE can be decomposed into bias and variance terms, as given below (Lebanon, 2010; Taboga, 2012).

$$\mathbb{E}[(\widehat{\boldsymbol{\Theta}} - \boldsymbol{\Theta})^2] = \operatorname{Bias}^2(\widehat{\boldsymbol{\Theta}}) + \operatorname{trace}(\operatorname{Var}(\widehat{\boldsymbol{\Theta}}))$$

where  $\operatorname{Bias}^2(\widehat{\Theta}) = \|\mathbb{E}[\widehat{\Theta}] - \Theta\|^2$  and  $\operatorname{Var}(\widehat{\Theta})$  is the covariance matrix of the estimator. Ideally, it is expected that the estimates result in low MSE values and it depends on the bias and variance of the parameter estimates. An estimate that results in lower values of MSE is usually preferred over the other estimates.

### 9.1.2 Kullback-Leibler (KL) divergence of the estimated distribution

The KL divergence is a similarity measure that is used to determine the "distance" between the true distribution and the distribution thats uses the estimated parameters. An estimate that results in lower KL divergence is considered a better estimate. The analytical form of the KL divergence between two  $FB_5$  distributions is derived in Section 8.4.3. We report the percentage of times (out of 1000 random simulations) that the KL divergence of a particular estimator is lower than that of others. An estimator wins when its associated KL divergence is less than that of the other estimates.

When the KL divergence of different estimates is compared, because of two different versions of MAP estimation, we present two separate frequency plots. The KL divergence of the moment, ML, and MML estimates is contrasted with KL divergence of MAP1 or MAP2 estimates.

### 9.1.3 Statistical hypothesis testing

The likelihood ratio test is typically used to determine the suitability of modelling data  $\mathcal{D}$  using a simpler or a nested model, corresponding to one with fewer free parameters (null hypothesis  $\mathcal{H}_0$ ) against a more general model (alternate hypothesis  $\mathcal{H}_A$ ). The likelihood ratio

 $\lambda$  is used to determine the preference of a null hypothesis  $\mathcal{H}_0$  over an alternate hypothesis  $\mathcal{H}_A$ , and is as follows:

$$\lambda = \frac{\underset{\mathcal{H}_{A}}{\text{max}} \text{ likelihood}(\mathcal{D}|\mathcal{H}_{0})}{\underset{\mathcal{H}_{A}}{\text{max}} \text{ likelihood}(\mathcal{D}|\mathcal{H}_{A})}$$

The test statistic resulting from the use of  $\lambda$  is related to the negative logarithm of the likelihood ratio and is given by  $\Lambda = -2 \log \lambda$ . The distribution of the statistic  $\Lambda$  is asymptotically approximated as a  $\chi^2$  distribution with degrees of freedom equal to the difference in the number of free parameters between the alternate and the null hypothesis (Wilks, 1938). If  $\lambda$  is sufficiently small, it would lead to a rejection of the null hypothesis. Conversely, if  $\Lambda$  exceeds some confidence threshold,  $\mathcal{H}_0$  is rejected.

In the current analysis of the various parameter estimates, we compare the likelihood ratio resulting from the use of a particular estimate  $\widehat{\Theta}$  (that is, moment, MAP or MML-based) against a general FB<sub>5</sub> distribution. It is equivalent to testing the null hypothesis  $\mathcal{H}_0: \Theta = \widehat{\Theta}$  (explicit parameters) against the alternate hypothesis  $\mathcal{H}_A: \Theta \neq \widehat{\Theta}$  (with 5 free parameters). Assuming a statistical significance of the test as 1%,  $\mathcal{H}_0$  is rejected when  $\Lambda > \tau$ , where  $\tau = 13.086$  corresponds to the 99<sup>th</sup> percentile of a  $\chi^2$  distribution with 5 degrees of freedom. Alternatively, the test statistic can be used to evaluate the p-value, which if less than 1% (significance of the test) amounts to rejection of  $\mathcal{H}_0$ .

For the various parameter estimates compared here, it is expected that at especially large sample sizes, the estimates are close to the maximum likelihood estimate as determined by the corresponding test statistic. In other words, the empirically determined test statistic is expected to be lower than the critical value  $\tau$ , which implies it has a corresponding p-value greater than 0.01.

### 9.2 Empirical analysis

The estimates are analyzed here in two controlled cases: (1) fixing sample size N with varying  $\kappa$  and e, and (2) varying N while fixing  $\kappa$  and e.

### 9.2.1 Fixed sample size, varying concentration $\kappa$ and eccentricity e

The results are presented when a random sample of size N=10 is generated from the FB<sub>5</sub> distribution for a  $\kappa$  that is increased by an order of magnitude starting from 1 to 100. The behaviour of the estimates is analyzed below.

•  $\kappa=1$ : The performance of the various estimates using the comparison methodologies (Section 9.1) is illustrated in Figure 11. It is observed that the bias and MSE of moment and ML estimates is greater than that of MAP and MML-based estimates. The two versions of the MAP estimates also have a greater bias and MSE as compared to the MML estimates shown in Figure 11(a) and (b).

It is also observed that the MML-based estimates result in lower KL divergence more than 80% of time as compared to other estimates when MAP1 is used (see Figure 11c). With MAP2, the frequency of wins for the MML-based estimates increases to more than 90% (see Figure 11d). This suggests that transforming the parameter space greatly impacts the MAP-based estimates. The ML estimates win less than 5% of

the time. This is in agreement with the relatively greater MSE observed for the ML estimates.

The boxplots shown in Figure 11(e) and (f) show the variation of the test statistics and the corresponding p-values. There is a greater variation for the MML-based estimates. However, across all values of eccentricity, the test statistic  $\Lambda$  is less than the threshold  $\tau=13.086$  and the smallest p-value is greater than 0.01. This is true across all estimation methods, thus, suggesting that the null hypothesis of modelling data using a particular estimate (moment, MAP or MML) is accepted at the 1% significance level.

•  $\kappa=10$ : The comparison results are presented in Figure 12. Similar to the previous case ( $\kappa=1$ ), the moment and ML estimates have greater bias and MSE. It is interesting to note that MAP2 has greater bias and MSE compared to MML estimates (Figure 12(a) and (b) respectively). However, MAP1 estimates are in close competition with the MML. The bias and MSE are lower for MML estimates until  $e \leq 0.5$  and greater compared to MAP1 estimates for e > 0.5.

The number of times KL divergence is lower for the MML estimates decreases with increasing eccentricity (for both versions of MAP estimates). For  $e \le 0.5$ , the percentage of wins for the MML estimates is greater than all other estimates. However, for e > 0.5, MAP1 wins majority of the time (Figure 12c). In the case of comparison with MAP2, the percentage of wins of MML estimates continuously decreases. However, the number of wins of MML estimates is always in the majority (Figure 12d).

The observations are in contrast to what was observed in the case of  $\kappa=1$  where MML estimates emerged as consistently better estimates. In terms of statistical hypothesis testing, the null hypotheses corresponding to modelling using moment, ML, MAP or MML estimates are accepted at the 1% significance level.

•  $\kappa = 100$ : The comparison results in this case follow the same pattern as that of  $\kappa = 10$  (not illustrated here as they are similar to Figure 12).

When  $\kappa=10$  and 100, the MAP1 estimates perform competitively compared to the MML estimates (with respect to bias and MSE). Further, the proportion of times MAP1 estimates win with respect to KL divergence progressively increases as the eccentricity increases. In general, similar results are observed for  $\kappa>10$ . However, as discussed previously, MAP-based estimation is subjective to the parameterization of the distribution as shown by the stark contrast between MAP1 and MAP2 estimates by the two parameterizations even though they are both reasonable. The moment, ML, and MML estimates, on the other hand, are not affected by parameterization. Amongst these, MML-based estimates outperform with respect to all objective metrics as described here.

### 9.2.2 Varying sample size N, fixed concentration $\kappa$ and eccentricity e

We have also explored the behaviour of different estimates with increasing sample size from N=10 to N=50. For space reasons, we only include the results for  $\kappa=10$ . The results are discussed for three specific eccentricity values, ranging from low eccentricity (e=0.1), to moderate eccentric (e=0.5) to high (e=0.9).

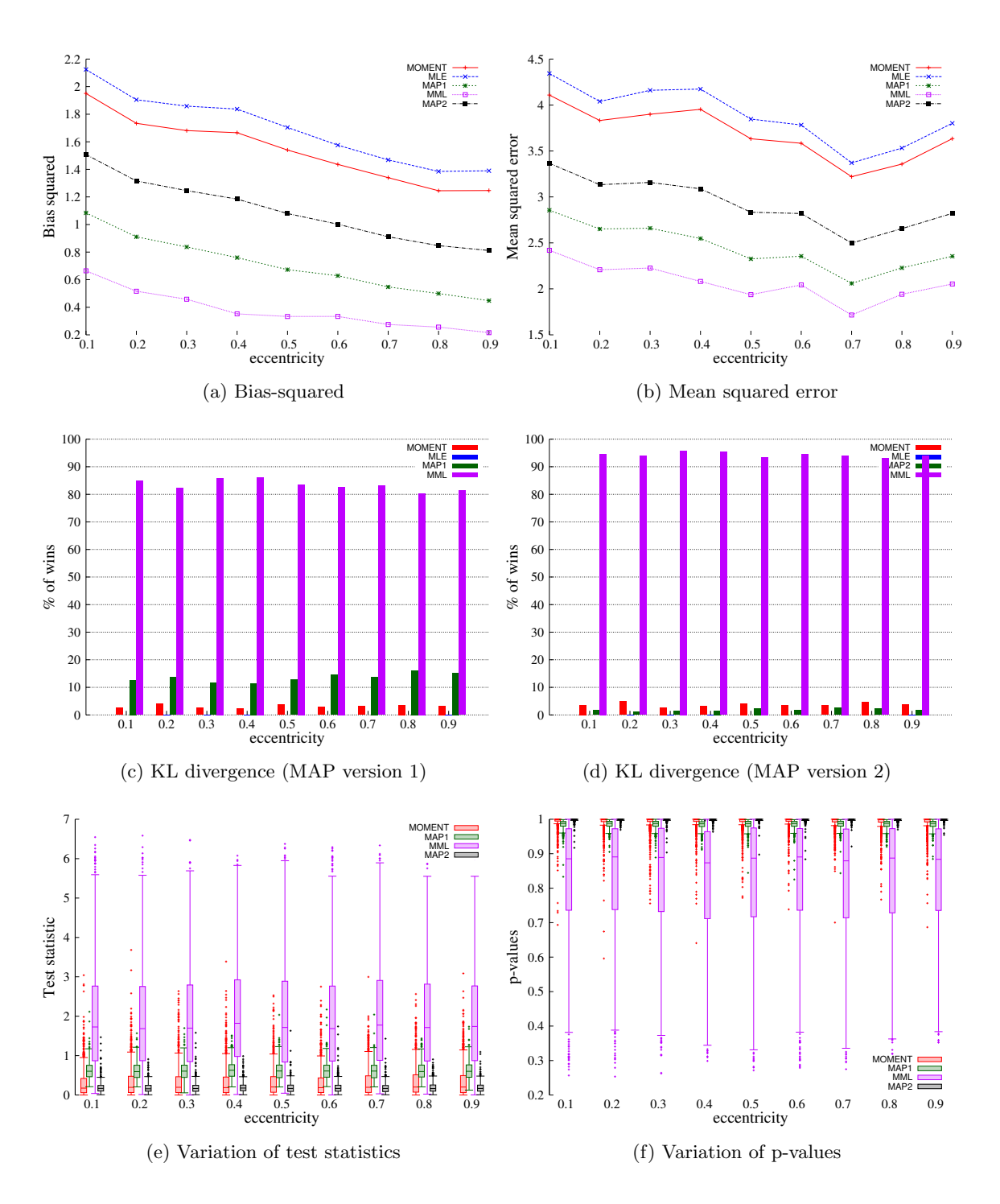


Figure 11:  $N = 10, \kappa = 1$ .

• e = 0.1: The comparison results are presented in Figure 13 which clearly shows how, across all estimators, the bias and MSE decrease as N increases. This is expected: as

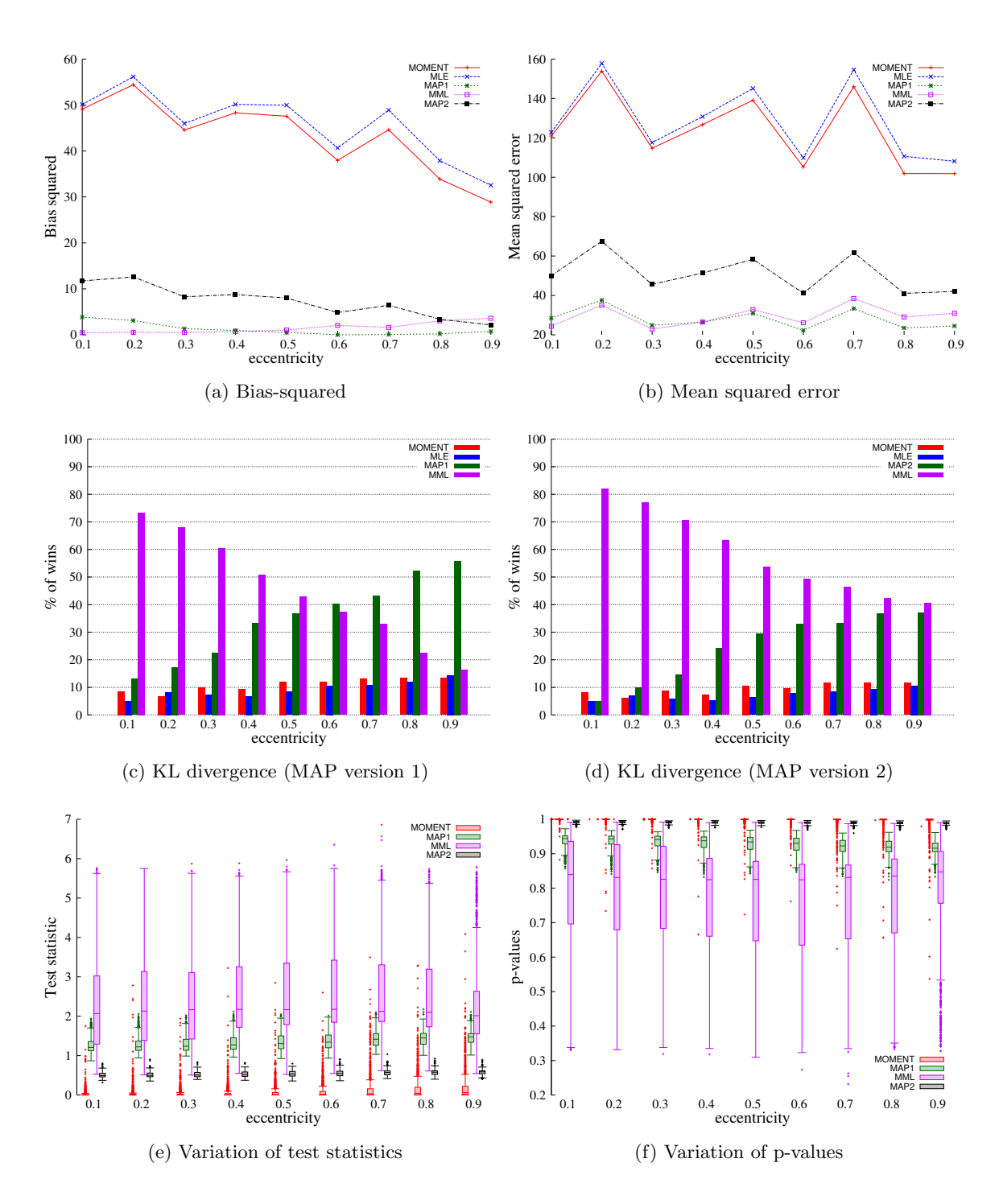


Figure 12:  $N = 10, \kappa = 10$ .

more data becomes available, the accuracy of estimation increases. Figure 13(a) and (b) illustrate that the bias and MSE are prominent for moment and ML estimators.

The bias of MML estimates is close to zero and convincingly lower than both versions of MAP estimates, especially when N < 25. The MSE of MML estimates is smaller but close to that of MAP1 estimate.

The proportion of wins of MML estimates with respect to KL-divergence is the highest with values of at least 70% and 80% when compared with MAP1 and MAP2, respectively (see Figure 13c,d). Also, hypothesis testing indicate that the respective estimates constituting the null hypothesis are accepted at the 1% significance level, as observed from the boxplots of test statistics and p-values in Figure 13(e) and (f).

• e = 0.5: The comparison results are presented in Figure 14. Similar to the previous case, the bias and MSE of moment and ML estimates are considerable high compared to those of the MAP and MML estimates. Also, MAP1 estimates have greater bias and MSE as compared to MAP2 estimates. In this case, the bias and MSE of MAP2 and MML are close to zero.

The proportion of wins of MML estimates with respect to KL divergence is higher with about 40% and 50% when compared against MAP1 and MAP2 estimates, respectively. The proportion of wins are, however, lower compared to the previous case when e = 0.1 as shown in Figure 14(c) and (d).

e = 0.9: The comparison results are presented in Figure 15. In this case, again, the bias and MSE of moment and ML estimates are greater compared to others. For N < 20, the bias of MML estimates is greater when compared to those of MAP1 and MAP2 (Figure 15a). Further, the MSE of MML estimates is greater than that of MAP1 and lower than that of MAP2. As the MSE combines the bias and variance terms, there is a tradeoff that leads to this result. When N > 25, there is almost no difference in the bias and MSE due to MAP and MML estimates.

Also, the proportion of wins of KL divergence for MAP1 is greater than all others (Figure 15c). This corresponds to the proportion of wins as illustrated through Figure 12(c), similar to the  $N=10, \kappa=10, e=0.9$  case. However, when compared with MAP2, the MML estimates have greater proportion of wins  $\sim 40\%$  (Figure 15d).

The traditional ML estimators are known to have considerable bias, especially at lower sample sizes (Dryden and Mardia, 1998; Dore et al., forthcoming). The ML estimates of  $\kappa$  in the case of a vMF distribution are known to be biased (Schou, 1978; Best and Fisher, 1981; Cordeiro and Vasconcellos, 1999). Similarly, the ML estimates of a Bingham distribution, which is a special case of a FB<sub>5</sub> distribution, are also shown to be biased and corrections have been proposed (Cordeiro and Klein, 1994; Kume and Wood, 2007; Dore et al., forthcoming).

The MML-based estimates have been shown to be effective in reducing bias in the case of a vMF distribution (Kasarapu and Allison, 2015). For an FB<sub>5</sub> distribution, we empirically demonstrated that, in comparison to the moment and ML estimates, the MML-based estimates have lower bias and MSE. Further, when compared to MAP estimates, MML estimates are competitive, particularly considering that MAP estimates are dependent on the parameterization. As a result, MAP estimates are inconsistent and should therefore be avoided. In contrast, MML-based estimates are invariant to alternative parameterizations

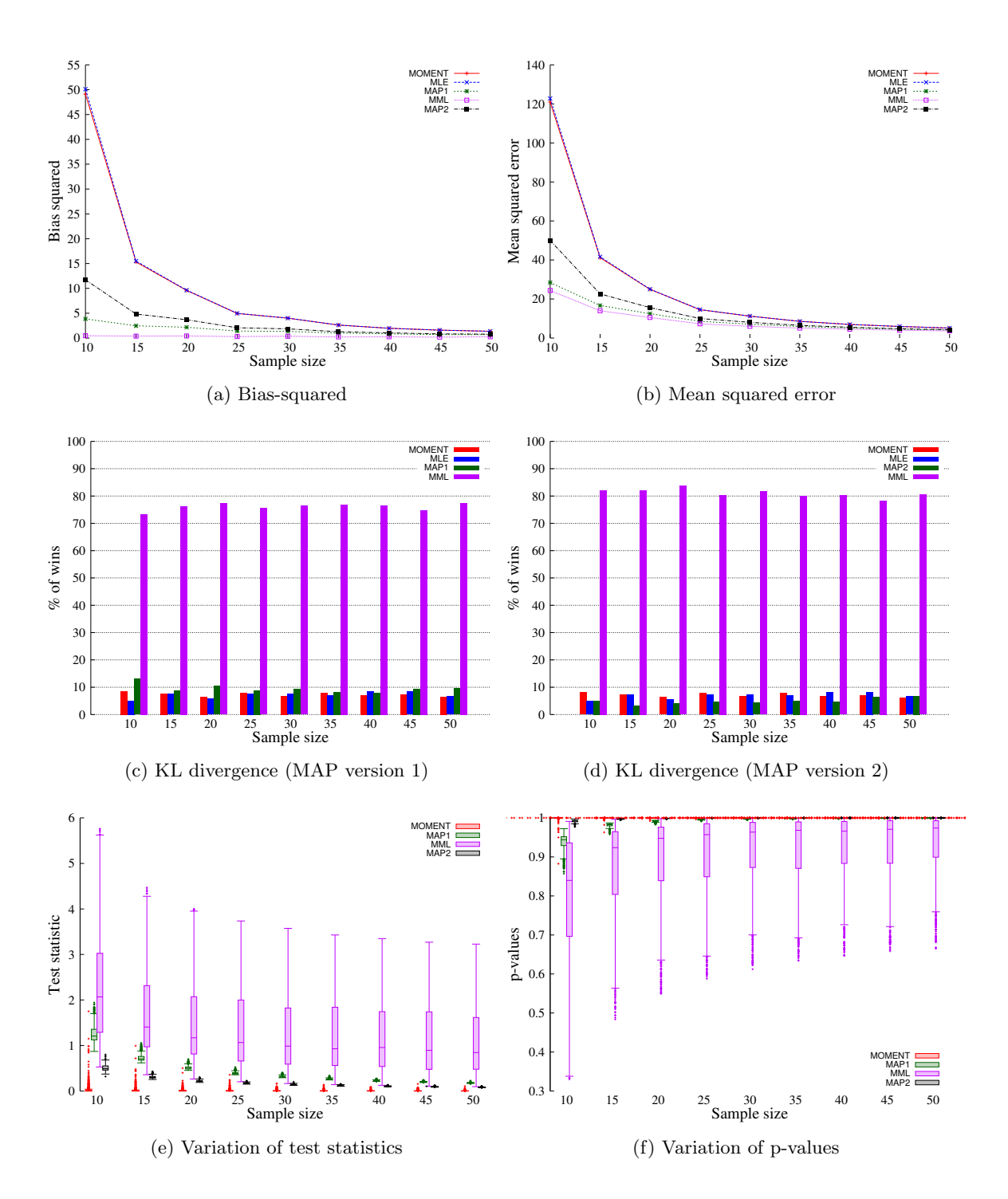


Figure 13:  $\kappa = 10$ , eccentricity = 0.1

(Oliver and Baxter, 1994; Wallace, 2005). In this regard, we discuss another parameteriza-

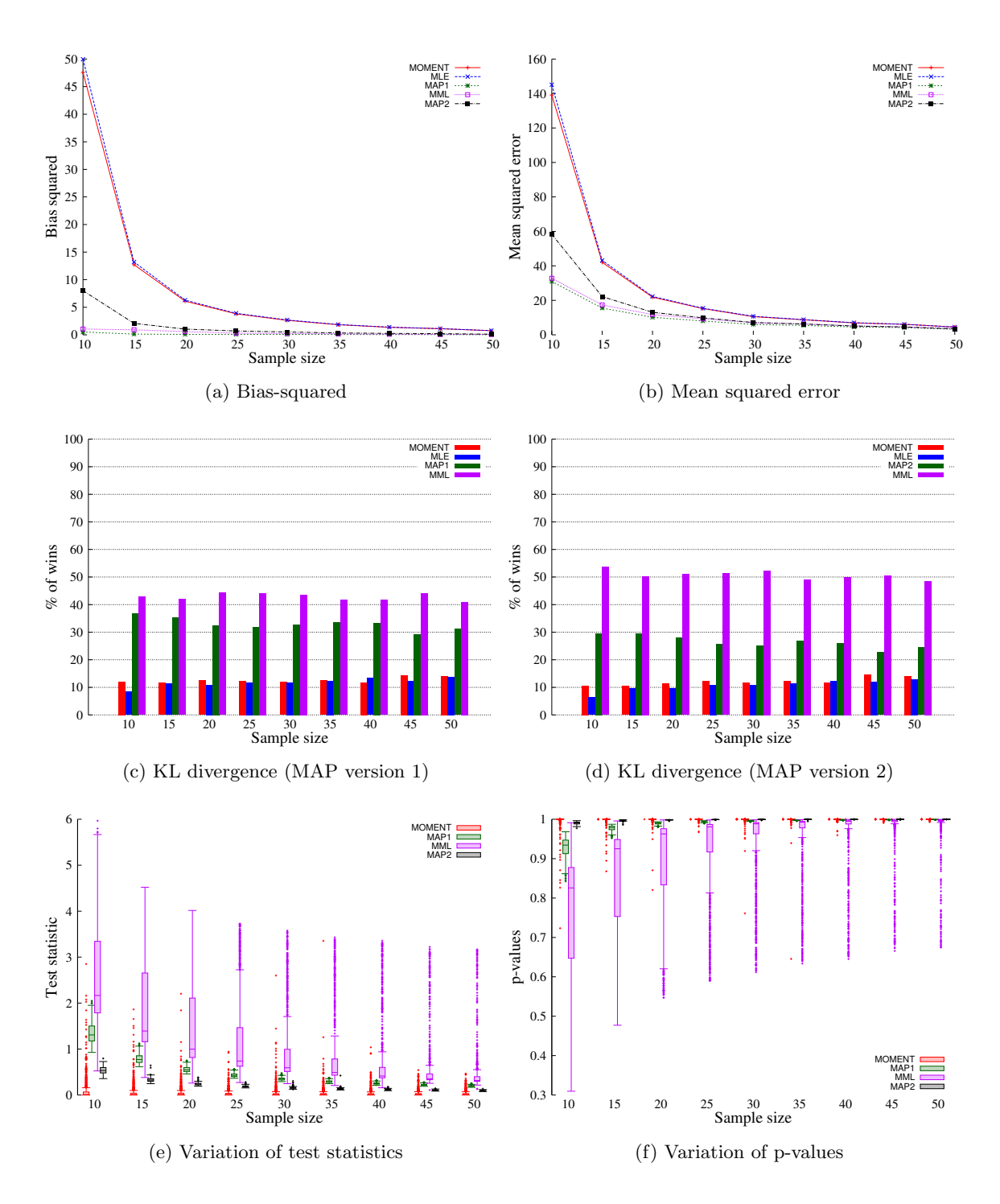


Figure 14:  $\kappa = 10$ , eccentricity = 0.5

tion in Appendix A involving all parameters of an  ${\rm FB}_5$  distribution to further strengthen our case.

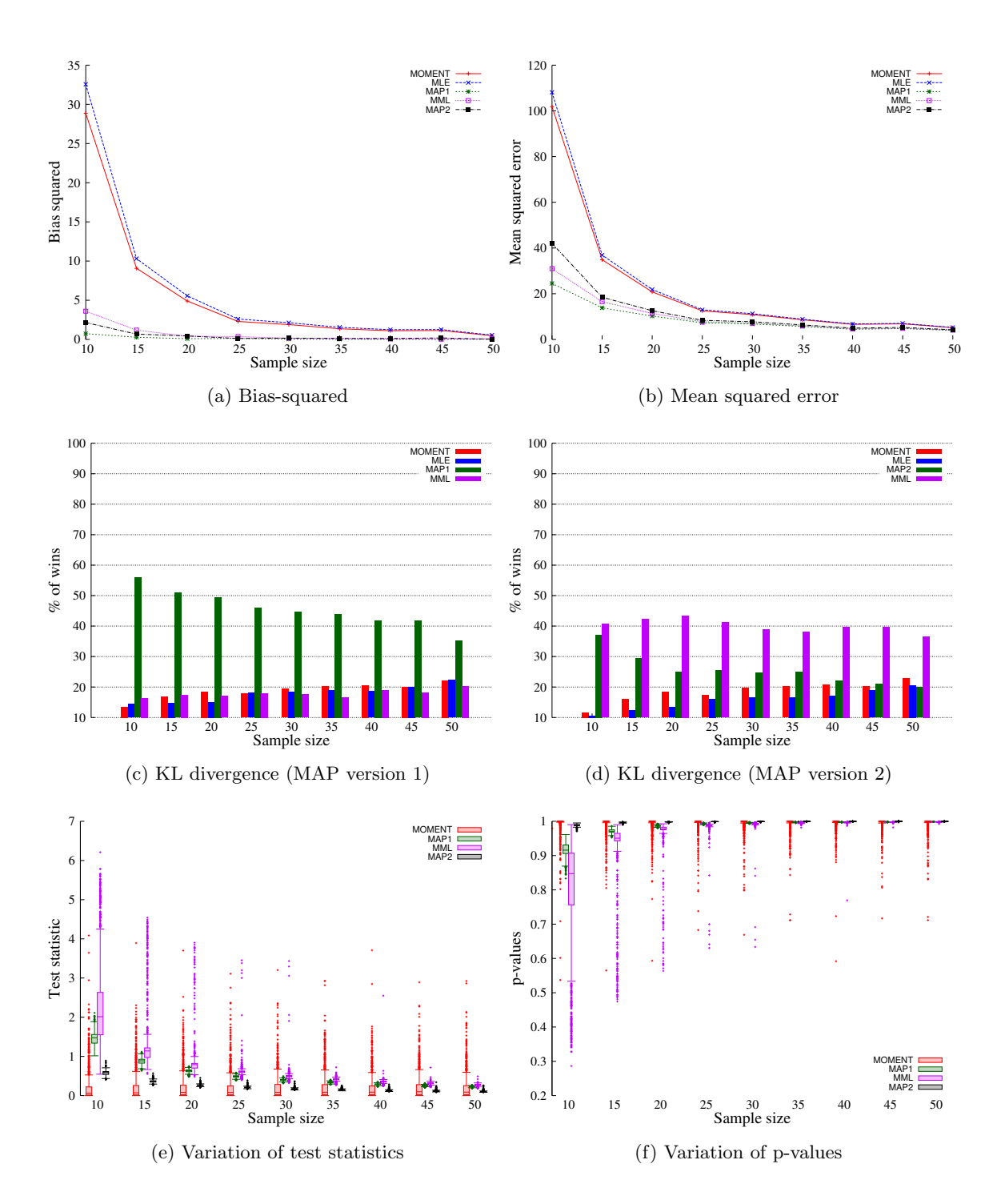


Figure 15:  $\kappa = 10$ , eccentricity = 0.9

# 10. Experiments involving $FB_5$ mixtures

To demonstrate the applicability of FB<sub>5</sub> mixtures, we consider the problem of mixture modelling of directional data arising out of protein three-dimensional conformations. A

protein chain consists of a sequence of amino acids (residues). Each residue has a central carbon atom  $C_{\alpha}$ . If  $C_{\alpha}^{i}$  and  $C_{\alpha}^{i+1}$  denote the carbon atoms at positions i and i+1 in the protein chain, then the distance between these successive atoms is highly constrained to be 3.8Å because of the chemical interactions between the constituent atoms. Thus,  $C_{\alpha}^{i+1}$  atom lies on a sphere of radius  $\sim 3.8$ Å whose centre is  $C_{\alpha}^{i}$ . The direction vector from  $C_{\alpha}^{i}$  to  $C_{\alpha}^{i+1}$  is considered a point in the data set. Given the Cartesian coordinates of a  $C_{\alpha}$  atom, its co-latitude ( $\theta$ ) and longitude ( $\phi$ ) are determined with respect to the previous  $C_{\alpha}$  atom in a consistent manner (Kasarapu and Allison, 2015). The set of all ( $\theta$ ,  $\phi$ ) pairs form the directional data corresponding to a given set of protein structures. The protein data set considered is the publicly available ASTRAL SCOP-40 (version 1.75) database (Murzin et al., 1995). Out of the entire dataset, the " $\beta$  class" proteins comprising of 1802 structures is a case in point. The empirical distribution consists of 251,346 ( $\theta$ ,  $\phi$ ) pairs and we infer mixtures on this directional data using the search method described in Section 8.4.

## 10.1 Evolution of vMF and FB<sub>5</sub> mixtures

Mixtures of vMF distributions were previously explored by Kasarapu and Allison (2015). This entailed estimating the vMF concentration parameter  $\kappa$  using MML. They use Taylor series approximations (Newton's and Halley's root-finding methods) in the computation of the MML estimates of  $\kappa$ . Both these root-finding approaches are truncated after two iterations in order to do a fair comparison with the other contemporary  $\kappa$  approximations that were discussed in that work (see Equations 8 and 9 in Kasarapu and Allison (2015)). The obtained vMF  $\kappa$  estimates were used as part of the mixture modelling apparatus. As a result, the search method employed for determining the optimal number of vMF components was terminated prematurely. Furthermore, the search heuristic employed in Kasarapu and Allison (2015) does a random selection of initial means of the child components while splitting a parent component. In contrast to these, the vMF  $\kappa$  estimates used in the current work correspond to the converged values (without truncating prematurely). Further, as per the search method described in this work, while splitting a parent component, the initial means of the children are chosen such that they are reasonably apart which gives them the best chance to form two distinct sub-components in order to escape a local optimum (explained in Section 8.4.1).

The search method infers a 37-component vMF mixture and terminates after 49 iterations involving split, delete, and merge operations. When modelled using  $FB_5$  distributions, the search method infers 23 components and terminates after 33 iterations. In each of these iterations, for every intermediate K-component mixture, each constituent component is split, deleted, and merged (with an appropriate component) to generate improved mixtures. The method terminates when these perturbations do not result in an improvement.

In the case of vMF mixture, the search method begins with a one-component mixture, continuously favours splits over delete and merge operations until a 17-component mixture is inferred. This corresponds to the steady increase in the first part of the message length as observed by the red curve in Figure 16(a) until the 17<sup>th</sup> iteration. Thereafter, a series of deletions and splits result in an intermediate sub-optimal 19-component mixture at the end of the 23<sup>rd</sup> iteration. This is characterized by the step-like behaviour of the red curve between the 17<sup>th</sup> and 24<sup>th</sup> iteration. The first part of the message is dependent on the

number of components (model complexity) and an increase in number of mixture components leads to an increase in the encoding cost of the parameters. From the 24<sup>th</sup> iteration, the method continues to split the constituent components until a 36-component mixture is inferred after 40 iterations. This is reflected in the continuous rise of the red curve in Figure 16(a) between 25<sup>th</sup> and 40<sup>th</sup> iterations. Thereafter, through a series of perturbations, the final resultant mixture has 37 components at the end of 49 iterations, characterized by a step-like behaviour towards the end between 40<sup>th</sup> and 49<sup>th</sup> iterations.

In the case of  $FB_5$  mixture, the search method infers a 23-component mixture at the end of 23 iterations by continuous splitting. This corresponds to the steady increase in the first part of the message length denoted by the red curve in Figure 16(b). From here on, after a series of perturbations, the final mixture stabilizes at the end of  $33^{\rm rd}$  iteration thereby resulting in a 23-component mixture. This is characterized by the step-like behaviour corresponding to intermediate reduction and increase in the number of mixture components between the  $24^{\rm th}$  and  $33^{\rm rd}$  iterations.

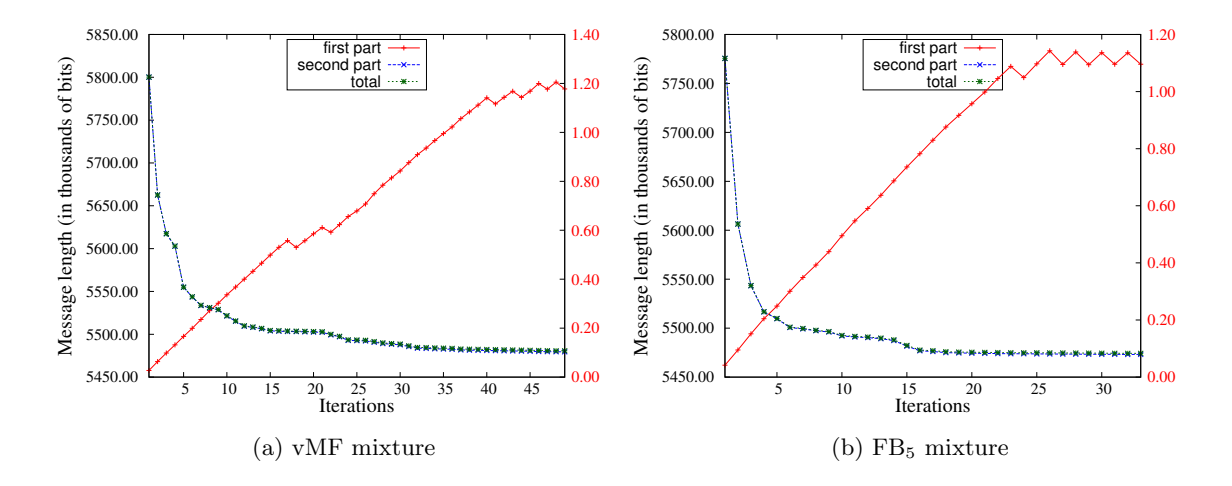


Figure 16: Evolution of mixtures inferred by the search method. Note there are two Y-axes in both (a) and (b) with different scales: the first part of the message follows the right side Y-axis (red); while the second part and total message lengths follow the left side Y-axis (black).

In both cases, the second part of the message length continues to decrease with an increase in the number of mixture components. An initial sharp decrease is observed in both mixture types. The search method terminates when the increase in first part dominates the reduction in the second part leading to an increase in total message length.

## 10.2 Comparison of vMF and FB<sub>5</sub> mixture models

The resulting vMF and FB<sub>5</sub> mixtures are shown in Figure 17. In order for effective visualization of the individual mixture components, the illustration includes the contours of the components such that they encompass 80% of the probability corresponding to each component. The data plotted is a random sample of 10000  $(\theta, \phi)$  pairs drawn from the empirical

distribution of  $\beta$  class of proteins. The regions in Figure 17 are coloured based on the empirical distribution (heat map). There are two distinguishable regions of the distribution of  $\theta$  and  $\phi$  values. At  $(\theta, \phi) \sim (90^{\circ}, 60^{\circ})$ , there is a concentrated mass which corresponds to the *helical* region in a typical protein. The area characterized by  $\theta \in (40^{\circ}, 80^{\circ})$ ,  $\phi \in (180^{\circ}, 240^{\circ})$  roughly corresponds to the *strand* region in a typical protein.

The search method inferred a 37-component vMF mixture and a 23-component FB<sub>5</sub> mixture. It is observed that the number of components used to model the entire collection of 251,346 ( $\theta$ , $\phi$ )-pairs using a FB<sub>5</sub> mixture model is fewer compared to a vMF mixture. This is expected as a vMF distribution is a specific case of a FB<sub>5</sub> distribution and, hence, a vMF mixture requires more number of components to model data that is asymmetrically distributed. In Figure 17(a), the vMF mixture components 1-11 are used to model the helical region (approximately), whereas in Figure 17(b), the same region is modelled using FB<sub>5</sub> mixture components 1-6. Similarly, the strand region in the proteins is modelled by components 12-17 in the vMF case, whereas, it is modelled by components 1-11 using FB<sub>5</sub> mixture. Further, components 18-24 in the vMF mixture and components 12, 13 in the FB<sub>5</sub> mixture model the same region. The other regions in the protein directional data space follow the same modelling pattern, that is, with fewer FB<sub>5</sub> components. These observations reflect the better explanatory power of FB<sub>5</sub> mixtures compared to vMF mixtures.

Compared to a singleton vMF distribution, the encoding cost of the parameters of a  $FB_5$  distribution would be greater as it is a complex model with more number of parameters. As shown in Table 1, the encoding cost of the parameters of the inferred 23-component FB<sub>5</sub> mixture is 1095 bits. A vMF mixture with the same number of components has a first part equal to 749 bits (a difference of 346 bits). However, the second part of the message (the fit to the data) is lower for the FB<sub>5</sub> mixture (a difference of  $\sim 17,000$  bits). Hence, the gain in the second part outweighs the greater cost of encoding the more complex FB<sub>5</sub> mixture. Thus, the total message length is lower for the FB<sub>5</sub> mixture and serves as a better model to explain the data. If the 23-component vMF mixture is compared with the 37-component vMF mixture inferred by our search method, the vMF mixture with 23 components has smaller first part and greater second part (Table 1). The 37-component mixture has a first part equal to 1177 bits compared to 749 bits in the 23-component case (a difference of 428 bits). However, there is a gain of 11,000 bits in the second part, thus, resulting in a lower total message length in the 37-component case. Through this analysis, it is shown how the tradeoff of choosing a complex model and the quality of fit is addressed using the MML framework.

Mixture	Number of	First part	Second part	Total message length	
model	components	(thousands of bits)	(millions of bits)		
vMF	23	0.749	5.490	5.491	
vMF	37	1.177	5.479	5.481	
$FB_5$	23	1.095	5.473	$\boldsymbol{5.474}$	

Table 1: Message lengths corresponding to mixtures inferred on the protein directional data.

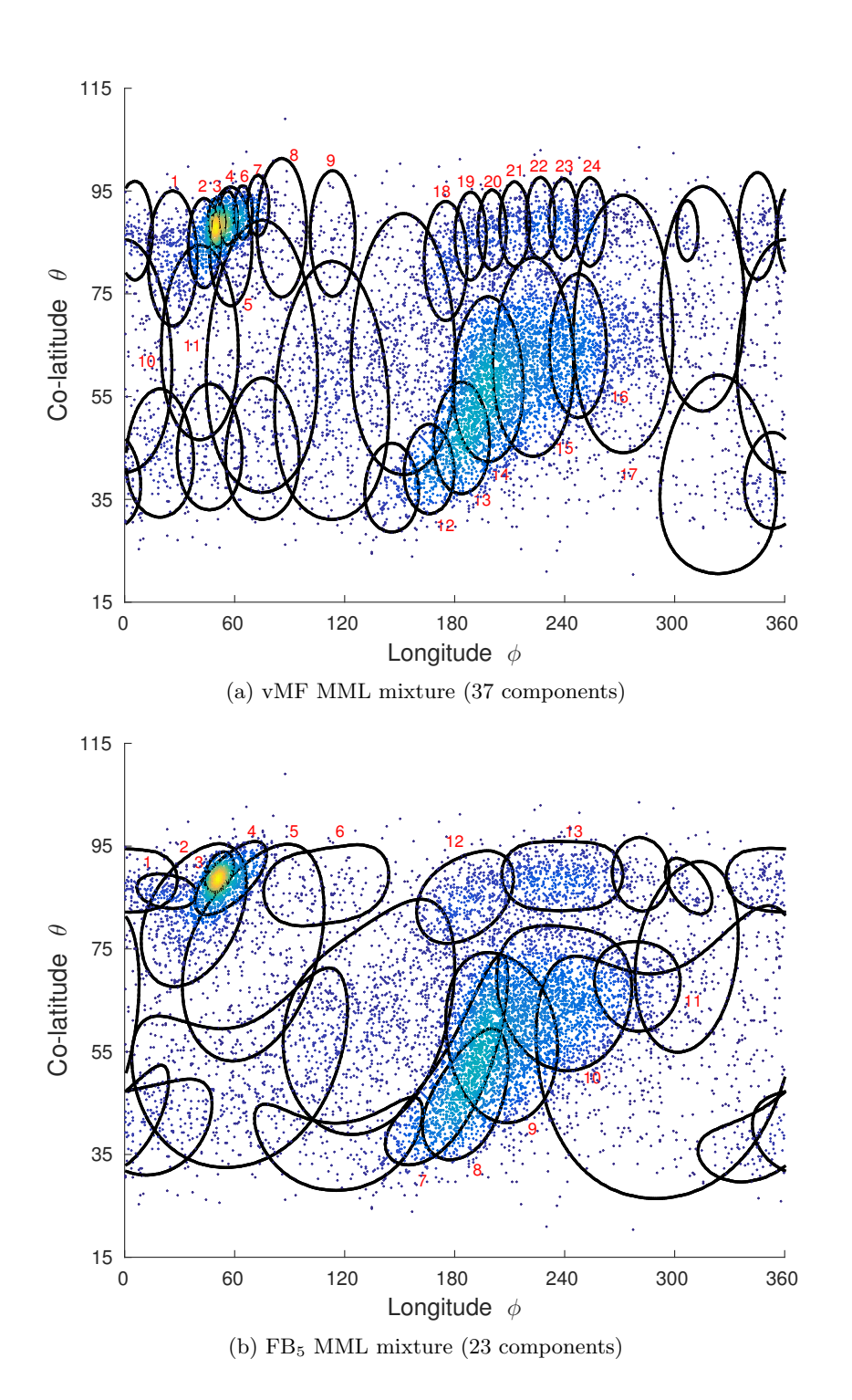


Figure 17: Mixtures inferred on the  $\beta$ -class proteins ( $\theta$  and  $\phi$  are in degrees).

It is also interesting to note the shape of the contours generated by both vMF and FB $_5$  mixtures. A vMF distribution caters to symmetrically distributed data and has circular

contours of constant probability on a spherical surface. Hence, in the  $\theta\phi$  space, we see regular oval-shaped contours as shown in Figure 17(a). In contrast, a FB<sub>5</sub> distribution has ellipse-like contours on a spherical surface (Figure 2). Thus, when projected onto the  $\theta\phi$  space, it results in a myriad of contour shapes (Figure 17b) depending on the parameters defining a FB<sub>5</sub> distribution.

Compressibility of protein structures: The better explanatory power of  $FB_5$  mixtures over vMF mixtures leads to enhanced data compression (demonstrated through Table 1), and hence, serve as efficient descriptors to model directional data. In the context of proteins, previous null model descriptors are based on the uniform distribution on the sphere (Konagurthu et al., 2012), and due to vMF mixtures (Kasarapu and Allison, 2015). The null model descriptions provide a baseline for encoding protein coordinate data in varied structure modelling tasks (Konagurthu et al., 2012, 2013; Collier et al., 2014). In this regard, the use of  $FB_5$  mixture offers a better alternative as opposed to encoding using uniform distribution or vMF mixtures.

The message length expressions to encode the orientation angles using uniform, vMF, and FB<sub>5</sub> null models are given by Equation 31 (Konagurthu et al., 2012; Kasarapu and Allison, 2015), where  $\mathbf{x}$  corresponds to a unit vector described by  $(\theta, \phi)$  on the surface of the sphere,  $\epsilon$  is the precision<sup>5</sup> to which each coordinate is measured, and r denotes the distance between successive  $C_{\alpha}$  atoms. In Equation 31, for the vMF mixture, K = 37 and the null model corresponding to the FB<sub>5</sub> mixture has K = 23 components.

Uniform Null = 
$$-\log_2\left(\frac{\epsilon^2}{4\pi r^2}\right) = \log_2(4\pi) - 2\log_2\left(\frac{\epsilon}{r}\right)$$
 bits.  
vMF & FB<sub>5</sub> Null =  $-\log_2\left(\sum_{j=1}^K w_j f_j(\mathbf{x}; \Theta_j)\right) - 2\log_2\left(\frac{\epsilon}{r}\right)$  bits. (31)

The inferred mixture models are then used to encode the entire protein data. After accounting for the distances between the successive atoms, the total message lengths obtained are given in Table 2. The uniform distribution is clearly not an appropriate descriptor and this can be reasoned from the empirical distribution which has multiple modes (Figure 17). The inferred vMF mixture has better explanatory power over the uniform distribution as it has a corresponding saving of 446,000 bits over 251,346 data points (residues). This translates to an enhanced compression of 1.778 bits per residue (on average). The inferred FB<sub>5</sub> mixture, however, encodes the same amount of data with a saving of 7,000 bits against the vMF mixture (an average of 0.026 bits extra compression per residue). The results following the application of FB<sub>5</sub> mixtures to modelling protein directional data demonstrate that that they supersede the vMF mixture models (Table 2). The ability of FB<sub>5</sub> distributions to model asymmetrical data leads to improved encoding of the protein data. Hence, they serve as natural successors to the vMF null model descriptors.

#### 10.3 Comparison of MML criterion with other information-theoretic criteria

The MML criterion is used in computing the score associated with a mixture model by separately encoding the parameters (first part) and the data given those parameters (second

<sup>5.</sup> Protein coordinate data is measured to an accuracy of  $\epsilon = 0.001 \text{Å}$ .

Null model	Total message length	Bits per
Null illodel	(millions of bits)	residue
Uniform	6.895	27.434
vMF mixture	6.449	25.656
FB <sub>5</sub> mixture	$\boldsymbol{6.442}$	25.630

Table 2: Comparison of the null model encoding lengths based on uniform distribution, vMF mixture (37 components), and FB<sub>5</sub> mixture (23 components).

part). This yields the total message length (Equation 29) which is used to find improved mixtures during the search process. In addition to the MML criterion, as discussed in Section 8.3, the traditional information-theoretic criteria used are AIC (Akaike, 1974) and BIC (Schwarz, 1978; Rissanen, 1978). These two criteria introduce constant term penalties depending on the number of free parameters in the mixture model. If p denotes the number of a model's free parameters<sup>6</sup>,  $\mathcal{L}(\mathcal{D}|\mathbf{\Phi})$  is the minimized negative log-likelihood of data given the parameters  $\mathbf{\Phi}$ , and N the sample size, then AIC and BIC are given by

$$AIC(p) = p + \mathcal{L}(\mathcal{D}|\mathbf{\Phi})$$
 and  $BIC(p) = \frac{p}{2}\log N + \mathcal{L}(\mathcal{D}|\mathbf{\Phi})$ 

Mixture modelling of some observed data based on these criteria can be done as follows:

- Exhaustive search: The search heuristic (Section 8.4) to determine the optimal mixture can be used alongside any objective function and not necessarily the MML criterion. The series of perturbations are carried out as described and the improvement to mixtures is determined based on the criterion in use.
- Traditional search: As discussed in Section 8.3, the traditional search method using AIC/BIC involves estimating the mixture parameters using the EM algorithm (Section 8.1) for varying number of components K and choosing the one which results in minimum criterion value.

It is to be noted that with the MML criterion, the EM algorithm in Section 8.2 is used to obtain the MML estimates of the mixture parameters. However, with AIC and BIC, the EM algorithm in Section 8.1 results in the maximum likelihood (ML) estimates for a given K. For FB<sub>5</sub> mixtures, the ML estimates are often approximated by the moment estimates which are used in the M-step of the EM algorithm (Peel et al., 2001; Kent and Hamelryck, 2005; Hamelryck et al., 2006). We compare the results for mixtures obtained using the ML estimates and their approximations against those obtained using MML-based estimates.

The results pertaining to the *exhaustive* search method are shown in Table 3. It is observed that when search is based on AIC, the mixtures resulting due to moment and ML estimation have 37 and 34 components respectively. The moment and the ML mixtures have the same AIC values in this case. With BIC, the mixture resulting from ML estimation has the lower BIC value. In this case, the moment and the ML mixtures have 23 and 24

<sup>6.</sup> The number of free parameters in a FB<sub>5</sub> mixture with K components is p = 5K + (K - 1) = 6K - 1.

components respectively. This number resembles the one obtained by the exhaustive search but MML-based parameter estimation. The ML mixture has the lowest BIC score.

Criterion	Moment mixtures			Maximum likelihood mixtures		
	K	Criterion	Message		Criterion	Message
		value	length	K	value	length
		$(\times 10^5 \text{ bits})$	$(\times 10^6 \text{ bits})$		$(\times 10^5 \text{ bits})$	$(\times 10^6 \text{ bits})$
AIC	37	2.313	5.474	34	2.313	5.474
BIC	23	4.647	5.475	24	$\boldsymbol{4.645}$	5.474

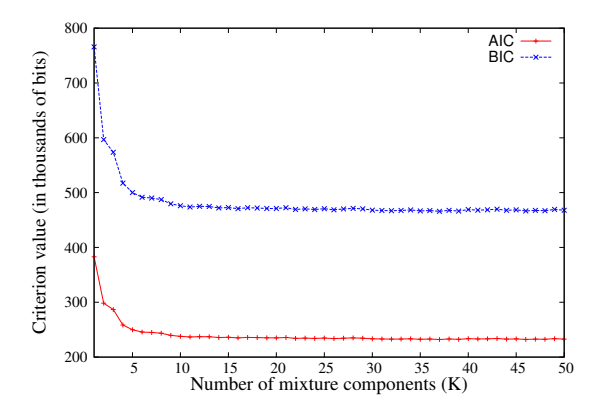
Table 3: FB<sub>5</sub> mixtures inferred by employing the *exhaustive search* method and changing the evaluation criteria and methods to estimate mixture parameters.

The results pertaining to the traditional search method are shown in Figure 18. As the number of components K is increased, it is expected that the AIC and BIC scores decrease until some minimum is reached and then increase thereafter. The value of K at which this behaviour happens is treated to be the optimal mixture that models the data. It is observed that initially, both criteria decrease and after K=30, the values do not change dramatically. By increasing K, the linear increase in penalty factors and the associated increase in log-likelihood are of the same magnitude, and hence, the difference in criteria is not apparent. Thus, using the traditional search, it is difficult to decide on an appropriate number of mixture components.

The trend observed in Figure 18 is the same for mixtures obtained using both moment and ML estimates. The expressions for AIC and BIC do not help in distinguishing the moment and ML mixtures because for different types of estimates and a given K, the penalty terms are the same. Also, the log-likelihood is approximately the same because for huge amounts of data, as is the case here, all the estimates converge to the same value.

In contrast, if we compute the first part message lengths corresponding to the moment and ML mixtures, for a given K, the differences in their encoding lengths become apparent. The variation in the first part message lengths for the moment and ML mixtures resulting from the traditional search are shown in Figure 20. It is observed that until K=30, the first part message lengths of moment and ML mixtures are close to each other. In Figure 20(b), when K>30, there are minute differences between encoding lengths of mixture parameters obtained using moment and ML estimates. Thus, unlike AIC/BIC, the MML criterion is able to distinguish mixtures with equal number of components. The first part corresponds to the model complexity and is dependent on not just the number of components K but also on the components' parameters themselves according to the MML framework.

The above discussion is aimed at projecting the limitations of the traditional search method and also the use of AIC and BIC as evaluation criteria. We find in MML an objective way to assess mixtures and in conjunction with the search method offers a better alternative to determine reliable mixture models. We further illustrate the behaviour of the search method with smaller amount of data. The previous discussion pertains to the entire empirical data set containing N=251,346 ( $\theta,\phi$ ) pairs. In the current context, from the empirical distribution, we randomly sample varying amounts of data ranging from N=1000



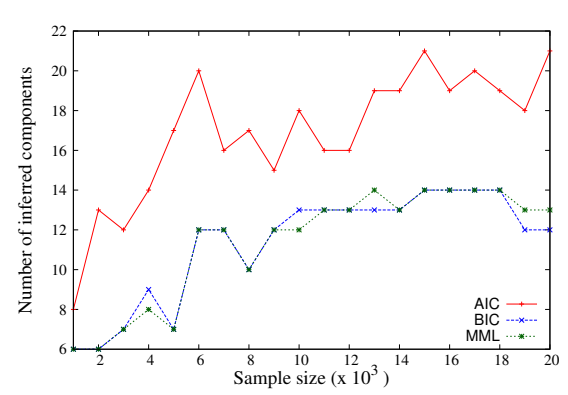


Figure 18: The criteria computed for maximum likelihood mixtures (moment mixtures have the same behaviour and are hence not shown)

Figure 19: Variation of the number of inferred components using the search method based on exhaustive perturbations.

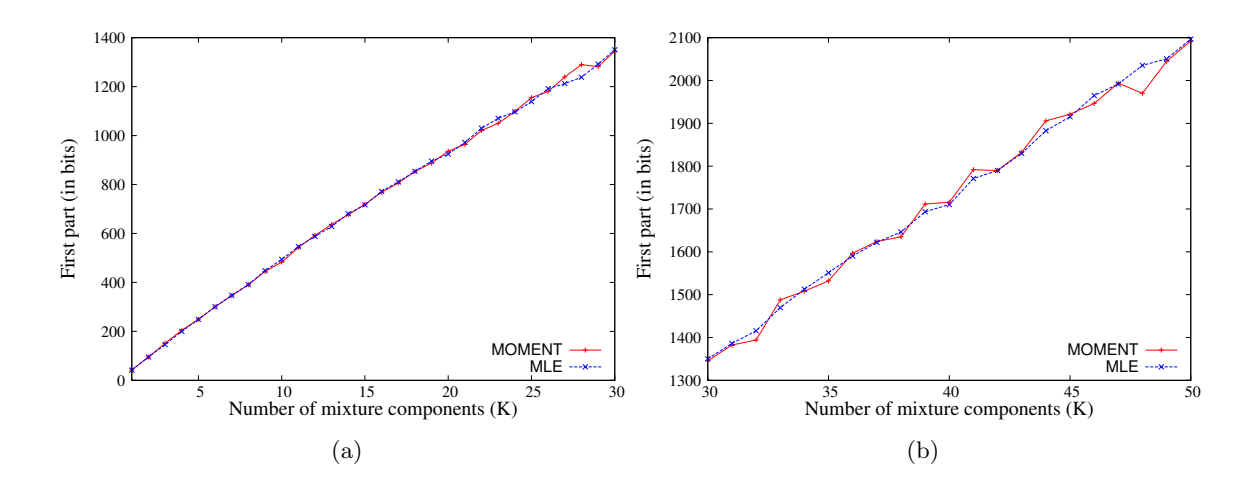


Figure 20: First part message length corresponding to mixtures evaluated using AIC. The results for BIC display the same pattern and are hence not shown. (the range of  $K \in [1, 50]$  is split into two sub-figures (a) and (b) in order to highlight the differences in the message lengths).

to N=20,000. The experiment is conducted by fixing the search method (exhaustive) but changing the evaluation criteria to infer suitable FB<sub>5</sub> mixtures. It is observed that mixtures based on AIC have greater number of components as compared to BIC and MML (see Figure 19). The mixtures corresponding to BIC and MML have the same number of

components in most of the experimental trials. These results are in agreement with what was observed on the complete protein data (Table 3), where AIC resulted in greater number of components.

### 11. Conclusion

We derived the parameter estimates of a FB<sub>5</sub> distribution defined on a three-dimensional unit sphere based on the Bayesian information-theoretic minimum message length criterion. The derived estimators have lower bias and mean squared error compared to the traditionally used moment and maximum likelihood estimators. The MML-based estimates are also invariant to transformations of the parameter space unlike the MAP estimates. Hence, the MML-based estimates are improvements over the traditionally used estimators. Further, we have designed the mixture modelling apparatus to be used in conjunction with FB<sub>5</sub> mixtures and demonstrated their applicability in modelling real-world directional data resulting from protein spatial orientations. The results obtained from modelling using FB<sub>5</sub> mixtures is contrasted with commonly used vMF mixtures. The FB<sub>5</sub> mixture models supersede the vMF models in describing protein data, and serve as improved null model descriptors that are important to modelling tasks in structural biology.

### References

- Milton Abramowitz and Irene A. Stegun. *Handbook of Mathematical Functions*. Dover, New York, 1965.
- Hirotugu Akaike. A new look at the statistical model identification. *IEEE Transactions on Automatic Control*,, 19(6):716–723, Dec 1974.
- Donald E. Amos. Computation of modified Bessel functions and their ratios. *Mathematics of Computation*, 28(125):239–251, 1974.
- Arindam Banerjee, Inderjit Dhillon, Joydeep Ghosh, and Suvrit Sra. Generative model-based clustering of directional data. In *Proceedings of the Ninth International Conference on Knowledge Discovery and Data Mining*, pages 19–28, New York, 2003.
- Arindam Banerjee, Inderjit Dhillon, Joydeep Ghosh, and Suvrit Sra. Clustering on the unit hypersphere using von Mises-Fisher distributions. *Journal of Machine Learning Research*, 6:1345–1382, 2005.
- Donald J. Best and Nicholas I. Fisher. The bias of the maximum likelihood estimators of the von Mises-Fisher concentration parameters. *Communications in Statistics-Simulation and Computation*, 10(5):493–502, 1981.
- Christophe Biernacki, Gilles Celeux, and Gérard Govaert. Assessing a mixture model for clustering with the integrated completed likelihood. *IEEE Transactions on Pattern Analysis and Machine Intelligence*, 22(7):719–725, 2000.
- Wouter Boomsma, John T. Kent, Kanti V. Mardia, Charles C. Taylor, and Thomas Hamelryck. Graphical models and directional statistics capture protein structure. *Interdisciplinary Statistics and Bioinformatics*, 25:91–94, 2006.

#### Kasarapu

- Hamparsum Bozdogan. Choosing the number of component clusters in the mixture-model using a new informational complexity criterion of the inverse-Fisher information matrix. Springer, Berlin, Heidelberg, 1993.
- James H. Collier, Lloyd Allison, Arthur M. Lesk, Maria Garcia de la Banda, and Arun S. Konagurthu. A new statistical framework to assess structural alignment quality using information compression. *Bioinformatics*, 30(17):i512–i518, 2014.
- John H. Conway and Neil J. A. Sloane. On the Voronoi regions of certain lattices. SIAM Journal on Algebraic and Discrete Methods, 5:294–305, 1984.
- Gauss M. Cordeiro and Ruben Klein. Bias correction in ARMA models. Statistics & Probability Letters, 19(3):169–176, 1994.
- Gauss M. Cordeiro and Klaus L. P. Vasconcellos. Theory & Methods: Second-order biases of the maximum likelihood estimates in von Mises regression models. *Australian & New Zealand Journal of Statistics*, 41(2):189–198, 1999.
- Arthur P. Dempster, Nan M. Laird, and Donald B. Rubin. Maximum likelihood from incomplete data via the EM algorithm. *Journal of the Royal Statistical Society: Series B (Methodological)*, 39(1):1–38, 1977.
- Luiz H. G. Dore, Getulio J. A. Amaral, Jorge T. M. Cruz, and Andrew T. A. Wood. Bias-corrected maximum likelihood estimation of the parameters of the complex bingham distribution. *Brazilian Journal of Probability and Statistics*, forthcoming.
- David L. Dowe, Lloyd Allison, Trevor I. Dix, Lawrence Hunter, Chris S. Wallace, and Timothy Edgoose. Circular clustering of protein dihedral angles by minimum message length. In *Pacific Symposium on Biocomputing*, volume 96, pages 242–255, 1996a.
- David L. Dowe, Jonathan J. Oliver, and Chris S. Wallace. MML estimation of the parameters of the spherical Fisher distribution. In *Proceedings of the Seventh International Workshop on Algorithmic Learning Theory*, volume 1160 of *Lecture Notes in Computer Science*, pages 213–227, Berlin, Heidelberg, 1996b. Springer.
- Ian L. Dryden and Kanti V. Mardia. Statistical shape analysis, volume 4. Wiley Chichester, 1998.
- Mario A. T. Figueiredo and Anil K. Jain. Unsupervised learning of finite mixture models. *IEEE Transactions on Pattern Analysis and Machine Intelligence*, 24(3):381–396, 2002.
- Nicholas I. Fisher. Statistical analysis of spherical data. Cambridge University Press, Cambridge, 1993.
- Ronald Fisher. Dispersion on a sphere. Proceedings of the Royal Society of London A: Mathematical, Physical and Engineering Sciences, 217(1130):295–305, 1953.
- Siddharth Gopal and Yiming Yang. Von Mises-Fisher clustering models. In *Proceedings of The 31st International Conference on Machine Learning*, pages 154–162, 2014.

- Thomas Hamelryck. Probabilistic models and machine learning in structural bioinformatics. Statistical Methods in Medical Research, 18(5):505–526, 2009.
- Thomas Hamelryck, John T. Kent, and Anders Krogh. Sampling realistic protein conformations using local structural bias. *PLoS Computational Biology*, 2(9):e131, 2006.
- Steven G. Johnson. The NLopt nonlinear-optimization package. http://ab-initio.mit.edu/nlopt.
- Parthan Kasarapu and Lloyd Allison. Minimum message length estimation of mixtures of multivariate Gaussian and von Mises-Fisher distributions. *Machine Learning*, 2015. doi: 10.1007/s10994-015-5493-0.
- John T. Kent. The Fisher-Bingham distribution on the sphere. Journal of the Royal Statistical Society: Series B (Methodological), 44(1):71–80, 1982.
- John T. Kent and Thomas Hamelryck. Using the Fisher-Bingham distribution in stochastic models for protein structure. *Quantitative Biology, Shape Analysis, and Wavelets*, 24: 57–60, 2005.
- John T. Kent, Asaad M. Ganeiber, and Kanti V. Mardia. A new method to simulate the Bingham and related distributions in directional data analysis with applications. arXiv:1310.8110[math.ST]. 2013.
- Arun S. Konagurthu, Arthur M. Lesk, and Lloyd Allison. Minimum message length inference of secondary structure from protein coordinate data. *Bioinformatics*, 28(12):i97–i105, 2012.
- Arun S. Konagurthu, Lloyd Allison, David Abramson, Peter J. Stuckey, and Arthur M. Lesk. Statistical inference of protein "LEGO bricks". In 2013 IEEE 13th International Conference on Data Mining (ICDM), pages 1091–1096. IEEE, 2013.
- Thriyambakam Krishnan and Geoffrey J. McLachlan. *The EM algorithm and extensions*. Wiley, New York, 1997.
- Solomon Kullback and Richard A. Leibler. On information and sufficiency. *The Annals of Mathematical Statistics*, 22(1):79–86, 1951.
- Alfred Kume and Andrew T. A. Wood. On the derivatives of the normalising constant of the Bingham distribution. Statistics & Probability Letters, 77(8):832–837, 2007.
- Guy Lebanon. Bias, Variance, and MSE of estimators, 2010.
- Kanti V. Mardia. Statistics of directional data (with discussion). Journal of the Royal Statistical Society: Series B (Methodological), 37:349–393, 1975.
- Kanti V. Mardia and Peter E. Jupp. Directional statistics. Wiley, Hoboken, NJ, USA, 2000.
- Kanti V. Mardia, Charles C. Taylor, and Ganesh K. Subramaniam. Protein bioinformatics and mixtures of bivariate von Mises distributions for angular data. *Biometrics*, 63(2): 505–512, 2007.

#### Kasarapu

- Geoffrey J. McLachlan and David Peel. Finite mixture models. Wiley, New York, 2000.
- Kevin P. Murphy. *Machine Learning: A probabilistic perspective*. The MIT Press, Cambridge, MA, USA, 2012.
- Alexey G. Murzin, Steven E. Brenner, Tim Hubbard, and Cyrus Chothia. SCOP: a structural classification of proteins database for the investigation of sequences and structures. Journal of Molecular Biology, 247(4):536–540, 1995.
- Jonathan J. Oliver and Rohan A. Baxter. MDL and MML: Similarities and differences (introduction to minimum encoding inference). Technical report, Monash University, 1994.
- Jonathan J. Oliver, Rohan A. Baxter, and Chris S. Wallace. Unsupervised learning using MML. In *Machine Learning: Proceedings of the 13th International Conference*, pages 364–372, 1996.
- David Peel, William J. Whiten, and Geoffrey J. McLachlan. Fitting mixtures of Kent distributions to aid in joint set identification. *Journal of the American Statistical Association*, 96(453):56–63, 2001.
- Michael J. D. Powell. A direct search optimization method that models the objective and constraint functions by linear interpolation. In *Advances in Optimization and Numerical Analysis*, pages 51–67. Kluwer Academic Publishers, Dordrecht, Netherlands, 1994.
- Jorma Rissanen. Modeling by shortest data description. Automatica, 14(5):465–471, 1978.
- Stephen J. Roberts, Dirk Husmeier, Iead Rezek, and William Penny. Bayesian approaches to Gaussian mixture modeling. *IEEE Transactions on Pattern Analysis and Machine Intelligence*, 20(11):1133–1142, Nov 1998.
- Murray Rosenblatt. Remarks on a multivariate transformation. The Annals of Mathematical Statistics, 23(3):470–472, 1952.
- Geert Schou. Estimation of the concentration parameter in von Mises–Fisher distributions. *Biometrika*, 65(2):369–377, 1978.
- Gideon Schwarz. Estimating the dimension of a model. The Annals of Statistics, 6(2): 461–464, 1978.
- Claude E. Shannon. A mathematical theory of communication. The Bell System Technical Journal, 27:379–423, 1948.
- Marco Taboga. Lectures on probability theory and mathematical statistics. CreateSpace Independent Pub., 2012.
- Naonori Ueda, Ryohei Nakano, Zoubin Ghahramani, and Geoffrey E. Hinton. SMEM algorithm for mixture models. *Neural Computation*, 12(9):2109–2128, 2000.
- Chris S. Wallace. An improved program for classification. In *Proceedings of the 9th Australian Computer Science Conference*, pages 357–366, 1986.

- Chris S. Wallace. Statistical and inductive inference using minimum message length. Springer-Verlag, Secaucus, NJ, USA, 2005.
- Chris S. Wallace and David M. Boulton. An information measure for classification. *Computer Journal*, 11(2):185–194, 1968.
- Chris S. Wallace and David L. Dowe. Estimation of the von Mises concentration parameter using minimum message length. In *Proceedings of the 12th Australian Statistical Society Conference, Monash University, Australia*, 1994.
- Chris S. Wallace and Peter R. Freeman. Estimation and inference by compact coding. Journal of the Royal Statistical Society: Series B (Methodological), 49(3):240–265, 1987.
- Geoffrey S. Watson and Evan J. Williams. On the construction of significance tests on the circle and the sphere. *Biometrika*, 43(3-4):344–352, 1956.
- Samuel S. Wilks. The large-sample distribution of the likelihood ratio for testing composite hypotheses. The Annals of Mathematical Statistics, 9(1):60–62, 1938.

## Appendix A. Prior density of $\Theta$ governed by the $\kappa$ prior for the 2D vMF

In the MML estimation of parameters of a vMF distribution on a circle, Wallace and Dowe (1994) use  $h(\kappa) = \frac{\kappa}{(1+\kappa^2)^{3/2}}$ . We discuss this prior additionally as this leads to an invertible transformation of all five parameters (described below) in the context of a FB<sub>5</sub> distribution. As in Section 5.1,  $h_A(\psi, \alpha, \eta) = \frac{\sin \alpha}{4\pi^2}$  and  $h(\beta|\kappa) = 2/\kappa$ . Hence, the joint prior density  $h_{\Theta}$  is formulated as shown below. Further, using the eccentricity transform described in Section 5.2.1, the joint prior density  $h_{\Theta'}$  in  $\Theta'$  parameterization is given below.

$$h_{\mathbf{\Theta}}(\psi, \alpha, \eta, \kappa, \beta) = \frac{\sin \alpha}{2\pi^2 (1 + \kappa^2)^{3/2}} \quad \text{and} \quad h_{\mathbf{\Theta}'}(\psi, \alpha, \eta, \kappa, e) = \frac{\kappa \sin \alpha}{4\pi^2 (1 + \kappa^2)^{3/2}}$$

### A.1 An alternative parameterization of the parameter vector $\Theta$

In addition to the eccentricity transform, we study a transformation proposed by Rosenblatt (1952), that transforms a given continuous k-variate probability distribution into the uniform distribution on the k-dimensional hypercube. Such a transformation applied on the prior density of the FB<sub>5</sub> parameter vector  $\boldsymbol{\Theta}$  results in the prior transforming to a uniform distribution. Hence, estimation in this transformed parameter space is equivalent to the corresponding maximum likelihood estimation. For the 5-parameter vector  $\boldsymbol{\Theta} = \{\psi, \alpha, \eta, \kappa, \beta\}$ , the Rosenblatt (1952) transformation to  $\boldsymbol{\Theta}'' = \{z_1, z_2, z_3, z_4, z_5\}$  is given by

$$\begin{split} z_1 &= \Pr(X_1 \leq \psi) = F_1(\psi) \\ z_2 &= \Pr(X_2 \leq \alpha | X_1 = \psi) = F_2(\alpha | \psi) \\ z_3 &= \Pr(X_3 \leq \eta | X_2 = \alpha, X_1 = \psi) = F_3(\eta | \alpha, \psi) \\ z_4 &= \Pr(X_4 \leq \kappa | X_3 = \eta, X_2 = \alpha, X_1 = \psi) = F_4(\kappa | \eta, \alpha, \psi) \\ z_5 &= \Pr(X_5 \leq \beta | X_4 = \kappa, X_3 = \eta, X_2 = \alpha, X_1 = \psi) = F_5(\beta | \kappa, \eta, \alpha, \psi) \end{split}$$

This transformation results in  $0 \le z_i \le 1, i = 1, ..., 5$ . Further, Rosenblatt (1952) argues that each  $z_i$  is uniformly and independently distributed on [0,1], so that the prior density in this transformed parameter space is  $h_{\Theta''}(z_1, z_2, z_3, z_4, z_5) = 1$ . In order to achieve such a transformation, we need to express  $z_i$  in terms of the original parameters. As per the definitions of the prior on  $\Theta$  (Section 5.1), the following relationships are derived:

$$z_{1} = \psi/\pi \implies \psi = \pi z_{1}$$

$$z_{2} = (1 - \cos \alpha)/2 \implies \alpha = \arccos(1 - 2z_{2})$$

$$z_{3} = \eta/(2\pi) \implies \eta = 2\pi z_{3}$$
(32)

Based on the independence assumption in the formulation of priors of angular and scale parameters (Section 5.1),  $z_4 = F_4(\kappa|\eta,\alpha,\psi) = F_4(\kappa)$ . Similarly,  $F_5(\beta|\kappa,\eta,\alpha,\psi) = F_5(\beta|\kappa)$ . Hence, the invertible transformations corresponding to  $\kappa$  and  $\beta$  are as follows:

$$z_4 = \int_0^{\kappa} h(\kappa) d\kappa = \int_0^{\kappa} \frac{\kappa}{(1 + \kappa^2)^{3/2}} d\kappa = 1 - \cos(\arctan \kappa) \implies \kappa = \tan(\arccos(1 - z_4))$$

$$z_5 = F_5(\beta | \kappa) = 2\beta / \kappa \implies \beta = \kappa z_5 / 2$$
(33)

With the 3D version of vMF  $\kappa$  prior (see Section 5.1),  $z_4$  evaluates to  $\frac{2}{\pi} \left( \arctan \kappa - \frac{\kappa}{1 + \kappa^2} \right)$ . This version of  $z_4$  is not invertible as it does not allow us to express  $\kappa$  as a closed form expression in  $z_4$ . Hence, the Rosenblatt (1952) transformation is discussed only in the context when 2D vMF  $\kappa$  prior is considered, as it is possible to find an inverse transformation.

## A.2 The example demonstrating the effects of alternative parameterizations

The above discussed prior and its variants are used in the MAP-based parameter estimation of the data from the example discussed in Section 5.3. The resulting estimates of  $\psi, \alpha, \eta$  are given below using:

$$h_{\Theta}: \widehat{\psi} = 2.070, \ \widehat{\alpha} = 1.493, \ \widehat{\eta} = 1.522$$
  
 $h_{\Theta'}: \widehat{\psi} = 2.070, \ \widehat{\alpha} = 1.493, \ \widehat{\eta} = 1.522$   
 $h_{\Theta''}: \widehat{z}_1 = 0.659, \ \widehat{z}_2 = 0.461, \ \widehat{z}_3 = 0.242$ 

As observed,  $\widehat{\psi}, \widehat{\alpha}$ , and  $\widehat{\eta}$  are the same when posteriors corresponding to  $h_{\Theta}$  and  $h_{\Theta'}$  are used. In the case of  $h_{\Theta''}$ , the mapping of  $\widehat{z}_1, \widehat{z}_2, \widehat{z}_3$  back to  $\widehat{\psi}, \widehat{\alpha}, \widehat{\eta}$  (Equation 32), results in the same estimates as that of  $h_{\Theta}$  and  $h_{\Theta'}$ . Hence, the MAP estimates of  $\psi, \alpha, \eta$  are the same across the different versions. The estimates of  $\kappa$  and  $\beta$  are, however, not the same under the various transformations. They are as follows depending on the parameterization:

$$h_{\mathbf{\Theta}}: \widehat{\kappa} = 16.975, \ \widehat{\beta} = 5.467$$
  
 $h_{\mathbf{\Theta}'}: \widehat{\kappa} = 20.547, \ \widehat{e} = 0.701 \implies \widehat{\beta} = \widehat{\kappa} \, \widehat{e}/2 = 7.205$   
 $h_{\mathbf{\Theta}''}: \widehat{z}_4 = 0.964, \ \widehat{z}_5 = 0.779 \implies \widehat{\kappa} = 28.065, \ \widehat{\beta} = 10.925$  (as per Equation 33)

The estimated value of  $\kappa$  using  $h_{\Theta}$  is 16.975 whereas it is 20.547 using  $h_{\Theta'}$ . The value of  $\hat{e}$  corresponds to a  $\hat{\beta} = 7.205$ . Similarly, the value of  $\hat{\kappa}$  and  $\hat{\beta}$  corresponding to  $\hat{z}_4 = 0.964$  and

 $\hat{z}_5 = 0.0.779$  are 28.065 and 10.925 respectively. Clearly, the value of the parameter estimates depend on the parameterization. However, it is required that the estimates obtained in different parameterizations should be the same irrespective of the space in which the parameters are defined. However, through this example, it is observed that for the various parameterizations, the value of MAP estimates differ.

The variation of the posterior density under various transformations of the parameter space are shown in Figure 21. These are plotted as a function of  $\kappa$ ,  $\beta$  (in case of  $h_{\Theta}$ ),  $\kappa$ , e (in case of  $h_{\Theta'}$ ), and  $z_4, z_5$  (in case of  $h_{\Theta''}$ ), each reflecting the space in which the posterior is defined. It is observed that the modes of the respective posterior distributions occur at different positions and they are not equivalent to each other. The posterior density plots in Figure 21(b) and (c) correspond to those in Figure 21(d) and (e) respectively. Ideally, (the modes in) Figure 21(a)-(c) should be the same. However, as demonstrated, that is not the case. Thus, maximizing the posterior density does not yield consistent estimates as observed through this example.

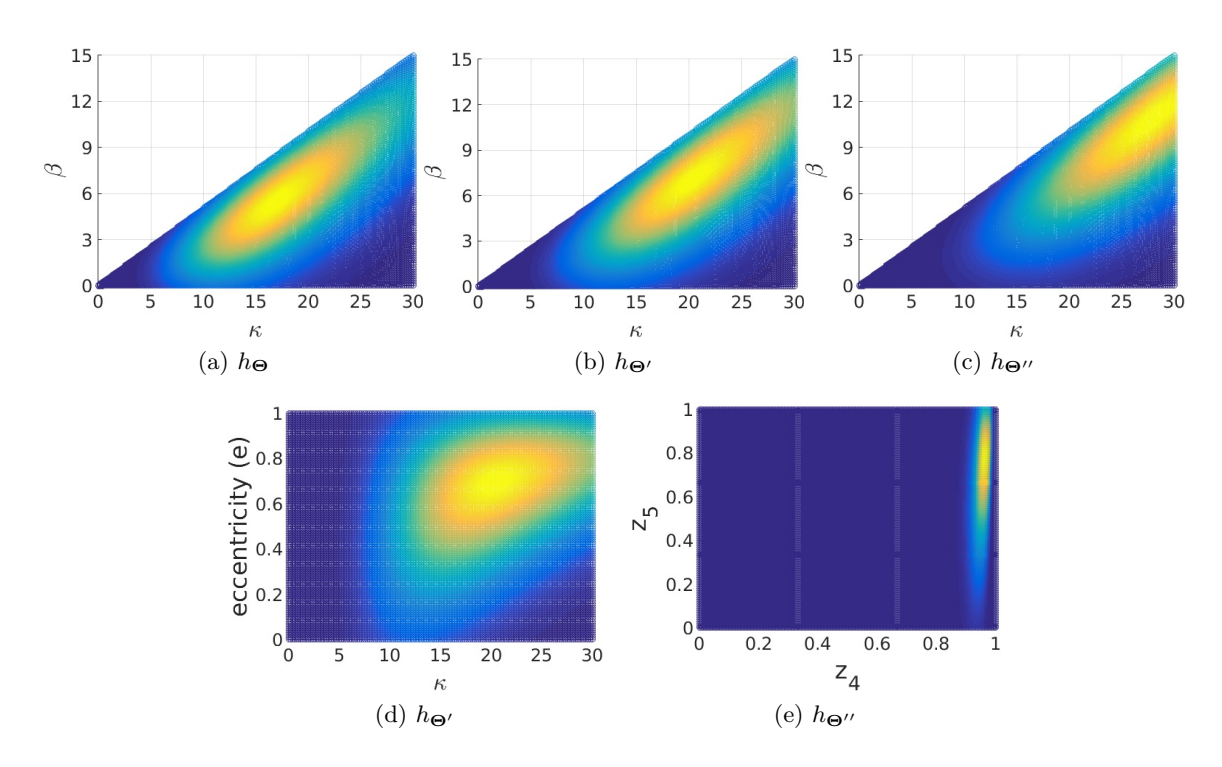


Figure 21: Heat maps depicting the modes (MAP estimates) of the posterior density resulting from different parameterizations.

# Appendix B. The partial derivatives of $\gamma_1, \gamma_2, \gamma_3$ with respect to $\psi, \alpha, \eta$

The first and second order partial derivatives of the axes are required for the evaluation of the elements of the Fisher information matrix (see Section 6.2.1). The expressions for  $\gamma_1, \gamma_2, \gamma_3$  as a function of  $\psi, \alpha, \eta$  are given by Equation 5.

• Derivatives of  $\gamma_1$ :

$$\frac{\partial \boldsymbol{\gamma}_{1}}{\partial \alpha} = \begin{pmatrix} \cos \alpha \\ \sin \alpha \cos \eta \\ \sin \alpha \sin \eta \end{pmatrix}, \quad \frac{\partial \boldsymbol{\gamma}_{1}}{\partial \eta} = \begin{pmatrix} 0 \\ -\sin \alpha \sin \eta \\ \sin \alpha \cos \eta \end{pmatrix}$$

$$\frac{\partial^{2} \boldsymbol{\gamma}_{1}}{\partial \alpha^{2}} = -\boldsymbol{\gamma}_{1}, \quad \frac{\partial^{2} \boldsymbol{\gamma}_{1}}{\partial \eta^{2}} = \begin{pmatrix} 0 \\ -\sin \alpha \cos \eta \\ -\sin \alpha \sin \eta \end{pmatrix}, \quad \frac{\partial^{2} \boldsymbol{\gamma}_{1}}{\partial \eta \partial \alpha} = \begin{pmatrix} 0 \\ -\cos \alpha \sin \eta \\ \cos \alpha \cos \eta \end{pmatrix}$$

The partial derivatives of  $\gamma_1$  involving the parameter  $\psi$  are zero vectors.

• Derivatives of  $\gamma_2$ :

$$\frac{\partial \mathbf{\gamma}_{2}}{\partial \alpha} = -\cos \psi \, \mathbf{\gamma}_{1} \,, \quad \frac{\partial \mathbf{\gamma}_{2}}{\partial \eta} = \begin{pmatrix} 0 \\ -\cos \psi \cos \alpha \sin \eta - \sin \psi \cos \eta \\ \cos \psi \cos \alpha \cos \eta - \sin \psi \sin \eta \end{pmatrix} \,, \quad \frac{\partial \mathbf{\gamma}_{2}}{\partial \psi} = \mathbf{\gamma}_{3}$$

$$\frac{\partial^{2} \mathbf{\gamma}_{2}}{\partial \alpha^{2}} = -\cos \psi \frac{\partial \mathbf{\gamma}_{1}}{\partial \alpha} \,, \quad \frac{\partial^{2} \mathbf{\gamma}_{2}}{\partial \eta^{2}} = \begin{pmatrix} 0 \\ -\cos \psi \cos \alpha \cos \eta + \sin \psi \sin \eta \\ -\cos \psi \cos \alpha \sin \eta - \sin \psi \cos \eta \end{pmatrix} \,, \quad \frac{\partial^{2} \mathbf{\gamma}_{2}}{\partial \psi^{2}} = -\mathbf{\gamma}_{2}$$

$$\frac{\partial^{2} \mathbf{\gamma}_{2}}{\partial \eta \partial \alpha} = -\cos \psi \frac{\partial \mathbf{\gamma}_{1}}{\partial \eta} \,, \quad \frac{\partial^{2} \mathbf{\gamma}_{2}}{\partial \psi \partial \alpha} = \sin \psi \, \mathbf{\gamma}_{1} \,, \quad \frac{\partial^{2} \mathbf{\gamma}_{2}}{\partial \psi \partial \eta} = \frac{\partial \mathbf{\gamma}_{3}}{\partial \eta}$$

• Derivatives of  $\gamma_3$ :

$$\begin{split} \frac{\partial \boldsymbol{\gamma}_3}{\partial \alpha} &= \sin \psi \, \boldsymbol{\gamma}_1 \,, \quad \frac{\partial \boldsymbol{\gamma}_3}{\partial \eta} = \begin{pmatrix} 0 \\ \sin \psi \cos \alpha \sin \eta - \cos \psi \cos \eta \\ -\sin \psi \cos \alpha \cos \eta - \cos \psi \sin \eta \end{pmatrix} \,, \quad \frac{\partial \boldsymbol{\gamma}_3}{\partial \psi} = -\boldsymbol{\gamma}_2 \\ \frac{\partial^2 \boldsymbol{\gamma}_3}{\partial \alpha^2} &= -\sin \psi \frac{\partial \boldsymbol{\gamma}_1}{\partial \alpha} \,, \quad \frac{\partial^2 \boldsymbol{\gamma}_3}{\partial \eta^2} = \begin{pmatrix} 0 \\ \sin \psi \cos \alpha \cos \eta + \cos \psi \sin \eta \\ \sin \psi \cos \alpha \sin \eta - \cos \psi \cos \eta \end{pmatrix} \,, \quad \frac{\partial^2 \boldsymbol{\gamma}_3}{\partial \psi^2} = -\boldsymbol{\gamma}_3 \\ \frac{\partial^2 \boldsymbol{\gamma}_3}{\partial \eta \partial \alpha} &= \sin \psi \frac{\partial \boldsymbol{\gamma}_1}{\partial \eta} \,, \quad \frac{\partial^2 \boldsymbol{\gamma}_3}{\partial \psi \partial \alpha} = \cos \psi \, \boldsymbol{\gamma}_1 \,, \quad \frac{\partial^2 \boldsymbol{\gamma}_3}{\partial \psi \partial \eta} = -\frac{\partial \boldsymbol{\gamma}_2}{\partial \eta} \end{split}$$

## Appendix C. The search process continued

The illustrations presented here are continuation of the example discussed in Section 8.5.1. Figure 22 illustrates the perturbations carried out on the component  $P_2$  in the mixture  $\mathcal{M}_3$ . None of the split, delete, and merge operations involving  $P_2$  result in improved mixtures. The same is the case with component  $P_3$  (depicted in Figure 23). It is interesting to note the different mixtures obtained by splitting  $P_2$  and  $P_3$  in Figure 22(c) and Figure 23(c) respectively. These 4-component mixtures are different to the mixture obtained by splitting  $P_1$  (Figure 9c). Also, the mixtures resulting from deleting and merging of  $P_2$  and  $P_3$  are different when compared to the mixtures obtained by the same operations on  $P_1$ . This example demonstrates how the search method evaluates various competing mixtures and selects the one which has the least overall message length.

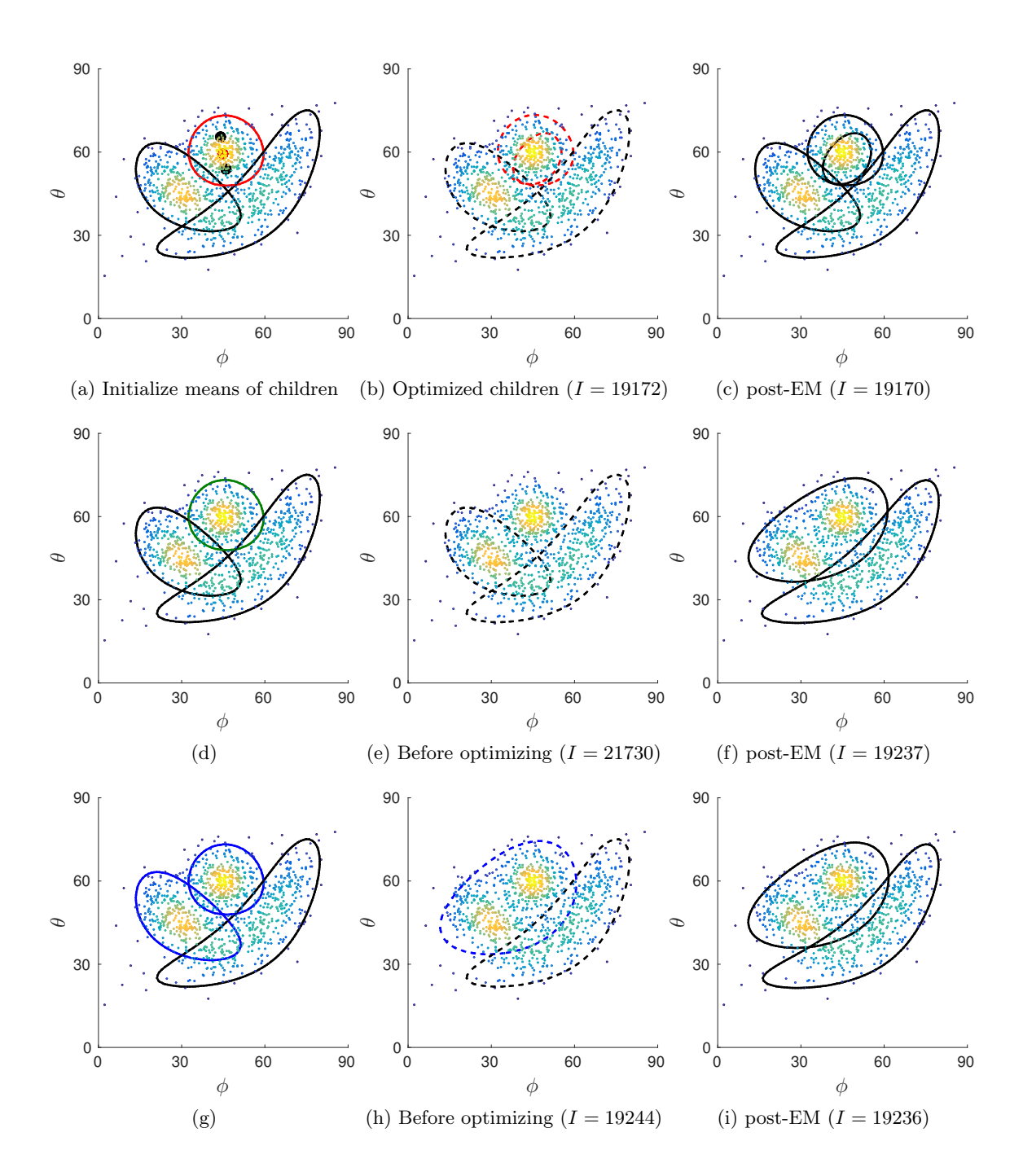


Figure 22: Iteration 3 – perturbations of  $P_2$  (a)-(c) splitting, (d)-(f) deletion, (g)-(i) merging

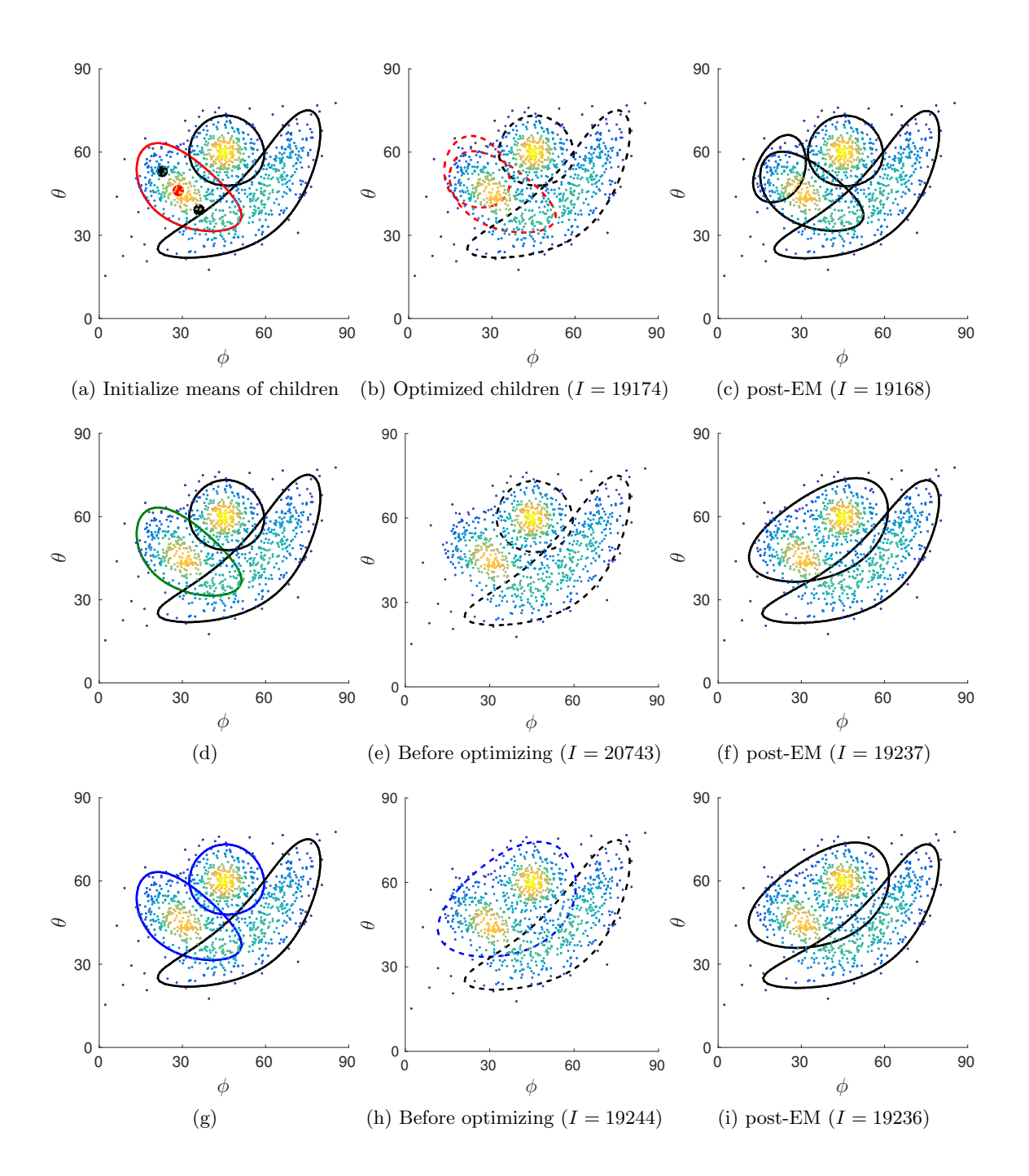


Figure 23: Iteration 3 – perturbations of  $P_3$  (a)-(c) splitting, (d)-(f) deletion, (g)-(i) merging